

CXCR4^{high} megakaryocytes regulate host-defense immunity against bacterial pathogens

Jin Wang^{1*}, Jiayi Xie^{2,3*}, Daosong Wang^{3*}, Xue Han^{2,3*}, Minqi Chen³, Guojun Shi^{1#},
Linjia Jiang^{2#}, Meng Zhao^{2,3,4#}

¹Department of Endocrinology & Metabolism, The Third Affiliated Hospital, Sun Yat-sen University, Guangzhou, Guangdong, 510630, China

²RNA Biomedical Institute, Sun Yat-sen Memorial Hospital, Sun Yat-sen University, Guangzhou, Guangdong, 510120, China

³Key Laboratory of Stem Cells and Tissue Engineering, Zhongshan School of Medicine, Sun Yat-sen University, Ministry of Education, Guangzhou, Guangdong, 510080, China

⁴Lead Contact

* These authors contributed equally to this work.

#Correspondence: Meng Zhao E-mail: zhaom38@mail.sysu.edu.cn; Linjia Jiang: E-mail: jianglj7@mail.sysu.edu.cn; Guojun Shi: E-mail: shigi6@mail.sysu.edu.cn

Abstract

Megakaryocytes (MKs) continuously produce platelets to support hemostasis and form a niche for hematopoietic stem cell maintenance in the bone marrow. MKs are also involved in inflammation responses; however, the mechanism remains poorly understood. Using single-cell sequencing, we identified a CXCR4 highly expressed MK subpopulation, which exhibited both MK-specific and immune characteristics. CXCR4^{high} MKs interacted with myeloid cells to promote their migration and stimulate the bacterial phagocytosis of macrophages and neutrophils by producing TNF α and IL-6. CXCR4^{high} MKs were also capable of phagocytosis, processing and presenting antigens to activate T cells. Furthermore, CXCR4^{high} MKs also egressed circulation and infiltrated into the spleen, liver, and lung upon bacterial infection. Ablation of MKs suppressed the innate immune response and T cell activation to impair the anti-bacterial effects in mice under the *Listeria monocytogenes* challenge. Using hematopoietic stem/progenitor cell lineage-tracing mouse lines, we show that CXCR4^{high} MKs were generated from infection-induced emergency megakaryopoiesis in response to bacterial infection. Overall, we identify the CXCR4^{high} MKs, which regulate host-defense immune response against bacterial infection.

Introduction

Megakaryocytes (MKs) are large and rare hematopoietic cells in the bone marrow, which continually produce platelets to support hemostasis and thrombosis (Deutsch & Tomer, 2006). MK progenitors undergo multiple rounds of endomitosis during maturation to

achieve polyploid (Chang et al., 2007; Deutsch & Tomer, 2013; Machlus & Italiano, 2013; Nagata et al., 1997; Patel et al., 2005). MKs and their progenitors migrate between distinct microenvironments and organs for their proliferation, maturation, and biological functions (Avecilla et al., 2004; Fuentes et al., 2010; Lefrancais et al., 2017; Pal et al., 2020; Tamura et al., 2016; Wang et al., 1998). Although platelet generation is the prominent role of MKs, emerging evidence suggests that MKs have other biological functions. Mature MKs interact with HSCs and constitute a unique niche to preserve HSC quiescence in the bone marrow (Bruns et al., 2014; Zhao et al., 2014). MKs also interact with other niche cells, such as osteoblasts (Dominici et al., 2009; Olson et al., 2013), non-myelinating Schwann cells (Jiang et al., 2018; Yamazaki et al., 2011), and blood vessels (Avecilla et al., 2004; Sacma et al., 2019) to further influence the attraction and retention of hematopoietic stem and progenitor cells during homeostasis and stress.

MK-biased hematopoietic stem cells (HSCs) induce emergency megakaryopoiesis to actively generate MKs upon acute inflammation, which can efficiently replenish the platelet loss during inflammatory insult (Haas et al., 2015). Studies suggested that MKs might participate in immune responses independent of their platelet generation role (Cunin & Nigrovic, 2019). MKs express multiple immune receptors, such as IgG Fc receptors and toll-like receptors (TLRs), enabling them to sense inflammation directly (Cunin & Nigrovic, 2019). Mature MKs also express major histocompatibility complex (MHC) to activate antigen-specific CD8⁺ T cells and enhance CD4⁺ T cells and Th17 cell responses through stimulating antigen processing (Finkielstein et al., 2015; Pariser et al., 2021; Zufferey et al., 2017). Furthermore, MKs release multiple cytokines and chemokines to influence immune cells. For example, MKs produce IL-1 α and IL-1 β to

promote arthritis susceptibility in mice resistant to arthritis (Cunin et al., 2017) and produce CXCL1 and CXCL2 to promote neutrophil efflux from the bone marrow (Köhler et al., 2011). Lung MKs contribute to thrombosis (Lefrancais et al., 2017) and, more interestingly, participate in immune responses (Pariser et al., 2021), although the relationship between lung MKs and bone marrow circulating MKs (Nishimura et al., 2015) remains unexplored. Furthermore, the recent single-cell atlas shows that MKs are heterogeneous and contain subpopulations that express multiple immune genes and are involved in inflammation response (C. Liu et al., 2021; Pariser et al., 2021; S. Sun et al., 2021; Yeung et al., 2020). Here, by combining scRNA-seq with functional assays, we identified a CXCR4^{high} MK population, which was generated by infection-induced emergency megakaryopoiesis, and stimulated innate immunity against bacterial infection.

Results

Single-cell atlas identifies an immune-modulatory subpopulation of MKs

We applied droplet-based scRNA-seq with CD41⁺ forward scatter (FSC)^{high} bone marrow MKs to explore the MK heterogeneity (Figure 1A; Figure 1-figure supplement 1A, B). To enrich accurate MKs, we further performed transcriptomic profile analysis in the phenotypically enriched MKs (Yeung et al., 2020). Our scRNA-seq successfully detected 5368 high-quality cells (Figure 1-figure supplement 1B, C), in which one MK cluster (1712 cells) and six immune cell clusters (3656 cells) were annotated according to their gene profile (Figure 1-figure supplement 1D-G) and the alignment with published scRNA-seq data (Almanzar et al., 2020; F. K. Hamey et al., 2021; Pariser et al., 2021; Xie et al., 2020; Yeung et al., 2020). Our annotated MKs were similar to MKs but distinct

to immune cells, including myeloid progenitors, basophils, neutrophils, monocytes, dendritic cells, macrophages, B cells, and T cells, in an integrated scRNA-seq analysis platform (Figure 1-figure supplement 2). Therefore, we re-clustered the transcriptionally enriched 1712 MKs into five subpopulations, termed MK1 to MK5 (Figure 1B; Figure 1-figure supplement 3A, B), which were further confirmed by the integrated scRNA-seq analysis platform to rule out the potential immune cell contamination (Pariser et al., 2021; Xie et al., 2020; Yeung et al., 2020) (Figure 1-figure supplement 3C, D). We noticed that mature MKs with huge sizes were captured at a relatively low rate, potentially due to the limitation in current techniques in cell purification and single-cell preparation (C. Liu et al., 2021; S. Sun et al., 2021).

Enriched signature genes by Gene Ontology exhibited that MK1 and MK2 highly expressed nuclear division, DNA replication and repair genes for endomitosis (Figure 1C, D). MK3 enriched blood coagulation and thrombosis genes for platelet generation (Figure 1C, D). No signature pathways were enriched in MK4. MK5 enriched cell migration and immune response genes (Figure 1C, D; Figure 1-figure supplement 4A-E), cytokine, chemokine (Figure 1E, F; Figure 1-figure supplement 4F), and genes involved in immune cell interaction (Figure 1G, Figure 1-figure supplement 5A). MK5 also expressed signature genes in recently reported inflammatory-related MKs (*Cd53*, *Lsp1*, *Anxa1*, *Spi*) (S. Sun et al., 2021) and immune MKs (*Ccl3*, *Cd52*, *Selp*, *Sell*, *Adam8*) (C. Liu et al., 2021) (Figure 1-figure supplement 5B). We also noticed that MK5 highly expressed *Cxcr4* than other MK subpopulations (Figure 1H, I), although most MKs express CXCR4 (Hamada et al., 1998) (Figure 1-figure supplement 6A). To confirm this, we found that CXCR4^{high} MKs expressed MK markers (Figure 1-figure supplement 6B), were mainly

polyloid cells (Figure 1-figure supplement 6C), and had platelet generation ability (Figure 1-figure supplement 6D), although they have relatively low polyploidy (Figure 1-figure supplement 6E) and smaller cell size (Figure 1-figure supplement 6F-H). CXCR4^{high} MKs generated platelets in lower efficiencies compared to CXCR4^{low} MKs (Figure 1-figure supplement 6D), suggesting CXCR4^{high} MKs might be specialized for immune functions. Overall, using scRNA-seq, we identified an MK subpopulation that exhibited both MK-specific and immune transcriptional characteristics.

CXCR4^{high} MKs enhance myeloid cell mobility and bacterial phagocytosis

As MK5 enriched genes involved in myeloid cell activation (Figure 1-figure supplement 4E) and myeloid cell interactions (Figure 1G, Figure 1-figure supplement 5A), we further explored the role of CXCR4^{high} MKs, which enriched MK5, in regulating myeloid immune cells, in regulating the innate immunity function of myeloid cells against pathogens. We challenged mice with *Listeria* (*L.*) *monocytogenes*, a Gram-positive facultative intracellular bacterium (Bishop & Hinrichs, 1987; Edelson & Unanue, 2000), which induce myelopoiesis (Eash et al., 2009) (Figure 2-figure supplement 1A, B). Interestingly, we noticed that CXCR4^{high} MKs were more dramatically associated with myeloid cells in the bone marrow of mice three days after *L. monocytogenes* infection, which was a significant increase than the association between myeloid cells and CXCR4^{low} MKs or the association between randomly placed myeloid cells and CXCR4^{high} MKs (Figure 2A, B). The myeloid cell-CXCR4^{high} MK association (mean distance 15.36 μ m) was significantly closer than the myeloid cell-CXCR4^{low} MKs association (Figure 2C; mean distance 25.62 μ m, $p = 7.0 \times 10^{-4}$ by KS test), and the

association between randomly placed myeloid cells and CXCR4^{high} MKs [35.37 μm , p ($\mu < 15.36$) = 1.8×10^{-10}] in the bone marrow of mice three days after *L. monocytogenes* infection. Whereas the observed mean distance of myeloid cells to CXCR4^{low} MKs (25.62 μm) is not different from random simulations [27.76 μm , p ($\mu < 25.62$) = 0.14] (Figure 2C). This suggested that the increased association between myeloid cell-CXCR4^{high} MK may not be due to the infection-induced expansion of myeloid cells. Furthermore, we did not observe a significant association between myeloid cells and MKs during homeostasis (Figure 2-figure supplement 1C, D). We also noticed that bone marrow myeloid cells were preferably adjacent to the CXCR4^{high} MK-blood vessel intersection in mice three days after *L. monocytogenes* infection (Figure 2-figure supplement 1E, F). These observations indicated that CXCR4^{high} MKs might regulate myeloid cells upon bacterial infection.

To explore how CXCR4^{high} MKs regulate myeloid cells, we interestingly found that CXCR4^{high} MKs, but not CXCR4^{low} MKs, effectively promoted myeloid cell mobilization in our transwell assays (Figure 2D). Furthermore, we asked whether CXCR4^{high} MKs regulate myeloid cell function against pathogens. To this aim, we incubated purified CXCR4^{low} MKs and CXCR4^{high} MKs with neutrophils or macrophages for bacterial phagocytosis analysis. We found that CXCR4^{high} MKs, but not CXCR4^{low} MKs, efficiently enhanced the bacterial phagocytosis of neutrophils and macrophages (Figure 2E-H; Figure 2-figure supplement 2A, B).

Our scRNA-seq also exhibited that the high expression of *Cxcr4* was positively correlated with immune cell-stimulating cytokines, such as *Ccl6*, *Tnf*, and *Il6* (Li et al., 2018; Rothe et al., 1993; Shapouri-Moghaddam et al., 2018) in MKs (Figure 2I). In line

with this, CXCR4^{high} MKs had higher TNF α and IL-6 protein levels than CXCR4^{low} MKs (Figure 2J; Figure 2-figure supplement 2C, D). The TNF α and IL-6 levels in CXCR4^{high} MKs were comparable to macrophages from mice three days after *L. monocytogenes* infection (Figure 2-figure supplement 2E), which are known as the primary cellular source of TNF α and IL-6 upon infection (Shapouri-Moghaddam et al., 2018). These observations suggested that CXCR4^{high} MKs might stimulate myeloid cell phagocytosis by producing TNF α and IL-6. Indeed, anti-TNF α and anti-IL-6 blocking antibodies compromised the role of CXCR4^{high} MKs in stimulating bacterial phagocytosis of neutrophils and macrophages (Figure 2K-N).

CXCR4^{high} MKs stimulate host-defense immunity against bacterial pathogens

To explore the *in vivo* role of MKs upon *L. monocytogenes* infection in mice, we employed *Pf4^{Cre}; Rosa26^{fs-iDTR}* mice, in which MKs were rendered sensitive to diphtheria toxin (DT) (Zhao et al., 2014) (Figure 3A, B). MK ablation increased the number of hematopoietic stem and progenitor cells and myelopoiesis in the bone marrow upon infection (Figure 3-figure supplement 1A-D). Notably, MK ablation dramatically increased the bacterial burdens in the liver and spleen three days after *L. monocytogenes* infection (Figure 3C). We also found that MK ablation reduced the number of myeloid cells, including monocytes, macrophages, dendritic cells (DCs), and neutrophils, in the liver and spleen (Figure 3D, E; Figure 3-figure supplement 1E, F), suggesting the role of MKs in promoting myeloid cells against pathogens. We further investigated whether MKs regulate adaptative immunity against pathogen infection. Interestingly, we noticed that CXCR4^{high} MKs were able to phagocytose bacteria and presented the ovalbumin (OVA)

antigens on their surface via MHC-I (Figure 3F, G). Furthermore, OVA antigens presented by CXCR4^{high} MKs activated OT-I CD8⁺ T cells (Figure 3H) and B3Z T cells (Figure 3-figure supplement 2), a T cell hybridoma which expresses TCR that specifically recognizes OVA (J. Karttunen et al., 1992). We challenged *Pf4^{Cre}; Rosa26^{fs-iDTR}* mice with OVA-expressing recombinant microbe (*L. monocytogenes*-OVA). Seven days after *L. monocytogenes*-OVA infection, splenocytes from control or MK ablated mice were re-stimulated with OVA peptide *in vitro* to assess OVA-specific T cell activation (Figure 3I). Notably, MK ablation dramatically reduced the number of CD4⁺ IFN γ ⁺ Th1, CD4⁺ IL4⁺ Th2, and CD8⁺ cytotoxic T lymphocytes but did not impact the total number of CD4⁺ T cells and CD8⁺ T cells (Figure 3J). These observations demonstrated that MKs regulate host-defense immunity against *L. monocytogenes* infection. To explore whether CXCR4^{high} MKs contribute to the immune response against bacterial pathogens, we infused the purified CXCR4^{high} MKs and CXCR4^{low} MKs into MK ablation mice during *L. monocytogenes* infection (Figure 3K). Notably, we found that the infusion with CXCR4^{high} MKs, but not CXCR4^{low} MKs, partially rescued the bacterial clearance defect in MK ablation mice (Figure 3L). This is potentially due to the reduced platelets known for regulating immune responses (Semple et al., 2011).

Bacterial infection stimulates the migration of CXCR4^{high} MKs

High *Cxcr4* expression indicated that CXCR4^{high} MKs might migrate between the bone marrow microenvironment and circulation in response to infection (Suraneni et al., 2018). In line with this, our spatial distribution analysis showed that ~80% of MKs directly contacted blood vessels three days after *L. monocytogenes* infection, which was much

higher than in control mice (~40%) (Figure 4A, B; Figure 4-figure supplement 1A). Furthermore, more CXCR4^{high} MKs, with small cell sizes (Figure 1-figure supplement 6F-H), were tightly associated with blood vessels and trapped in the sinusoid than CXCR4^{low} MKs three days after *L. monocytogenes* infection (Figure 4C, D). However, *L. monocytogenes* infection did not influence the association between MKs and HSCs (Figure 4A, E), albeit the critical role of perivascular MKs in maintaining HSC quiescence (Bruns et al., 2014; Itkin et al., 2016; Zhao et al., 2014) and the dramatic HSC activation upon infection (Figure 4-figure supplement 1B).

To further explore the dynamic migration of MKs upon pathogen infection, we adapted an *ex vivo* real-time imaging method to trace MK migration in the bone marrow (Xie et al., 2009). Using *Pf4^{Cre}; Rosa26^{fs-tdTomato}* mice and *ex vivo* live imaging approach, we observed that small tdTomato⁺ MKs rapidly migrated into sinusoids without rupture or platelet release upon infection (Figure 4F, Figure 4-video 1). In contrast, MKs with large sizes showed much slower migration (Figure 4-video 1). Additionally, CXCR4^{high} MKs were decreased in the bone marrow three days after *L. monocytogenes* infection but with a similar proliferation and apoptosis rate compared to CXCR4^{low} MKs (Figure 4G; Figure 4-figure supplement 1C-F), indicating CXCR4^{high} MKs might migrate out of bone marrow. Consistent with this, the frequency of MK5, which enriched CXCR4^{high} MKs, decreased in bone marrow after *L. monocytogenes* infection in our single-cell atlas (Figure 4-figure supplement 2). Furthermore, we found that *L. monocytogenes* infection decreased the expression of CXCL12, the ligand of CXCR4 (Sugiyama et al., 2006), in bone marrow but increased CXCL12 expression in the lung, liver, and spleen (Figure 4-figure supplement 3), suggesting that the distinguished CXCL12 levels between tissues

might drive the migration of CXCR4^{high} MKs between tissues. In line with this, CXCR4^{high} MKs were increased in the peripheral blood and organs, including the liver, spleen, and lung three days after *L. monocytogenes* infection without an alternation of cell cycle and apoptosis, whereas CXCR4^{low} MKs did not differ except for a slight increase in the liver (Figure 4G; Figure 4-figure supplement 4A-C). Moreover, inflammatory stresses, such as IFN γ and Lipopolysaccharides (LPS), or *L. monocytogenes* treatment did not increase CXCR4 expression in CXCR4^{low} MKs (Figure 4H; Figure 4-figure supplement 4D).

To further explore how MKs migrate between organs during bacterial infection *in vivo*, we employed *Pf4^{Cre}; Rosa26^{fs-tdTomato}*, and *Pf4^{Cre}; cell membrane-localized tdTomato cell membrane-localized EGFP (Rosa26^{fs-mTmG})* mice in which Tomato or cell membrane-localized EGFP (mGFP) were exclusively expressed in MK lineage (Tiedt et al., 2007). mGFP expressing MKs or Tomato expressing CXCR4^{high} MKs were increased in the liver and spleen three days after *L. monocytogenes* infection (Figure 4I; Figure 4-figure supplement 4E-H), whereas Tomato expressing CXCR4^{low} MKs did not change (Figure 4-figure supplement 4I). To further confirm the tissue infiltration of MKs upon infection, we intravenously injected membrane-localized tdTomato (mTomato) expressing bone marrow cells from *Rosa26R^{fs-mTmG}* mice into control recipients or recipients infected with *L. monocytogenes* one day before mTomato⁺ cell perfusion (Figure 4J). We found that two days after mTomato⁺ cell perfusion, engrafted mTomato⁺ CXCR4^{high} MKs more efficiently infiltrated into the liver (92.1%) and spleen (92.5%); by contrast, most mTomato⁺ CXCR4^{low} MKs (66.7%) migrated to the bone marrow (Figure 4K).

As the lung is an important site for platelet generation (Lefrancais et al., 2017), we aligned our MK sc-RNAseq data with lung MKs (Pariser et al., 2021; Yeung et al., 2020), and found that MK5, MK4, and MK3 showed similar gene profiles with lung MKs (Figure 4L). Moreover, MK5 enriched more inflammatory pathway genes, antigen processing, and presentation pathway after *L. monocytogenes* infection, which enabled MK5 to achieve a more similar transcriptional profile as the lung MKs than normal MK5 (Figure 4-figure supplement 5). Interestingly, we found that engrafted Tomato⁺ MKs (from *Pf4^{Cre}; Rosa26^{fs-tdTomato}* mice) more efficiently infiltrated the lungs in the infected recipients as extravascular MKs than in the control recipients (Figure 4M-O and Figure 4-figure supplement 6).

Acute inflammation-induced emergency megakaryopoiesis generates CXCR4^{high} MKs upon infection

Infection-induced emergency megakaryopoiesis compensates the platelet consumption (Verschoor et al., 2011). Consistently, we observed that MKs were ruptured in the bone marrow three days after *L. monocytogenes* infection to recover the reduced platelets post-*L. monocytogenes* infection (Couldwell & Machlus, 2019; Nishimura et al., 2015) (Figure 5A-C). However, CXCR4^{high} MKs were increased at 18 hours after *L. monocytogenes* infection and substantially declined at 72 hours in bone marrow, whereas CXCR4^{low} MKs remained unchanged upon infection (Figure 5D). As MK-committed HSCs drive infection-induced emergency megakaryopoiesis (Haas et al., 2015), we asked whether emergency megakaryopoiesis also generates CXCR4^{high} MKs to participate in the host-defense response. To this aim, we employed *Scl^{CreER}; Rosa26^{fs-tdTomato}* mice

(Göthert et al., 2005) to monitor the HSPC derived emergency megakaryopoiesis upon bacterial infection. Eighteen hours after tamoxifen recombining Tomato in HSPCs and *L. monocytogenes* infection (Figure 5E), we observed that Tomato⁺ HSPCs derived Tomato⁺ CXCR4^{high} MKs rapidly increased in the bone marrow, similar to the platelet-generating MKs (tdTomato⁺ CXCR4^{low} MKs) (Figure 5F), without a noticeable rise of hematopoietic progenitors (Figure 5G). Overall, our observations indicated that CXCR4^{high} MKs might be generated by emergency megakaryopoiesis to stimulate pathogen defense.

Discussion

MKs participate in megakaryocyte maturation, platelet activation, and potentially influence neutrophils and the adaptive immune cells (Cunin & Nigrovic, 2019). Accordingly, MKs prevent the spread of dengue virus infection by enhancing the type 1 interferons pathway in murine and clinical biospecimens (Campbell et al., 2019) and contribute to cytokine storms in severe COVID-19 patients (Bernardes et al., 2020; Ren et al., 2021; Stephenson et al., 2021). MKs were reported to express multiple inflammation receptors, such as Fcγ receptors (Markovic et al., 1995), Toll-like receptors (Beaulieu et al., 2011; Ward et al., 2005), interleukin receptors (Navarro et al., 1991; Yang et al., 2000), and IFN receptors (Negrotto et al., 2011), which might enable MKs to receive inflammation signals and express cytokines. Recent scRNA-seq studies suggested the existence of MK subpopulations for inflammation responses (C. Liu et al., 2021; Pariser et al., 2021; S. Sun et al., 2021; Wang et al., 2021). Here, we identified that MK5 has both MK and immune cell characteristics for platelet generation and immune responses. More importantly, we demonstrated that CXCR4^{high} MKs recruited and

stimulated innate myeloid cells by producing TNF α and IL-6, for bacterial phagocytosis. Furthermore, CXCR4^{high} MKs had the ability for antigen processing and antigen presentation capacity, which suggested that CXCR4^{high} MKs might contribute to the regulation of adaptive immune function. This is consistent with a previous observation that lung MKs are able to process and present antigens (Pariser et al., 2021). Our data suggested that CXCR4^{high} MKs might contribute to the regulation of adaptive immune function. However, as the distinction between CXCR4^{high} MKs and CXCR4^{low} MKs is not entirely objective, additional markers are warranted to further enrich CXCR4^{high} MKs.

We observed that MK ablation increased HSPCS and myeloid granulocyte/macrophage progenitor (GMP) in bone marrow under bacterial infection, which is consistent with 5-FU stress (Hérault et al., 2017). However, increased GMP only increased myeloid cells in the bone marrow but not in other organs, which further supported the role of CXCR4^{high} MKs in promoting the migration of myeloid cells. Normal HSC to MK development takes 11-12 days in humans and 4 days in mice; However, emergency megakaryopoiesis takes less than a day to generate MKs upon inflammation stress (Couldwell & Machlus, 2019; C. Liu et al., 2021; S. Sun et al., 2021) (Figure 5D). Previously, researchers believed that emergency megakaryopoiesis mainly contributes to the replenishment of damaged platelets upon acute inflammation (Haas et al., 2015). We found that inflammation signals could not upregulate CXCR4 in CXCR4^{low} MKs *in vitro*, although we cannot entirely exclude the plasticity of MKs *in vivo*. Our data showed that CXCR4^{high} MKs might be generated from the emergency megakaryopoiesis, instead of CXCR4^{low} MKs, to facilitate host-defense responses against

bacterial infection.

A recent report showed that the lung is a reservoir of MKs for platelet production (Lefrancais et al., 2017). Other works also indicate that lung MKs share a similar transcriptional profile with lung DCs and participate in pathogen infection (Boilard & Machlus, 2021; Pariser et al., 2021). However, the correspondence between MKs in the lung and bone marrow remains unexplored. Neonatal lung MKs lack the immune molecules in adult lung MKs (Pariser et al., 2021), which indicates that lung MKs might have distinct developmental origins. Similarly, MKs are observed to egress and migrate to the pulmonary capillary under stresses (Davis et al., 1997). Our works suggested lung MKs might migrate from bone marrow upon infection challenges, although more detailed investigations are warranted in future studies.

Materials and Methods

Mice

C57BL/6-Tg(*Pf4-cre*)Q3Rsko/J (*Pf4^{Cre}*), C57BL/6-Gt(ROSA) 26Sortm1(HBEGF) Awai/J (*Rosa26^{fs-iDTR}*), C57BL/6-Gt(ROSA)26Sortm4(ACTB-tdTomato,-EGFP)Luo/J (*Rosa26^{fs-mTmG}*), Gt(ROSA)26Sortm9(CAG-tdTomato)Hze (*Rosa26^{fs-tdTomato}*), CXCL12tm2.1Sjm/J (*Cxcl12^{DsRed}*) and C57BL/6-Tg(TcraTcrb)1100Mjb/J (*OT-I*) mice were obtained from the Jackson Laboratory. *Scf^{CreER}* mice were provided by J. R. Göthert. All mice were maintained in the C57BL/6 background. Animals were blindly included in the experiments according to genotyping results as a mix of male and female. All animal experiments were performed according to protocols approved by the Sun Yat-sen University animal care and use committee (approval No. SYSU-IACUC-2021-B0617).

322 **Cell line**

323 B3Z hybridoma T cells were kindly gifted by Dr. Nilabh Shastri (Johns Hopkins
324 University). This cell line was verified to be mycoplasma free by EZdetect PCR Kit for
325 Mycoplasma Detection (HiMedia).

326 **Bacteria and infections**

327 *Listeria (L.) monocytogenes* infection was performed as described with minor
328 modifications (Edelson & Unanue, 2000; Verschoor et al., 2011). In brief, wild type *L.*
329 *monocytogenes* strain 10403S grown to exponential phase at 37 °C in TSB media was
330 injected intravenously at a dose of 2 500 colony-forming units (CFUs) to determine
331 spleen and liver bacterial burdens three days after infection. Recombinant *L.*
332 *monocytogenes* expressing the chicken ovalbumin peptide (OVA₂₅₇₋₂₆₄) (*L.m.* –
333 OVA₂₅₇₋₂₆₄) was injected intravenously at a dose of 2500 CFUs to determine activated
334 spleen T cells seven days after infection. *Escherichia (E.) coli* wild type strain 85344
335 expressing GFP was constructed as previously described (Feng et al., 2020). GFP labeled
336 *E. coli* was grown to exponential phase at 37 °C in LB media and washed with PBS
337 before being suspended for phagocytosis assays.

338 **Antibodies for flow cytometry analysis and cell sorting**

339 For cell sorting and analysis, monoclonal antibodies to CD41 (MWReg30, eBioscience),
340 CXCR4 (2B11, eBioscience), CD11b (M1/70, eBioscience), F4/80 (BM8, eBioscience),
341 Gr-1 (RB6-8C5, Biolegend), Ly6C (HK1.4, Biolegend), CD11c (N418, eBioscience),
342 CD45.1 (A20, eBioscience), CD45.2 (104, Biolegend), CD4 (GK1.5, eBioscience), CD8
343 (53-6.7, Biolegend), INF- γ (XMG1.2, Biolegend), IL4 (11B11, Biolegend), CD34
344 (RAM34, eBioscience), Sca-1 (D7, Biolegend), c-kit (2B8, Biolegend), CD135 (A2F10,

Biolegend), CD3 ϵ (145-2C11, Biolegend), CD45R (RA3-6B2, Biolegend), TER-119 (Ter-119, Biolegend), IgM (II/41, eBioscience), F γ RII (93, Biolegend), IL-7R (A7R34, Biolegend), TNF α (MP6-XT22, Invitrogen), IL-6 (MP5-20F3, Biolegend), OVA257-264 (SIINFEKL) peptide bound to H-2K^b (eBio25-D1.16 (25-D1.16), Invitrogen) and IL-2 (JES6-5H4, eBioscience) were used where indicated.

Flow cytometry and cell sorting

Bone marrow cells were isolated from mouse femora and tibiae as previously reported (Jiang et al., 2018). Splenocytes were mechanically dissociated in PBS with 2% FBS. Peripheral blood was collected from the retro-orbital sinus and anticoagulated by K2-EDTA. Those three kinds of cells then underwent red blood cell lysis for 5 min using 0.16 M ammonium chloride solution. Liver cells were mechanically dissociated and lysed using 0.16 M ammonium chloride solution, followed by gradient sedimentation using a density reagent (LTS1077, TBD Science) following the manufacturer's instruction. Cell sorting was performed using a cell sorter (MoFlo Astrios, Beckman Coulter) with a 100 μ m nozzle at a speed of around 5000 cells sec⁻¹. For intracellular cytokine staining, cells were pretreated with Brefeldin-A (BFA, 10 μ g ml⁻¹) for 4 hours at 37°C before staining. For MK antigen presentation detection, MKs were co-culture with 100 μ g ml⁻¹ soluble full-length OVA for 24 hours before staining. For IFN γ , LPS and *L. monocytogenes* treatment, cells were co-culture with 10 ng ml⁻¹ IFN- γ or 30 μ g ml⁻¹ LPS for 4, 18 or 24 hours, or 10⁶ *L. monocytogenes* for 4 hours in a 37°C incubator before staining. Cell analysis was performed on either one of the flow cytometers (Attune NxT, Thermo Fisher; Cytex AURORA, Aurora).

Single-cell library construction and sequencing

Sorted CD41⁺ FSC^{high} single cells from four mice of a control MK group and an MK group from mice three days upon *L. monocytogenes* infection each were processed through the Chromium Single Cell Platform using the Chromium Single Cell 3' Library and Gel Bead Kit v3 (PN-1000075, 10x Genomics) and the Chromium Single Cell B Chip Kit (PN-1000074, 10x Genomics) as the manufacturer's protocol. In brief, over 7000 cells were loaded onto the Chromium instrument to generate single-cell barcoded droplets. Cells were lysed and barcoded reverse transcription of RNA occurred. The library was prepared by following amplification, fragmentation, adaptor, and index attachment then sequenced on an Illumina NovaSeq platform.

scRNA-seq processing

The scRNA-seq reads were aligned to the mm10 reference genomes, and unique molecular identifier (UMI) counts were obtained by Cell Ranger 3.0.2. Normalization, dimensionality reduction, and clustering were performed with the Seurat 3.0 R package (Butler et al., 2018). For the control and *Listeria (L.) monocytogenes* infection group, we loaded one 10x Genomics well each and detected 5663 and 5948 cells that passed the Cell Ranger pipeline, respectively. To ruled out low quality cells, cells with >12% mitochondrial content or <200 detected genes were excluded with Seurat function subset (percent.mt<12 & nFeature_RNA>200). We ruled out doublets with default parameters of DoubletDecon R package, and 54 control cells and 939 *L. monocytogenes* infected cells were excluded. Following the standard procedure in Seurat's pipeline, we identified 3272 MKs from control mice (1712 MKs) and mice with *L. monocytogenes* infection (1560 MKs) (3897 and 3449 immune cells were discarded respectively) in combination with MetaNeighbor method. Preprocessed dataset normalization was performed by dividing

the UMI counts per gene by the total UMI counts in the corresponding cell and log-transforming before scaling and centering. SCT normalization was performed with the script: `object <- SCTransform(object, vars.to.regress = "percent.mt", verbose = FALSE)`. Signature genes of each cluster were obtained using the Seurat function `FindMarkers` with Wilcox test with fold change > 1.5 and p value < 0.05 after clustering. Heatmaps, individual UMAP plots, and violin plots were generated by the Seurat functions in conjunction with `ggplot2` and `pheatmap` R packages.

Similarities and UMAP projection between our scRNA-seq data and published datasets GSE152574 (Yeung et al., 2020), GSE158358 (Pariser et al., 2021), GSE137540 (Xie et al., 2020), GSE128074 (F. K. Hamey et al., 2021), or GSE132042 (Almanzar et al., 2020) were conducted by `MetaNeighbor` R package (Crow et al., 2018), `iMAP.py` and `Symphony` R package (Kang et al., 2021). `iMAP` integration was performed using the default parameters except `n_top_genes=2000`, `min_genes=0`, `min_cells=0`, and `n_epochs=100` before doing dimensionality reduction using Uniform Manifold Approximation and Projection method (UMAP, `n_neighbors=30`, `n_pca=30`). Radar charts were generated with JavaScript written by Nadieh Bremer (VisualCinnamon.com). Euclidean distances denote the distances between the centroid of each cluster.

Correlations were calculated based on normalized RNA values, with the function `cor` and the parameter `method= "spearman"`. Multiple testing correction using the function `cor.test` with the parameter `method = "spearman"` and it was applied for *Cxcr4* expression correlations. We calculated the similarities between MK1 to 5 with the published MK, immune cell, and myeloid progenitor datasets (Almanzar et al., 2020; F. K. Hamey et al., 2021; Pariser et al., 2021; Xie et al., 2020; Yeung et al., 2020) using `scmap`

R package (Kiselev et al., 2018). Default parameters and 1 000 features were used and threshold > 0 was set. Cell-type matches are selected based on the highest value of similarities and the second-highest value which is not 0.01 less than the highest value across all reference cell types.

Cytokine, inflammatory, chemokine, and antigen processing and presentation scores were evaluated with the AddModuleScore function of Seurat using genes from KEGG pathway ko04060, cytokine-cytokine receptor interaction; GO:0006954, inflammatory response; chemokine ligands from CellPhoneDB.mouse (Jin et al., 2021) and GO:0019882, antigen processing and presentation.

Interaction analysis of MKs and immune cells were conducted by CellPhoneDB (Efremova et al., 2020) (transformed to human orthologous genes (Davidson et al., 2020)) and CellChat R package (Jin et al., 2021). Only interactions involving cytokines were shown. Gene Ontology (GO) analysis was performed using clusterProfiler R package (Yu et al., 2012) and visualized using enrichplot R package (Yu, 2019).

Gene set enrichment analysis (GSEA) was performed using gsea R package (Subramanian et al., 2005) and visualized using enrichplot R package. Gene lists were pre-ranked by the fold change values of the differential expression analysis using Seurat function FindMarkers. Gene sets for GSEA were obtained from GO database (GO:0002367, cytokine production involved in immune response; GO:0006954, inflammatory response; GO:0008009, chemokine activity; GO:0022409, positive regulation of cell-cell adhesion; GO:0002275, myeloid cell activation involved in immune response).

Gene set variation analysis (GSVA) was performed using GSVA R package

(Hanzelmann et al., 2013). GSVA was performed to calculate GSVA score of indicated pathway genes in single cell datasets with the whole protein encoding genes after log normalization of expression values. Gene sets for GSVA were obtained from GO database (GO:0022409, positive regulation of cell-cell adhesion; GO:0002275, myeloid cell activation involved in immune response; GO:0002367, cytokine production involved in immune response; GO:0007596, blood coagulation; GO:0019882, antigen processing and presentation; GO:0034340: response to type I interferon; GO:0034341: response to interferon-gamma; GO:0045088, regulation of innate immune response; GO:0042742, defense response to bacterium; GO:0002819, regulation of adaptive immune response; GO:1903708, positive regulation of hemopoiesis).

Lung cells preparation for flow cytometry

Lungs were removed and digested as described with minor modifications (Lefrancais et al., 2017). In brief, removed lungs were placed in 1.5 ml tubes, minced with scissors, and digested with 1 ml digestion buffer (HBSS with 1mg ml⁻¹ collagenase D, 0.1 mg ml⁻¹ DNase I, 25 mM HEPES, 2 mM L-glutamine, and 2% FBS) for 30 min at 37°C before filtration through a 100-µm cell strainer and red blood cell lysis for 5 min. Samples were then filtered through 70-µm strainers and resuspended for subsequent surface marker staining for flow cytometry.

Megakaryocyte ablation induction

Pf4^{Cre} mice were mated with the *Rosa26^{fs-iDTR}* line to generate *Pf4^{Cre}; Rosa26^{fs-iDTR}* mice. Diphtheria toxin (DT, Sigma-Aldrich) was injected intraperitoneally every day at a dose of 40 ng g⁻¹ bodyweight into *Pf4^{Cre+}; Rosa26^{fs-iDTR+/-}* mice and their cre negative counterparts to induce megakaryocyte ablation as indicated.

Cre-ER recombinase induction

Scl^{CreER} mice were mated with the *Rosa26*^{fs-tdTomato} line to generate *Scl*^{CreER}; *Rosa26*^{fs-tdTomato} mice. For induction of cre-ER recombinase, *Scl*^{CreER}, *Rosa26*^{fs-tdTomato+/-} mice were injected with tamoxifen intraperitoneally once (2 mg in 0.1 ml corn oil; Sigma-Aldrich).

BrdU incorporation assay

5-bromo-2-deoxyuridine (BrdU) was administered at a single dose of 125 mg kg⁻¹ body mass by intraperitoneal injection. Whole bone marrow cells were collected 12 hours later and incubated with anti-CD41 and anti-CXCR4 for one hour. Cells were washed and then fixed with 4% PFA at 4 °C overnight. Cells were then permeabilized with 0.5% TritonX-100 for 15 minutes at room temperature and incubated with 1mg ml⁻¹ DNase I (Roche) for one hour at 37 °C followed by incubating with anti-BrdU (BU20A, eBioscience) for one hour at room temperature before being analyzed.

Annexin V binding assay

For Annexin V binding assay, bone marrow cells were incubated with cell surface markers for one hour at 4 °C and then washed with PBS before being resuspended with Annexin V binding buffer (Biolegend). Cells were then incubated with FITC Annexin V (Biolegend) for 15 minutes at room temperature in dark, and then 300 µl Annexin V binding buffer was added to each tube. Cells were analyzed by a flow cytometer.

Immunostaining

Immunostaining of frozen sections was performed as described (Jiang et al., 2018). For bone sections, mice were perfused with PBS and 4% paraformaldehyde (PFA). Then the bones were fixed with 4% PFA for 24 hours, decalcified with 0.5 M EDTA for 2 days,

and gradient dehydrated by 15% and 30% sucrose for another 2 days. The thick of sections was 30 μ m. We used CD41 (MWReg30; eBioscience; 1:200), Endomucin (R&D; 1:100), CD150 (TC15-12F12.2; Biolegend; 1:100), CD48 (HM48-1; Biolegend; 1:100), CXCR4 (2B11, eBioscience; 1:100) antibodies, and lineage panel (Biolegend; cat #133307; 1:50). Secondary staining was done with donkey anti-goat AlexaFluor 488 (Invitrogen; 1:1000). For the liver and spleen from *Pf4^{Cre}+*; *Rosa26^{fs-mTmG+/-}* mice, and lung from *Pf4-cre⁺*; *Rosa26^{fs-tdTomato+/-}* mice, we used DAPI (Thermo Fisher; 0.5 μ g ml⁻¹) to stain the frozen sections. For phagocytosis analysis, F4/80 (BM8, eBioscience; 1:100), CD11b (M1/70; Invitrogen; 1:100), CD41 (MWReg30; Thermo Fisher; 1:200) and DAPI was used. For sorted MKs, we used CXCR4 (2B11, eBioscience; 1:100), TNF α (R023, Sino Biological; 1:100) and IL-6 (MP5-20F3, Biolegend; 1:100) antibody. Secondary staining was performed with donkey anti-rabbit AlexaFluor 488 (Invitrogen; 1:1000). Confocal images were obtained using a spinning-disk confocal microscope (Dragonfly, Andor) and analyzed using Imaris 9.0 software (Oxford Instruments). Three-Dimension plots were generated using Matplotlib (Hunter, 2007).

Quantitative real-time (qRT-) PCR

For RT-qPCR, MKs were dissociated in Trizol (Magen), and RNA was extracted following the manufacture's instruction. RNA was reverse transcribed into cDNA using the TransCripT All-in-One First-Strand cDNA Synthesis kit (Transgene). Quantitative PCR was performed using a Bio-Rad CFX 96 touch. The primers for *Pf4* were 5'-GGGATCCATCTTAAGCACATCAC-3' (forward) and 5'-CCATTCTTCAGGGTGGCTATG-3' (reverse). The primers for *Vwf* were 5'-CTTCTGTACGCCTCAGCTATG-3' (forward) and

506 5'-GCCGTTGTAATTCCCACACAAG-3' (reverse). The primers for *Mpl* were
507 5'-AACCCGGTATGTGTGCCAG-3' (forward) and
508 5'-AGTTCATGCCTCAGGAAGTCA-3' (reverse). The primers for *Cxcl12* were
509 5'-AGGTTCTTATTTCACGGCTTGT-3' (forward) and
510 5'-TGGGTGCTGAGACCTTTGAT-3' (reverse). The primers for *Gapdh* were
511 5'-AGGTCGGTGTGAACGGATTTG-3' (forward) and
512 5'-GGGGTCGTTGATGGCAACA-3' (reverse). *Gapdh* was used as the reference gene
513 for qRT-PCR analysis.

514 **Transwell migration**

515 Transmigration assays were performed on a transwell with a pore size of 5 μ m (Biofil).
516 CXCR4^{low} MKs or CXCR4^{high} MKs from bone marrow were sorted (5000 cells per well)
517 from control mice and added to the lower chamber with 600 μ l IMDM (Thermo Fisher)
518 plus 10% FBS (Gibco). Peripheral blood cells were collected as described in the “Flow
519 cytometry and cell sorting” section. 6×10^5 peripheral blood cells were resuspended in
520 100 μ l RPMI 1640 (Gibco) plus 10% FBS and added to the upper insert to continue for
521 two-hour incubation at 37 °C, 5% CO₂. Cells in the lower chamber were harvested,
522 washed with PBS once, and resuspended with 100 μ l PBS for staining and FACS
523 counting.

524 **Phagocytosis**

525 Bone marrow-derived macrophages (BMDM) from C57BL/6 mice at 6-8 weeks of age
526 were differentiated from bone marrow precursors with minor modifications (Minutti et al.,
527 2019). In brief, bone marrow cells were isolated and propagated for seven days in
528 DMEM without sodium pyruvate or HEPES (Gibco), containing 20% FBS (Gibco), 30%

supernatants of L929 conditioned media, and 1% Pen/Strep (Hyclone) at 37 °C. Macrophage phagocytosis assays were performed on a transwell plate with a pore size of 3 µm (Biofil) as described with modifications (Sharif et al., 2014). Briefly, attached cells were replated into 24-well plates, 5×10^4 cells per well, on glass coverslips for 24-hour culture. Then 5 000 sorted CXCR4^{low} MKs or CXCR4^{high} MKs were added in the upper inserts and placed onto macrophages chambers for additional 16 hours incubation without or with 2 µg ml⁻¹ TNFα neutralizing antibody (R023, Sino Biological; 1:100) or 2 µg ml⁻¹ IL-6 neutralizing antibody (MP5-20F3, Biolegend) at 37 °C, 5% CO₂. The upper inserts were discarded and macrophages were washed with PBS without antibiotics and incubated with 10⁵ GFP-labeled *E. coli* for two hours at 37 °C, 5% CO₂. Cells were washed three times with PBS and incubated with DMEM without sodium pyruvate or HEPES (Gibco) with gentamycin (50 µg ml⁻¹) for 30 minutes at 37 °C, 5% CO₂ to remove adherent bacteria. Cells were then detected by flow cytometry or fixed by cold methanol for 15 minutes and blocked with 10% BSA overnight, followed by incubation with F4/80 (BM8, eBioscience; 1:100) for two hours at room temperature before being quantified using a spinning disk confocal microscope (Dragonfly, Andor).

For neutrophil phagocytosis, CD11b⁺ Gr1⁺ Ly6c⁻ neutrophils were sorted from the spleen and propagated in RPMI 1640 (Gibco) containing 10% FBS. Neutrophil phagocytosis was performed as described in macrophage phagocytosis assay, except cells were sedimented for 30 minutes and fixed on glass coverslips after incubated with GFP-*E. coli* and gentamycin. The capacity of phagocytosis was evaluated by flow cytometry or by fluorescence intensity of GFP-*E. coli*. using the confocal microscope within macrophages and neutrophils.

For megakaryocyte phagocytosis, CXCR4^{low} and CXCR4^{high} MKs were sorted from the bone marrow and propagated in RPMI 1640 (Gibco) containing 10% FBS without antibiotics and incubated with 10⁵ GFP-labeled *E. coli* for two hours at 37 °C, 5% CO₂. Cells were washed three times with PBS and incubated with DMEM without sodium pyruvate or HEPES (Gibco) with gentamycin (50 µg ml⁻¹) for 30 minutes at 37 °C, 5% CO₂ to remove adherent bacteria. Cells were then detected by flow cytometry.

Bone marrow *ex vivo* live imaging

Pf4^{Cre+}; Rosa26^{fs-tdTomato+/-} mice were infected with *L. monocytogenes* for 24 hours. FITC-Dextran (average mol wt 2000000, Sigma-Aldrich) was injected intravenously at a dose of 1.25 mg per mouse before being sacrificed. The ends of the femur below the end of the marrow cavity were cut. The bone marrow plug was gently flushed out of the end of the bone with a 21-gauge blunt needle not to break up the marrow plug. Bone marrow was flushed integrally and fixed onto a glass slide in a chamber, rinsed with RPMI 1640 (Gibco), and covered slightly with a coverslip. The integrity of the vascular structure in the bone marrow was observed and warranted through FITC-Dextran inflorescence before capturing images. Confocal images were obtained every minute on the spinning-disk confocal microscope (Dragonfly, Andor) and analyzed using Imaris 9.0 software (Oxford Instruments).

***In vitro* MK culture, MK size, and proplatelet formation measurement**

MKs were sorted using a cell sorter (MoFlo Astrios, Beckman Coulter) and cultured in 24-well plates in SFEM (Stem Cell Technologies) plus 100 ng ml⁻¹ mTPO (Novoprotein) and 1% Pen/Strep (Hyclone), and incubated at 37 °C, 5% CO₂ for four days. Images were taken by a Nikon Ts2R microscope equipped with a Nikon DS-Ri2 camera. Cell size and

proplatelet formation were measured on day three or day five post-cultured, respectively, using Nikon NIS-Elements BR.

Bone marrow transfer experiments

Pf4^{Cre} mice were mated with the *Rosa26^{fs-tdTomato}* line to generate *Pf4^{Cre+}*; *Rosa26^{fs-tdTomato+/-}* mice. tdTomato⁺ MKs were isolated from *Pf4^{Cre+}*; *Rosa26^{fs-tdTomato+/-}* mice. 6-8-week-old recipient mice were pre-treated with PBS or 2500 CFUs of *L. monocytogenes* as previously described one day before cell perfusion. 1×10^5 tdTomato⁺ MKs were sorted and intravenously injected into control or *L. monocytogenes* infected mice. tdTomato⁺ MKs were detected in lungs with immunostaining two days after cell perfusion.

mtdTomato⁺ bone marrow cells were isolated from *Pf4^{Cre-}*; *Rosa26^{fs-mTmG+/-}* mice. 1×10^6 mtdTomato⁺ bone marrow cells were intravenously injected into control or one-day-*L. monocytogenes* infected mice. mtdTomato⁺ MKs were detected in bone marrow, liver, and spleen two days after cell perfusion.

For *in vivo* CXCR4^{high} MK function assay in MK ablation mice, DT was intraperitoneally injected every day for five days. On the second and fourth days, 2×10^5 sorted wild type CXCR4^{high} MKs or CXCR4^{low} MKs were intravenously injected into indicated groups. PBS or 2500 CFUs of *L. monocytogenes* as previously described were injected intravenously on the third day. Spleen and liver were harvested three days after infection to determine the bacterial burdens as described.

T cell reactivation *in vitro*

Splenocytes (1×10^6 cells well⁻¹) from control or MK ablated mice after seven days *L.m.*-OVA infection were re-stimulated for four hours *in vitro* with OVA peptide (10 μ M)

in the presence of Brefeldin-A (BFA, 10 $\mu\text{g ml}^{-1}$). Activated T cells were then analyzed by a flow cytometer.

For MK-induced T cell activation, 3×10^4 MK subpopulations for each sample were sorted and co-cultured with 100 $\mu\text{g ml}^{-1}$ soluble full-length OVA for 24 hours, then co-cultured with 6×10^4 OT-I CD8^+ T cells or B3Z T cells (J Karttunen et al., 1992) for 48 hours at 37°C in a 5% CO_2 incubator as described (Zufferey et al., 2017). OT-I T cell activation was detected by measuring intracellular IL-2 levels. B3Z T cell activation was detected using β -galactosidase Assay Kit (RG0036, Beyotime). Bone marrow-derived dendritic cells (DCs) were adopted as positive controls for T cell activation assay. To obtain bone marrow-derived DCs, isolated bone marrow cells were cultured in RPMI 1640 with 10 ng ml^{-1} of GM-CSF and 10 ng ml^{-1} of IL-4 as described (Roney, 2019).

Computational modeling of random myeloid cell localization

We have performed randomized simulations as in previous reports (Bruns et al., 2014; Jiang et al., 2018) in Python. Images of a $400 \mu\text{m} \times 400 \mu\text{m}$ bone marrow region with $\text{CXCR4}^{\text{high}}$ and $\text{CXCR4}^{\text{low}}$ MKs, in which background staining was removed, were used to generate MKs onto which 200 myeloid cells were randomly placed, consistent with an average density of 200 myeloid cells per field. Each simulated run placed 200 random myeloid cells (mean diameter 5 μm) was repeated 500 times. The shortest Euclidean distance was calculated for each myeloid cell to $\text{CXCR4}^{\text{high}}$ or $\text{CXCR4}^{\text{low}}$ MKs. Random and observed distance distributions were compared using the modified nonparametric two-dimensional (2D) KS test as described (Bruns et al., 2014; Jiang et al., 2018).

Statistical analyses

Data are presented as means \pm s.e.m or presented medians, first and third quartiles. For

phagocytosis assay and MK size measurement, data were analyzed by a one-dimensional KS test. Differences were considered statistically significant if $p < 0.05$. For the comparison of three-dimensional distances, a two-dimensional KS test was used. The difference was considered statistically significant if $p < 0.05$. For multiple comparisons analysis, data were analyzed by repeated-measures one-way analysis of variance (ANOVA) followed by Dunnett's test. Differences were considered statistically significant if $p < 0.05$. ‡ $P < 0.05$, # $P < 0.01$, ## $P < 0.001$, n.s., not significant. For pairs of measurements, data were analyzed by paired Student's t -test. Differences were considered statistically significant if $p < 0.05$. # $P < 0.05$, ## $P < 0.01$, ### $P < 0.001$, n.s., not significant. For other experiments except for scRNA-seq analysis, data were analyzed by a two-tailed Student's t -test. Differences were considered statistically significant if $p < 0.05$. * $p < 0.05$, ** $p < 0.01$, *** $p < 0.001$, n.s., not significant.

Data availability

The scRNA-seq data generated in this study are deposited in GEO (GSE168224, <https://www.ncbi.nlm.nih.gov/geo/query/acc.cgi?acc=GSE168224>). The code used in the study can be accessed at GitHub (https://github.com/JYCathyXie/MK_infection).

Acknowledgments

We thank the National Key Research and Development Program of China (2018YFA0107200), the National Natural Science Foundation of China (82170112, 81900101), The Key Research and Development Program of Guangdong Province (2019B020234002), China Postdoctoral Science Foundation (2021M693614), Guangdong Innovative and Entrepreneurial Research Team Program (2016ZT06S029,

2019ZT08Y485), Sanming Project of Medicine in Shenzhen (No.SZSM201911004) for generous support.

Competing interests

The authors declare no competing interests.

References

- Almanzar, N., Antony, J., Baghel, A. S., Bakerman, I., Bansal, I., Barres, B. A., Beachy, P. A., Berdnik, D., Bilen, B., Brownfield, D., Cain, C., Chan, C. K. F., Chen, M. B., Clarke, M. F., Conley, S. D., Darmanis, S., Demers, A., Demir, K., de Morree, A., Divita, T., du Bois, H., Ebadi, H., Espinoza, F. H., Fish, M., Gan, Q., George, B. M., Gillich, A., Gómez-Sjöberg, R., Green, F., Genetiano, G., Gu, X., Gulati, G. S., Hahn, O., Haney, M. S., Hang, Y., Harris, L., He, M., Hosseinzadeh, S., Huang, A., Huang, K. C., Iram, T., Isobe, T., Ives, F., Jones, Robert C., Kao, K. S., Karkanias, J., Karnam, G., Keller, A., Kershner, A. M., Khoury, N., Kim, S. K., Kiss, B. M., Kong, W., Krasnow, M. A., Kumar, M. E., Kuo, C. S., Lam, J., Lee, D. P., Lee, S. E., Lehallier, B., Leventhal, O., Li, G., Li, Q., Liu, L., Lo, A., Lu, W.-J., Lugo-Fagundo, M. F., Manjunath, A., May, A. P., Maynard, A., McGeever, A., McKay, M., Mc Nerney, M. W., Merrill, B., Metzger, R. J., Mignardi, M., Min, D., Nabhan, A. N., Neff, N. F., Ng, K. M., Nguyen, P. K., Noh, J., Nusse, R., Pálovics, R., Patkar, R., Peng, W. C., Penland, L., Pisco, A. O., Pollard, K., Puccinelli, R., Qi, Z., Quake, S. R., Rando, T. A., Rulifson, E. J., Schaum, N., Segal, J. M., Sikandar, S. S., Sinha, R., Sit, R. V., Sonnenburg, J., Staehli, D., Szade, K., Tan, M., Tan, W., Tato, C., Tellez, K., Dulgeroff, L. B. T., Travaglini, K. J., Tropini, C., Tsui, M., Waldburger, L., Wang, B. M., van Weele, L. J., Weinberg, K., Weissman, I. L., Wosczyzna, M. N., Wu, S. M., Wyss-Coray, T., Xiang, J., Xue, S., Yamauchi, K. A., Yang, A. C., Yerra, L. P., Youngunpipatkul, J., Yu, B., Zanini, F., Zardeneta, M. E., Zee, A., Zhao, C., Zhang, F., Zhang, H., Zhang, M. J., Zhou, L., Zou, J., & The Tabula Muris, C. (2020). A single-cell transcriptomic atlas characterizes ageing tissues in the mouse. *Nature*, 583(7817), 590-595. <https://doi.org/10.1038/s41586-020-2496-1>
- Avecilla, S. T., Hattori, K., Heissig, B., Tejada, R., Liao, F., Shido, K., Jin, D. K., Dias, S., Zhang, F., Hartman, T. E., Hackett, N. R., Crystal, R. G., Witte, L., Hicklin, D. J., Bohlen, P., Eaton, D., Lyden, D., de Sauvage, F., & Rafii, S. (2004). Chemokine-mediated interaction of hematopoietic progenitors with the bone marrow vascular niche is required for thrombopoiesis. *Nat Med*, 10(1), 64-71. <https://doi.org/10.1038/nm973>
- Beaulieu, L. M., Lin, E., Morin, K. M., Tanriverdi, K., & Freedman, J. E. (2011). Regulatory effects of TLR2 on megakaryocytic cell function. *Blood*, 117(22), 5963-5974.

<https://doi.org/10.1182/blood-2010-09-304949>

Bernardes, J. P., Mishra, N., Tran, F., Bahmer, T., Best, L., Blase, J. I., Bordoni, D., Franzenburg, J., Geisen, U., Josephs-Spaulding, J., Köhler, P., Künstner, A., Rosati, E., Aschenbrenner, A. C., Bacher, P., Baran, N., Boysen, T., Brandt, B., Bruse, N., Dörr, J., Dräger, A., Elke, G., Ellinghaus, D., Fischer, J., Forster, M., Franke, A., Franzenburg, S., Frey, N., Friedrichs, A., Fuß, J., Glück, A., Hamm, J., Hinrichsen, F., Hoepfner, M. P., Imm, S., Junker, R., Kaiser, S., Kan, Y. H., Knoll, R., Lange, C., Laue, G., Lier, C., Lindner, M., Marinos, G., Markewitz, R., Nattermann, J., Noth, R., Pickkers, P., Rabe, K. F., Renz, A., Röcken, C., Rupp, J., Schaffarzyk, A., Scheffold, A., Schulte-Schrepping, J., Schunk, D., Skowasch, D., Ulas, T., Wandinger, K.-P., Wittig, M., Zimmermann, J., Busch, H., Hoyer, B. F., Kaleta, C., Heyckendorf, J., Kox, M., Rybníček, J., Schreiber, S., Schultze, J. L., Rosenstiel, P., Banovich, N. E., Desai, T., Eickelberg, O., Haniffa, M., Horvath, P., Kropinski, J. A., Lafyatis, R., Lundeberg, J., Meyer, K., Nawijn, M. C., Nikolic, M., Ordovas Montanes, J., Pe'er, D., Tata, P. R., Rawlins, E., Regev, A., Reyfman, P., Samakovlis, C., Schultze, J., Shalek, A., Shepherd, D., Spence, J., Teichmann, S., Theis, F., Tsankov, A., van den Berge, M., von Papen, M., Whitsett, J., Zaragosi, L. E., Angelov, A., Bals, R., Bartholomäus, A., Becker, A., Bezdan, D., Bonifacio, E., Bork, P., Clavel, T., Colme-Tatche, M., Diefenbach, A., Dillthey, A., Fischer, N., Förstner, K., Frick, J.-S., Gagneur, J., Goesmann, A., Hain, T., Hummel, M., Janssen, S., Kalinowski, J., Kallies, R., Kehr, B., Keller, A., Kim-Hellmuth, S., Klein, C., Kohlbacher, O., Korbel, J. O., Kurth, I., Landthaler, M., Li, Y., Ludwig, K., Makarewicz, O., Marz, M., McHardy, A., Mertes, C., Nöthen, M., Nürnberg, P., Ohler, U., Ossowski, S., Overmann, J., Peter, S., Pfeffer, K., Poetsch, A. R., Pühler, A., Rajewsky, N., Ralser, M., Rieß, O., Ripke, S., Nunes da Rocha, U., Rosenstiel, P., Saliba, A.-E., Sander, L. E., Sawitzki, B., Schiffer, P., Schulte, E.-C., Schultze, J. L., Sczyrba, A., Stegle, O., Stoye, J., Theis, F., Vehreschild, J., Vogel, J., von Kleist, M., Walker, A., Walter, J., Wieczorek, D., & Ziebuhr, J. (2020). Longitudinal Multi-omics Analyses Identify Responses of Megakaryocytes, Erythroid Cells, and Plasmablasts as Hallmarks of Severe COVID-19. *Immunity*, 53(6), 1296-1314.e1299. <https://doi.org/10.1016/j.immuni.2020.11.017>

Bishop, D. K., & Hinrichs, D. J. (1987). Adoptive transfer of immunity to *Listeria monocytogenes*. The influence of in vitro stimulation on lymphocyte subset requirements. *J Immunol*, 139(6), 2005-2009. <https://www.ncbi.nlm.nih.gov/pubmed/3114382>

Boilard, E., & Machlus, K. R. (2021). Location is everything when it comes to megakaryocyte function. *J Clin Invest*, 131(1). <https://doi.org/10.1172/JCI144964>

Bruns, I., Lucas, D., Pinho, S., Ahmed, J., Lambert, M. P., Kunisaki, Y., Scheiermann, C., Schiff, L., Poncz, M., Bergman, A., & Frenette, P. S. (2014). Megakaryocytes regulate hematopoietic stem cell quiescence through CXCL4 secretion [Letter]. *Nat Med*, 20(11), 1315-1320. <https://doi.org/10.1038/nm.3707>

Butler, A., Hoffman, P., Smibert, P., Papalexi, E., & Satija, R. (2018). Integrating single-cell transcriptomic data across different conditions, technologies, and species. *Nature Biotechnology*, 36(5), 411-420. <https://doi.org/10.1038/nbt.4096>

Campbell, R. A., Schwartz, H., Hottz, E. D., Rowley, J. W., Manne, B. K., Washington, A. V., Hunter-Mellado, R., Tolley, N. D., Christensen, M., Eustes, A. S., Montenont, E., Bhatlekar, S.,

Ventrone, C. H., Kirkpatrick, B. D., Pierce, K. K., Whitehead, S. S., Diehl, S. A., Bray, P. F., Zimmerman, G. A., Kosaka, Y., Bozza, P. T., Bozza, F. A., Weyrich, A. S., & Rondina, M. T. (2019). Human megakaryocytes possess intrinsic antiviral immunity through regulated induction of IFITM3. *Blood*, 133(19), 2013-2026. <https://doi.org/10.1182/blood-2018-09-873984>

Chang, Y., Bluteau, D., Debili, N., & Vainchenker, W. (2007). From hematopoietic stem cells to platelets. *J Thromb Haemost*, 5 Suppl 1, 318-327. <https://doi.org/10.1111/j.1538-7836.2007.02472.x>

Couldwell, G., & Machlus, K. R. (2019). Modulation of megakaryopoiesis and platelet production during inflammation. *Thromb Res*, 179, 114-120. <https://doi.org/10.1016/j.thromres.2019.05.008>

Crow, M., Paul, A., Ballouz, S., Huang, Z. J., & Gillis, J. (2018). Characterizing the replicability of cell types defined by single cell RNA-sequencing data using MetaNeighbor. *Nat Commun*, 9(1), 884. <https://doi.org/10.1038/s41467-018-03282-0>

Cunin, P., & Nigrovic, P. A. (2019). Megakaryocytes as immune cells. *Journal of Leukocyte Biology*, 105(6), 1111-1121. <https://doi.org/10.1002/Jlb.Mr0718-261rr>

Cunin, P., Penke, L. R., Thon, J. N., Monach, P. A., Jones, T., Chang, M. H., Chen, M. M., Melki, I., Lacroix, S., Iwakura, Y., Ware, J., Gurish, M. F., Italiano, J. E., Boilard, E., & Nigrovic, P. A. (2017). Megakaryocytes compensate for Kit insufficiency in murine arthritis. *J Clin Invest*, 127(5), 1714-1724. <https://doi.org/10.1172/JCI84598>

Davidson, S., Efremova, M., Riedel, A., Mahata, B., Pramanik, J., Huuhtanen, J., Kar, G., Vento-Tormo, R., Hagai, T., Chen, X., Haniffa, M. A., Shields, J. D., & Teichmann, S. A. (2020). Single-Cell RNA Sequencing Reveals a Dynamic Stromal Niche That Supports Tumor Growth. *Cell Rep*, 31(7), 107628. <https://doi.org/10.1016/j.celrep.2020.107628>

Davis, R. E., Stenberg, P. E., Levin, J., & Beckstead, J. H. (1997). Localization of megakaryocytes in normal mice and following administration of platelet antiserum, 5-fluorouracil, or radiostrontium: evidence for the site of platelet production. *Exp Hematol*, 25(7), 638-648. <https://www.ncbi.nlm.nih.gov/pubmed/9216740>

Deutsch, V. R., & Tomer, A. (2006). Megakaryocyte development and platelet production. *Br J Haematol*, 134(5), 453-466. <https://doi.org/10.1111/j.1365-2141.2006.06215.x>

Deutsch, V. R., & Tomer, A. (2013). Advances in megakaryocytopoiesis and thrombopoiesis: from bench to bedside. *Br J Haematol*, 161(6), 778-793. <https://doi.org/10.1111/bjh.12328>

Dominici, M., Rasini, V., Bussolari, R., Chen, X., Hofmann, T. J., Spano, C., Bernabei, D., Veronesi, E., Bertoni, F., Paolucci, P., Conte, P., & Horwitz, E. M. (2009). Restoration and reversible expansion of the osteoblastic hematopoietic stem cell niche after marrow radioablation. *Blood*, 114(11), 2333-2343. <https://doi.org/10.1182/blood-2008-10-183459>

Dong, F., Hao, S., Zhang, S., Zhu, C., Cheng, H., Yang, Z., Hamey, F. K., Wang, X., Gao, A., Wang, F., Gao, Y., Dong, J., Wang, C., Wang, J., Lan, Y., Liu, B., Ema, H., Tang, F., Gottgens, B., Zhu, P., & Cheng, T. (2020). Differentiation of transplanted haematopoietic stem cells tracked by single-cell transcriptomic analysis. *Nat Cell Biol*, 22(6), 630-639. <https://doi.org/10.1038/s41556-020-0512-1>

Eash, K. J., Means, J. M., White, D. W., & Link, D. C. (2009). CXCR4 is a key regulator of neutrophil release from the bone marrow under basal and stress granulopoiesis conditions. *Blood*, 113(19), 4711-4719. <https://doi.org/10.1182/blood-2008-09-177287>

- Edelson, B. T., & Unanue, E. R. (2000). Immunity to *Listeria* infection. *Curr Opin Immunol*, 12(4), 425-431. [https://doi.org/10.1016/s0952-7915\(00\)00112-6](https://doi.org/10.1016/s0952-7915(00)00112-6)
- Efremova, M., Vento-Tormo, M., Teichmann, S. A., & Vento-Tormo, R. (2020). CellPhoneDB: inferring cell-cell communication from combined expression of multi-subunit ligand-receptor complexes. *Nature Protocols*, 15(4), 1484-1506. <https://doi.org/10.1038/s41596-020-0292-x>
- Feng, S., Liu, Y., Liang, W., El-Sayed Ahmed, M. A. E., Zhao, Z., Shen, C., Roberts, A. P., Liang, L., Liao, L., Zhong, Z., Guo, Z., Yang, Y., Wen, X., Chen, H., & Tian, G. B. (2020). Involvement of Transcription Elongation Factor GreA in *Mycobacterium* Viability, Antibiotic Susceptibility, and Intracellular Fitness. *Front Microbiol*, 11, 413. <https://doi.org/10.3389/fmicb.2020.00413>
- Finkielsztejn, A., Schlinker, A. C., Zhang, L., Miller, W. M., & Datta, S. K. (2015). Human megakaryocyte progenitors derived from hematopoietic stem cells of normal individuals are MHC class II-expressing professional APC that enhance Th17 and Th1/Th17 responses. *Immunology Letters*, 163(1), 84-95. <https://doi.org/https://doi.org/10.1016/j.imlet.2014.11.013>
- Fuentes, R., Wang, Y. H., Hirsch, J., Wang, C., Rauova, L., Worthen, G. S., Kowalska, M. A., & Poncz, M. (2010). Infusion of mature megakaryocytes into mice yields functional platelets. *Journal of Clinical Investigation*, 120(11), 3917-3922. <https://doi.org/10.1172/Jci43326>
- Göthert, J. R., Gustin, S. E., Hall, M. A., Green, A. R., Göttgens, B., Izon, D. J., & Begley, C. G. (2005). In vivo fate-tracing studies using the Scl stem cell enhancer: embryonic hematopoietic stem cells significantly contribute to adult hematopoiesis. *Blood*, 105(7), 2724-2732. <https://doi.org/10.1182/blood-2004-08-3037>
- Haas, S., Hansson, J., Klimmeck, D., Loeffler, D., Velten, L., Uckelmann, H., Wurzer, S., Prendergast, A. M., Schnell, A., Hexel, K., Santarella-Mellwig, R., Blaszkiewicz, S., Kuck, A., Geiger, H., Milsom, M. D., Steinmetz, L. M., Schroeder, T., Trumpp, A., Krijgsveld, J., & Essers, M. A. (2015). Inflammation-Induced Emergency Megakaryopoiesis Driven by Hematopoietic Stem Cell-like Megakaryocyte Progenitors. *Cell Stem Cell*, 17(4), 422-434. <https://doi.org/10.1016/j.stem.2015.07.007>
- Hamada, T., Mohle, R., Hesselgesser, J., Hoxie, J., Nachman, R. L., Moore, M. A., & Rafii, S. (1998). Transendothelial migration of megakaryocytes in response to stromal cell-derived factor 1 (SDF-1) enhances platelet formation. *J Exp Med*, 188(3), 539-548. <https://doi.org/10.1084/jem.188.3.539>
- Hamey, F. K., Lau, W. W. Y., Kucinski, I., Wang, X., Diamanti, E., Wilson, N. K., Gottgens, B., & Dahlin, J. S. (2021). Single-cell molecular profiling provides a high-resolution map of basophil and mast cell development. *Allergy*, 76(6), 1731-1742. <https://doi.org/10.1111/all.14633>
- Hanzelmann, S., Castelo, R., & Guinney, J. (2013). GSVA: gene set variation analysis for microarray and RNA-seq data. *Bmc Bioinformatics*, 14, 7. <https://doi.org/10.1186/1471-2105-14-7>
- Hérault, A., Binnewies, M., Leong, S., Calero-Nieto, F. J., Zhang, S. Y., Kang, Y.-A., Wang, X., Pietras, E. M., Chu, S. H., Barry-Holson, K., Armstrong, S., Göttgens, B., & Passegué, E. (2017). Myeloid progenitor cluster formation drives emergency and leukaemic myelopoiesis. *Nature*, 544(7648), 53-58. <https://doi.org/10.1038/nature21693>
- Hunter, J. D. (2007). Matplotlib: A 2D graphics environment. *Computing in Science & Engineering*, 9, 90--95. <https://doi.org/10.1109/MCSE.2007.55>

- Itkin, T., Gur-Cohen, S., Spencer, J. A., Schajnovitz, A., Ramasamy, S. K., Kusumbe, A. P., Ledergor, G., Jung, Y., Milo, I., Poulos, M. G., Kalinkovich, A., Ludin, A., Kollet, O., Shakhar, G., Butler, J. M., Rafii, S., Adams, R. H., Scadden, D. T., Lin, C. P., & Lapidot, T. (2016). Distinct bone marrow blood vessels differentially regulate haematopoiesis. *Nature*, 532(7599), 323-328. <https://doi.org/10.1038/nature17624>
- Jiang, L., Han, X., Wang, J., Wang, C., Sun, X., Xie, J., Wu, G., Phan, H., Liu, Z., Yeh, E. T. H., Zhang, C., Zhao, M., & Kang, X. (2018). SHP-1 regulates hematopoietic stem cell quiescence by coordinating TGF-beta signaling. *J Exp Med*, 215(5), 1337-1347. <https://doi.org/10.1084/jem.20171477>
- Jin, S., Guerrero-Juarez, C. F., Zhang, L., Chang, I., Ramos, R., Kuan, C. H., Myung, P., Plikus, M. V., & Nie, Q. (2021). Inference and analysis of cell-cell communication using CellChat. *Nat Commun*, 12(1), 1088. <https://doi.org/10.1038/s41467-021-21246-9>
- Kang, J. B., Nathan, A., Weinand, K., Zhang, F., Millard, N., Rumker, L., Moody, D. B., Korsunsky, I., & Raychaudhuri, S. (2021). Efficient and precise single-cell reference atlas mapping with Symphony. *Nat Commun*, 12(1), 5890. <https://doi.org/10.1038/s41467-021-25957-x>
- Karttunen, J., Sanderson, S., & Shastri, N. (1992). Detection of rare antigen-presenting cells by the lacZ T-cell activation assay suggests an expression cloning strategy for T-cell antigens. *Proc Natl Acad Sci U S A*, 89(13), 6020-6024. <https://doi.org/10.1073/pnas.89.13.6020>
- Karttunen, J., Sanderson, S., & Shastri, N. (1992). Detection of rare antigen-presenting cells by the lacZ T-cell activation assay suggests an expression cloning strategy for T-cell antigens. *Proceedings of the National Academy of Sciences*, 89(13), 6020-6024. <https://doi.org/doi:10.1073/pnas.89.13.6020>
- Kiselev, V. Y., Yiu, A., & Hemberg, M. (2018). scmap: projection of single-cell RNA-seq data across data sets. *Nat Methods*, 15(5), 359-362. <https://doi.org/10.1038/nmeth.4644>
- Köhler, A., De Filippo, K., Hasenberg, M., van den Brandt, C., Nye, E., Hosking, M. P., Lane, T. E., Männ, L., Ransohoff, R. M., Hauser, A. E., Winter, O., Schraven, B., Geiger, H., Hogg, N., & Gunzer, M. (2011). G-CSF-mediated thrombopoietin release triggers neutrophil motility and mobilization from bone marrow via induction of Cxcr2 ligands. *Blood*, 117(16), 4349-4357. <https://doi.org/10.1182/blood-2010-09-308387>
- Lefrancais, E., Ortiz-Munoz, G., Caudrillier, A., Mallavia, B., Liu, F., Sayah, D. M., Thornton, E. E., Headley, M. B., David, T., Coughlin, S. R., Krummel, M. F., Leavitt, A. D., Passegue, E., & Looney, M. R. (2017). The lung is a site of platelet biogenesis and a reservoir for haematopoietic progenitors. *Nature*, 544(7648), 105-109. <https://doi.org/10.1038/nature21706>
- Li, B., Jones, L. L., & Geiger, T. L. (2018). IL-6 Promotes T Cell Proliferation and Expansion under Inflammatory Conditions in Association with Low-Level ROR γ t Expression. *Journal of immunology (Baltimore, Md. : 1950)*, 201(10), 2934-2946. <https://doi.org/10.4049/jimmunol.1800016>
- Liu, C., Wu, D., Xia, M., Li, M., Sun, Z., Shen, B., Liu, Y., Jiang, E., Wang, H., Su, P., Shi, L., Xiao, Z., Zhu, X., Zhou, W., Wang, Q., Gao, X., Cheng, T., & Zhou, J. (2021). Characterization of Cellular Heterogeneity and an Immune Subpopulation of Human Megakaryocytes. *Adv Sci (Weinh)*,

e2100921. <https://doi.org/10.1002/advs.202100921>

Machlus, K. R., & Italiano, J. E., Jr. (2013). The incredible journey: From megakaryocyte development to platelet formation. *J Cell Biol*, 201(6), 785-796. <https://doi.org/10.1083/jcb.201304054>

Markovic, B., Wu, Z., Chesterman, C. N., & Chong, B. H. (1995). Quantitation of soluble and membrane-bound Fc gamma RIIA (CD32A) mRNA in platelets and megakaryoblastic cell line (Meg-01). *Br J Haematol*, 91(1), 37-42. <https://doi.org/10.1111/j.1365-2141.1995.tb05241.x>

Minutti, C. M., Modak, R. V., Macdonald, F., Li, F. Q., Smyth, D. J., Dorward, D. A., Blair, N., Husovsky, C., Muir, A., Giampazolias, E., Dobie, R., Maizels, R. M., Kendall, T. J., Griggs, D. W., Kopf, M., Henderson, N. C., & Zaiss, D. M. (2019). A Macrophage-Pericyte Axis Directs Tissue Restoration via Amphiregulin-Induced Transforming Growth Factor Beta Activation. *Immunity*, 50(3), 645-+. <https://doi.org/10.1016/j.immuni.2019.01.008>

Nagata, Y., Muro, Y., & Todokoro, K. (1997). Thrombopoietin-induced polyploidization of bone marrow megakaryocytes is due to a unique regulatory mechanism in late mitosis. *J Cell Biol*, 139(2), 449-457. <https://doi.org/10.1083/jcb.139.2.449>

Navarro, S., Debili, N., Le Couedic, J. P., Klein, B., Breton-Gorius, J., Doly, J., & Vainchenker, W. (1991). Interleukin-6 and its receptor are expressed by human megakaryocytes: in vitro effects on proliferation and endoreplication. *Blood*, 77(3), 461-471. <https://www.ncbi.nlm.nih.gov/pubmed/1991163>

Negrotto, S., C, J. D. G., Lapponi, M. J., Etulain, J., Rivadeneyra, L., Pozner, R. G., Gomez, R. M., & Schattner, M. (2011). Expression and functionality of type I interferon receptor in the megakaryocytic lineage. *J Thromb Haemost*, 9(12), 2477-2485. <https://doi.org/10.1111/j.1538-7836.2011.04530.x>

Nishimura, S., Nagasaki, M., Kunishima, S., Sawaguchi, A., Sakata, A., Sakaguchi, H., Ohmori, T., Manabe, I., Italiano, J. E., Jr., Ryu, T., Takayama, N., Komuro, I., Kadowaki, T., Eto, K., & Nagai, R. (2015). IL-1 α induces thrombopoiesis through megakaryocyte rupture in response to acute platelet needs. *Journal of Cell Biology*, 209(3), 453-466. <https://doi.org/10.1083/jcb.201410052>

Olson, T. S., Caselli, A., Otsuru, S., Hofmann, T. J., Williams, R., Paolucci, P., Dominici, M., & Horwitz, E. M. (2013). Megakaryocytes promote murine osteoblastic HSC niche expansion and stem cell engraftment after radioablative conditioning. *Blood*. <https://doi.org/blood-2012-10-463414> [pii] 10.1182/blood-2012-10-463414

Pal, K., Nowak, R., Billington, N., Liu, R., Ghosh, A., Sellers, J. R., & Fowler, V. M. (2020). Megakaryocyte migration defects due to nonmuscle myosin IIA mutations underlie thrombocytopenia in MYH9-related disease. *Blood*, 135(21), 1887-1898. <https://doi.org/10.1182/blood.2019003064>

Pariser, D. N., Hilt, Z. T., Ture, S. K., Blick-Nitko, S. K., Looney, M. R., Cleary, S. J., Roman-Pagan, E., Saunders, J., 2nd, Georas, S. N., Veazey, J., Madere, F., Santos, L. T., Arne, A., Huynh, N. P., Livada, A. C., Guerrero-Martin, S. M., Lyons, C., Metcalf-Pate, K. A., McGrath, K. E., Palis, J., & Morrell, C. N. (2021). Lung megakaryocytes are immune modulatory cells. *J Clin Invest*, 131(1). <https://doi.org/10.1172/JCI137377>

- Patel, S. R., Hartwig, J. H., & Italiano, J. E., Jr. (2005). The biogenesis of platelets from megakaryocyte proplatelets. *J Clin Invest*, 115(12), 3348-3354. <https://doi.org/10.1172/JCI26891>
- Ren, X., Wen, W., Fan, X., Hou, W., Su, B., Cai, P., Li, J., Liu, Y., Tang, F., Zhang, F., Yang, Y., He, J., Ma, W., He, J., Wang, P., Cao, Q., Chen, F., Chen, Y., Cheng, X., Deng, G., Deng, X., Ding, W., Feng, Y., Gan, R., Guo, C., Guo, W., He, S., Jiang, C., Liang, J., Li, Y. M., Lin, J., Ling, Y., Liu, H., Liu, J., Liu, N., Liu, S. Q., Luo, M., Ma, Q., Song, Q., Sun, W., Wang, G., Wang, F., Wang, Y., Wen, X., Wu, Q., Xu, G., Xie, X., Xiong, X., Xing, X., Xu, H., Yin, C., Yu, D., Yu, K., Yuan, J., Zhang, B., Zhang, P., Zhang, T., Zhao, J., Zhao, P., Zhou, J., Zhou, W., Zhong, S., Zhong, X., Zhang, S., Zhu, L., Zhu, P., Zou, B., Zou, J., Zuo, Z., Bai, F., Huang, X., Zhou, P., Jiang, Q., Huang, Z., Bei, J. X., Wei, L., Bian, X. W., Liu, X., Cheng, T., Li, X., Zhao, P., Wang, F. S., Wang, H., Su, B., Zhang, Z., Qu, K., Wang, X., Chen, J., Jin, R., & Zhang, Z. (2021). COVID-19 immune features revealed by a large-scale single-cell transcriptome atlas. *Cell*, 184(7), 1895-1913 e1819. <https://doi.org/10.1016/j.cell.2021.01.053>
- Roney, K. (2019). Bone Marrow-Derived Dendritic Cells. In I. C. Allen (Ed.), *Mouse Models of Innate Immunity: Methods and Protocols* (pp. 57-62). Springer New York. https://doi.org/10.1007/978-1-4939-9167-9_4
- Rothe, G., Kellermann, W., Briegel, J., Schaerer, B., & Valet, G. (1993). Activation of Neutrophils by Tumor Necrosis Factor- α During Sepsis. In E. Faist, J. L. Meakins, & F. W. Schildberg (Eds.), *Host Defense Dysfunction in Trauma, Shock and Sepsis: Mechanisms and Therapeutic Approaches* (pp. 727-735). Springer Berlin Heidelberg. https://doi.org/10.1007/978-3-642-77405-8_94
- Sacma, M., Pospiech, J., Bogeska, R., de Back, W., Mallm, J. P., Sakk, V., Soller, K., Marka, G., Vollmer, A., Karns, R., Cabezas-Wallscheid, N., Trumpp, A., Mendez-Ferrer, S., Milsom, M. D., Mulaw, M. A., Geiger, H., & Florian, M. C. (2019). Haematopoietic stem cells in perisinusoidal niches are protected from ageing. *Nat Cell Biol*, 21(11), 1309-1320. <https://doi.org/10.1038/s41556-019-0418-y>
- Semple, J. W., Italiano, J. E., Jr., & Freedman, J. (2011). Platelets and the immune continuum. *Nat Rev Immunol*, 11(4), 264-274. <https://doi.org/10.1038/nri2956>
- Shapouri-Moghaddam, A., Mohammadian, S., Vazini, H., Taghadosi, M., Esmacili, S. A., Mardani, F., Seifi, B., Mohammadi, A., Afshari, J. T., & Sahebkar, A. (2018). Macrophage plasticity, polarization, and function in health and disease. *J Cell Physiol*, 233(9), 6425-6440. <https://doi.org/10.1002/jcp.26429>
- Sharif, O., Gawish, R., Warszawska, J. M., Martins, R., Lakovits, K., Hladik, A., Doninger, B., Brunner, J., Korosec, A., Schwarzenbacher, R. E., Berg, T., Kralovics, R., Colinge, J., Mesteri, I., Gilfillan, S., Salmaggi, A., Verschoor, A., Colonna, M., & Knapp, S. (2014). The triggering receptor expressed on myeloid cells 2 inhibits complement component 1q effector mechanisms and exerts detrimental effects during pneumococcal pneumonia. *PLoS Pathog*, 10(6), e1004167. <https://doi.org/10.1371/journal.ppat.1004167>
- Stephenson, E., Reynolds, G., Botting, R. A., Calero-Nieto, F. J., Morgan, M. D., Tuong, Z. K., Bach, K., Sungnak, W., Worlock, K. B., Yoshida, M., Kumasaka, N., Kania, K., Engelbert, J., Olabi, B., Spegarova, J. S., Wilson, N. K., Mende, N., Jardine, L., Gardner, L. C. S., Goh, I., Horsfall, D.,

McGrath, J., Webb, S., Mather, M. W., Lindeboom, R. G. H., Dann, E., Huang, N., Polanski, K., Prigmore, E., Gothe, F., Scott, J., Payne, R. P., Baker, K. F., Hanrath, A. T., Schim van der Loeff, I. C. D., Barr, A. S., Sanchez-Gonzalez, A., Bergamaschi, L., Mescia, F., Barnes, J. L., Kilich, E., de Wilton, A., Saigal, A., Saleh, A., Janes, S. M., Smith, C. M., Gopee, N., Wilson, C., Coupland, P., Coxhead, J. M., Kiselev, V. Y., van Dongen, S., Bacardit, J., King, H. W., Cambridge Institute of Therapeutic, I., Infectious Disease-National Institute of Health Research, C.-B. C., Rostron, A. J., Simpson, A. J., Hambleton, S., Laurenti, E., Lyons, P. A., Meyer, K. B., Nikolic, M. Z., Duncan, C. J. A., Smith, K. G. C., Teichmann, S. A., Clatworthy, M. R., Marioni, J. C., Gottgens, B., & Haniffa, M. (2021). Single-cell multi-omics analysis of the immune response in COVID-19. *Nat Med*, 27(5), 904-916. <https://doi.org/10.1038/s41591-021-01329-2>

Subramanian, A., Tamayo, P., Mootha, V. K., Mukherjee, S., Ebert, B. L., Gillette, M. A., Paulovich, A., Pomeroy, S. L., Golub, T. R., Lander, E. S., & Mesirov, J. P. (2005). Gene set enrichment analysis: a knowledge-based approach for interpreting genome-wide expression profiles. *Proc Natl Acad Sci U S A*, 102(43), 15545-15550. <https://doi.org/10.1073/pnas.0506580102>

Sugiyama, T., Kohara, H., Noda, M., & Nagasawa, T. (2006). Maintenance of the hematopoietic stem cell pool by CXCL12-CXCR4 chemokine signaling in bone marrow stromal cell niches [Research Support, Non-U.S. Gov't]. *Immunity*, 25(6), 977-988. <https://doi.org/10.1016/j.immuni.2006.10.016>

Sun, S., Jin, C., Si, J., Lei, Y., Chen, K., Cui, Y., Liu, Z., Liu, J., Zhao, M., Zhang, X., Tang, F., Rondina, M. T., Li, Y., & Wang, Q. F. (2021). Single-Cell Analysis of Ploidy and Transcriptome Reveals Functional and Spatial Divergency in Murine Megakaryopoiesis. *Blood*. <https://doi.org/10.1182/blood.2021010697>

Suraneni, P. K., Corey, S. J., Hession, M. J., Ishaq, R., Awomolo, A., Hasan, S., Shah, C., Liu, H., Wickrema, A., Debili, N., Crispino, J. D., Eklund, E. A., & Chen, Y. (2018). Dynamins 2 and 3 control the migration of human megakaryocytes by regulating CXCR4 surface expression and ITGB1 activity. *Blood Adv*, 2(23), 3540-3552. <https://doi.org/10.1182/bloodadvances.2018021923>

Tamura, S., Suzuki-Inoue, K., Tsukiji, N., Shirai, T., Sasaki, T., Osada, M., Satoh, K., & Ozaki, Y. (2016). Podoplanin-positive periaarteriolar stromal cells promote megakaryocyte growth and proplatelet formation in mice by CLEC-2. *Blood*, 127(13), 1701-1710. <https://doi.org/10.1182/blood-2015-08-663708>

Tiedt, R., Schomber, T., Hao-Shen, H., & Skoda, R. C. (2007). Pf4-Cre transgenic mice allow the generation of lineage-restricted gene knockouts for studying megakaryocyte and platelet function in vivo. *Blood*, 109(4), 1503-1506. <https://doi.org/10.1182/blood-2006-04-020362>

Verschoor, A., Neuenhahn, M., Navarini, A. A., Graef, P., Plaumann, A., Seidlmeier, A., Nieswandt, B., Massberg, S., Zinkernagel, R. M., Hengartner, H., & Busch, D. H. (2011). A platelet-mediated system for shuttling blood-borne bacteria to CD8 alpha(+) dendritic cells depends on glycoprotein GPIb and complement C3. *Nature Immunology*, 12(12), 1194-U1186. <https://doi.org/10.1038/ni.2140>

Wang, H., He, J., Xu, C., Chen, X., Yang, H., Shi, S., Liu, C., Zeng, Y., Wu, D., Bai, Z., Wang, M., Wen, Y., Su, P., Xia, M., Huang, B., Ma, C., Bian, L., Lan, Y., Cheng, T., Shi, L., Liu, B., & Zhou, J. (2021).

Decoding Human Megakaryocyte Development. *Cell Stem Cell*, 28(3), 535-549 e538.
<https://doi.org/10.1016/j.stem.2020.11.006>

Wang, J. F., Liu, Z. Y., & Groopman, J. E. (1998). The alpha-chemokine receptor CXCR4 is expressed on the megakaryocytic lineage from progenitor to platelets and modulates migration and adhesion. *Blood*, 92(3), 756-764. <http://www.ncbi.nlm.nih.gov/pubmed/9680341>

Ward, J. R., Bingle, L., Judge, H. M., Brown, S. B., Storey, R. F., Whyte, M. K., Dower, S. K., Buttle, D. J., & Sabroe, I. (2005). Agonists of toll-like receptor (TLR)2 and TLR4 are unable to modulate platelet activation by adenosine diphosphate and platelet activating factor. *Thromb Haemost*, 94(4), 831-838. <https://www.ncbi.nlm.nih.gov/pubmed/16270639>

Xie, X., Shi, Q., Wu, P., Zhang, X., Kambara, H., Su, J., Yu, H., Park, S. Y., Guo, R., Ren, Q., Zhang, S., Xu, Y., Silberstein, L. E., Cheng, T., Ma, F., Li, C., & Luo, H. R. (2020). Single-cell transcriptome profiling reveals neutrophil heterogeneity in homeostasis and infection. *Nat Immunol*, 21(9), 1119-1133. <https://doi.org/10.1038/s41590-020-0736-z>

Xie, Y., Yin, T., Wiegand, W., He, X. C., Miller, D., Stark, D., Perko, K., Alexander, R., Schwartz, J., Grindley, J. C., Park, J., Haug, J. S., Wunderlich, J. P., Li, H., Zhang, S., Johnson, T., Feldman, R. A., & Li, L. (2009). Detection of functional haematopoietic stem cell niche using real-time imaging. *Nature*, 457(7225), 97-101. <https://doi.org/10.1038/nature07639>

Yamazaki, S., Ema, H., Karlsson, G., Yamaguchi, T., Miyoshi, H., Shioda, S., Taketo, M. M., Karlsson, S., Iwama, A., & Nakauchi, H. (2011). Nonmyelinating Schwann cells maintain hematopoietic stem cell hibernation in the bone marrow niche. *Cell*, 147(5), 1146-1158.
<https://doi.org/10.1016/j.cell.2011.09.053>

Yang, M., Li, K., Chui, C. M., Yuen, P. M., Chan, P. K., Chuen, C. K., Li, C. K., & Fok, T. F. (2000). Expression of interleukin (IL) 1 type I and type II receptors in megakaryocytic cells and enhancing effects of IL-1beta on megakaryocytopoiesis and NF-E2 expression. *Br J Haematol*, 111(1), 371-380. <https://doi.org/10.1046/j.1365-2141.2000.02340.x>

Yeung, A. K., Villacorta-Martin, C., Hon, S., Rock, J. R., & Murphy, G. J. (2020). Lung megakaryocytes display distinct transcriptional and phenotypic properties. *Blood Adv*, 4(24), 6204-6217.
<https://doi.org/10.1182/bloodadvances.2020002843>

Yu, G. (2019). enrichplot: Visualization of Functional Enrichment Result.
<https://github.com/GuangchuangYu/enrichplot>

Yu, G., Wang, L. G., Han, Y., & He, Q. Y. (2012). clusterProfiler: an R package for comparing biological themes among gene clusters. *OMICS*, 16(5), 284-287. <https://doi.org/10.1089/omi.2011.0118>

Zhao, M., Perry, J. M., Marshall, H., Venkatraman, A., Qian, P., He, X. C., Ahamed, J., & Li, L. (2014). Megakaryocytes maintain homeostatic quiescence and promote post-injury regeneration of hematopoietic stem cells. *Nat Med*, 20(11), 1321-1326. <https://doi.org/10.1038/nm.3706>

Zufferey, A., Speck, E. R., Machlus, K. R., Aslam, R., Guo, L., McVey, M. J., Kim, M., Kapur, R., Boilard, E., Italiano, J. E., & Semple, J. W. (2017). Mature murine megakaryocytes present antigen-MHC class I molecules to T cells and transfer them to platelets. *Blood Advances*, 1(20), 1773-1785.
Retrieved 2017/09//, from <https://doi.org/10.1182/bloodadvances.2017007021>

Figures and figure legends

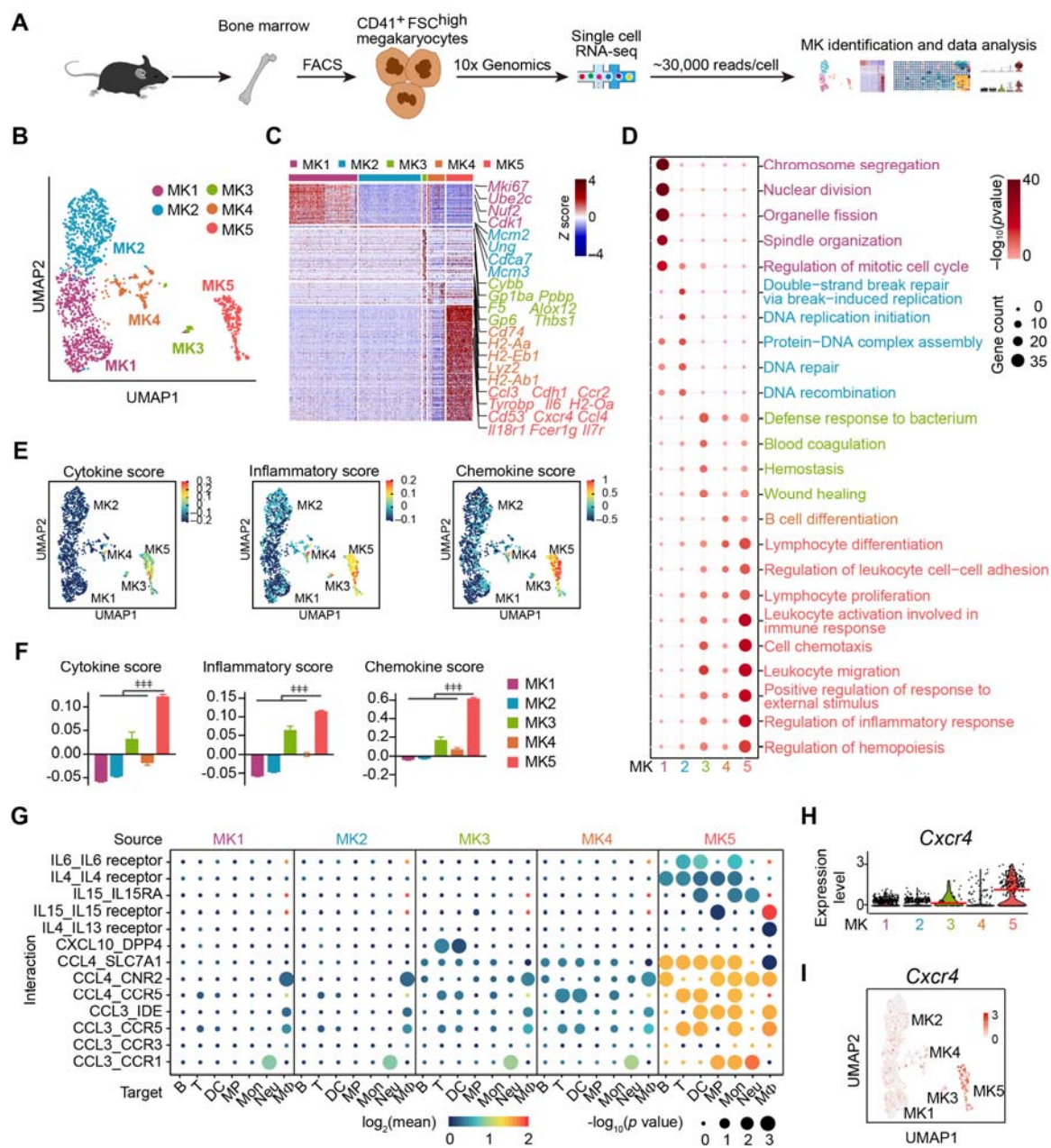


Figure 1. Single-cell atlas identifies an immune-modulatory subpopulation of MKs

(A) Schematic strategy for MK preparation, scRNA-seq and data analysis. (B) Clustering of 1 712 bone marrow MKs. (C) Heatmap of signature gene expression in MK

subpopulations (fold-change > 1.5, p value < 0.05) with exemplar genes listed on the right (top, color-coded by subpopulations). Columns denote cells; rows denote genes. Z score, row-scaled expression of the signature genes in each subpopulation. **(D)** Gene Ontology (GO) analysis of signature genes (fold-change > 1.5, p value < 0.05) for each MK subpopulations. GO terms selected with Benjamini–Hochberg-corrected p values < 0.05 and colored by $-\log_{10}(p \text{ value})$. Bubble size indicates the enriched gene number of each term. **(E-F)** UMAP visualization **(E)** and statistical analysis **(F)** of cytokine score (left), inflammatory score (middle) and chemokine score (right) in MK1 to 5. **(G)** Dotplots of significant cytokine ligand (source) -receptor (target) interactions between MKs and immune cells discovered. The color indicates the means of the receptor-ligand pairs between two cell types and bubble size indicates p values. Mon, monocytes; $M\Phi$, macrophages (Dong et al., 2020); DC, dendritic cells; Neu, neutrophils; MP, myeloid progenitors; T, T cells; B, B cells. **(H-I)** Violin plot **(H)** and feature plot **(I)** of selected signature genes of MK5. Red lines in **(H)** indicate the median gene expression. Repeated-measures one-way ANOVA followed by Dunnett’s test for multiple comparisons in **(F)**, # p < 0.01, ## p < 0.001.

The following figure supplements are available for figure 1:

Figure 1-figure supplement 1. Cell isolation, quality control and annotation of scRNA-seq data.

Figure 1-figure supplement 2. Cell type identification by alignment with published scRNA-seq data.

Figure 1-figure supplement 3. Identification of MK subpopulations.

Figure 1-figure supplement 4. Enriched genes in MK1 to 4 and MK5.

Figure 1-figure supplement 5. MK5 interacts with immune cells and express signature genes of immune MKs.

Figure 1-figure supplement 6. Polyploidy, platelet generation ability and cell size of CXCR4^{low} and CXCR4^{high} MKs.

Figure 1-source data 1. Signature genes of MK1 to MK5.

Figure 1-source data 2. The means and *p* value of the average expression level of interacting molecule 1 in cluster 1 and interacting molecule 2 in cluster 2 by CellPhoneDB.

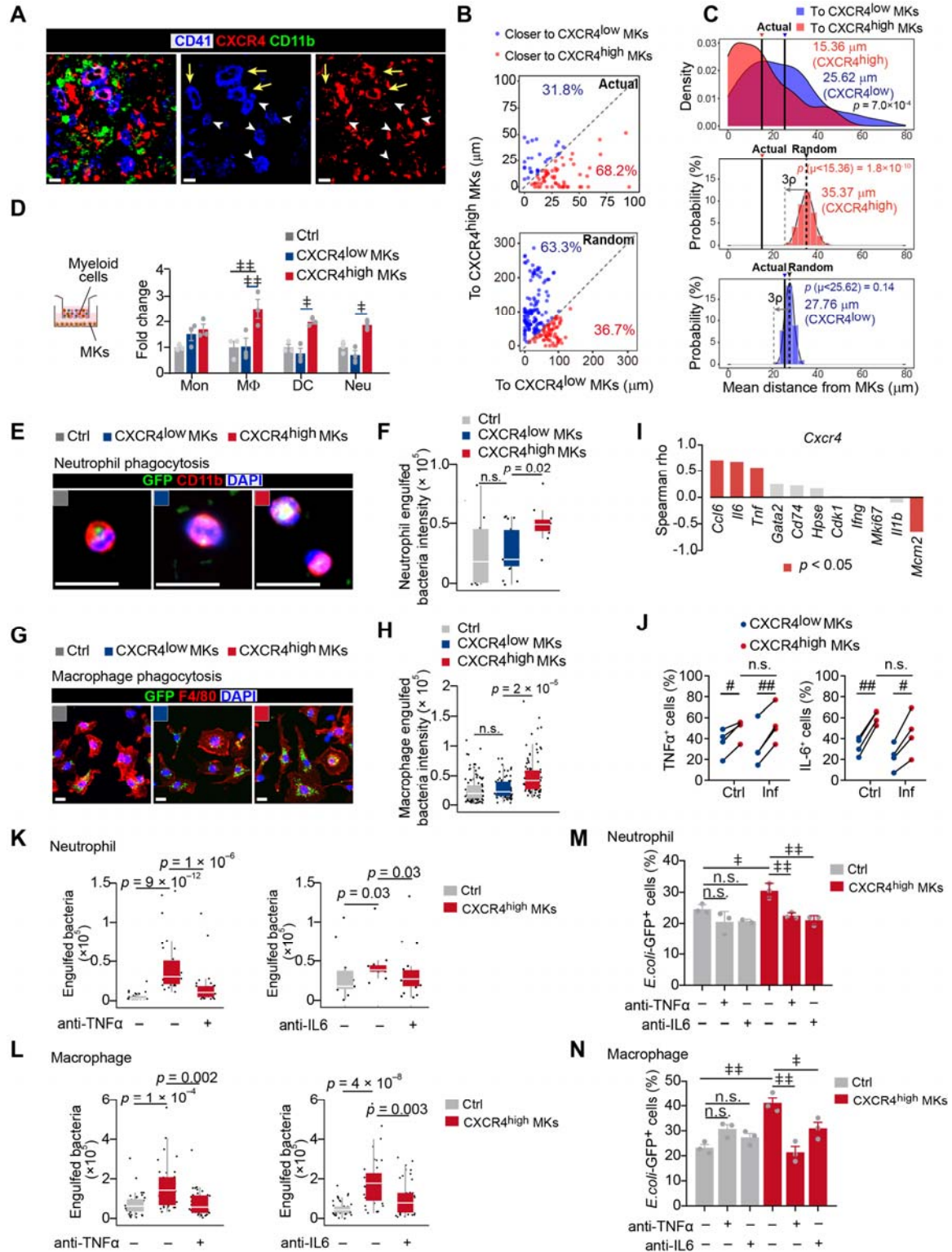


Figure 2. CXCR4^{high} MKs enhance myeloid cell mobility and bacteria phagocytosis

(A) Distribution of myeloid cells to CXCR4^{low} or CXCR4^{high} MKs three days after *L. monocytogenes* infection. Representative images of MKs (blue), CXCR4 (red), and myeloid cells (green) in mouse bone marrow. Yellow arrows indicate CXCR4^{high} MKs and white arrowheads indicate CXCR4^{low} MKs. (B-C) Distance (B) and mean distance (C) of actual or randomly positioned myeloid cells to the closest CXCR4^{low} and CXCR4^{high} MKs three days after *L. monocytogenes* infection. (D) Numbers of transmigrated myeloid cells normalized to Ctrl (without MKs in the lower chambers) as indicated by transwell assays. Mon, monocytes; MΦ, macrophages; DC, dendritic cells; Neu, neutrophils. (E-F) Representative images (E) and quantification (F) of neutrophil phagocytosis capacity with or without MK co-culture as indicated. CD11b, red; *E. coli*, green; DAPI, blue. Ctrl, neutrophil without MK co-culture. (G-H) Representative images (G) and quantification (H) of macrophage phagocytosis capacity with or without MK co-culture as indicated. F4/80, red; *E. coli*, green; DAPI, blue. Ctrl, macrophage without MK co-culture. (I) Spearman correlation analysis between expression profiles of *Cxcr4* and feature genes in MK subpopulations. (J) Quantification of TNFα⁺ and IL-6⁺ cells in CXCR4^{low} MKs and CXCR4^{high} MKs from control mice or mice three days after *L. monocytogenes* infection. (K-L) Quantification of neutrophil (K) and macrophage (L) phagocytosis with or without CXCR4^{high} MK co-culture in the absence or presence of anti-TNFα or anti-IL-6 neutralizing antibodies. (M-N) Quantification of the phagocytosis abilities by neutrophils (M) and macrophages (N) with or without CXCR4^{low} MK or CXCR4^{high} MK co-culture in the absence or presence of anti-TNFα or anti-IL-6 neutralizing antibodies by flow cytometry. Ctrl, neutrophils (M) or macrophages (N) without MKs co-culture. Scale bars, 20 μm (A, E, G). Data represent mean ± s.e.m (D) and boxplots show medians, first and

third quartiles (**F, H, K-L**). Repeated-measures one-way ANOVA followed by Dunnett's test for multiple comparisons in (**D, M, N**), ‡ $p < 0.05$, # $p < 0.01$, n.s., not significant. A two-sample KS test was performed to assess statistically significant (**C, F, H, K, L**), n.s., not significant. Paired Student's t -test was performed to assess statistical significance (**J**), # $p < 0.05$, ## $p < 0.01$, n.s., not significant.

The following figure supplements are available for figure 2:

Figure 2-figure supplement 1. *L. monocytogenes* promote myelopoiesis and the association of myeloid cells and the CXCR4^{high} MK-blood vessel intersection.

Figure 2-figure supplement 2. CXCR4^{high} MKs promote myeloid cell phagocytosis and produce TNF α and IL-6.

Figure 2-source data 1. Distance of actual myeloid cells to the closest CXCR4^{low} and CXCR4^{high} MKs three days after *L. monocytogenes* infection.

Figure 2-source data 2. Distance of randomly positioned myeloid cells to the closest CXCR4^{low} and CXCR4^{high} MKs three days after *L. monocytogenes* infection.

Figure 2-source data 3. Mean distance of randomly positioned myeloid cells to the closest CXCR4^{low} and CXCR4^{high} MKs three days after *L. monocytogenes* infection from 500 times simulations.

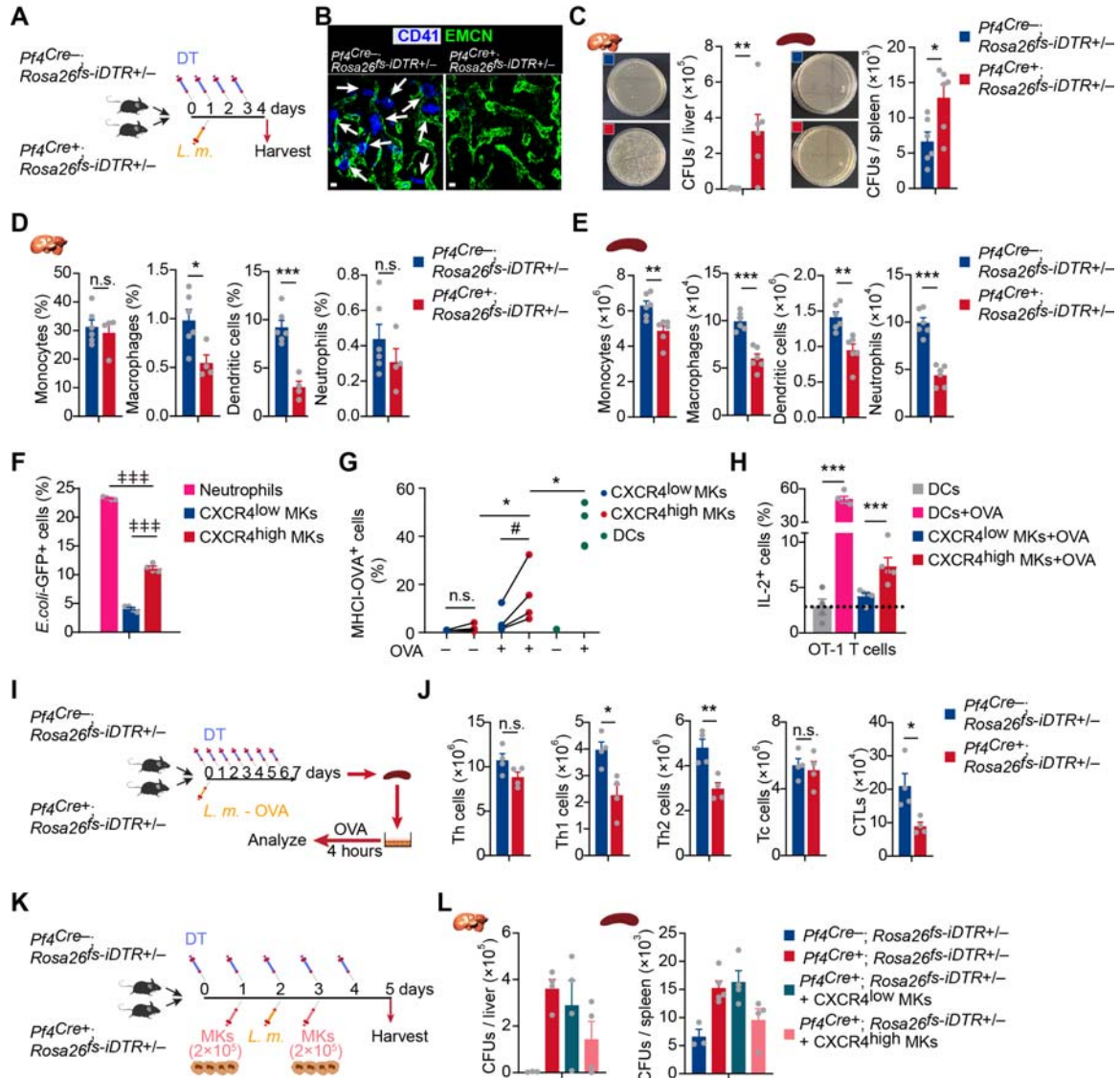


Figure 3. CXCR4^{high} MKs stimulate host-defense immunity against bacterial pathogens

(A) Schema for diphtheria toxin (DT) and *L. monocytogenes* administration used for the experiments shown in (B-E). (B) Representative images of MKs (blue, indicated by arrows) and vascular endothelial cells (green) in the bone marrow of mice after four daily DT treatments. (C) Bacterial burdens in the liver and spleen of *Pf4Cre^{-/-}; Rosa26^{fls-iDTR}* mice three days after *L. monocytogenes* (*L.m.*) infection with four-time DT injections. (D-E)

Myeloid cells in the liver (**D**) and spleen (**E**) of *Pf4^{Cre}; Rosa26^{fs-iDTR}* mice three days after *L. monocytogenes* (*L.m.*) infection with four-time DT injections. (**F**) Quantification of bacterial phagocytosis capacities of neutrophils, CXCR4^{low} MKs and CXCR4^{high} MKs. (**G**) Quantification of MHCI-OVA levels on CXCR4^{low} MKs, CXCR4^{high} MKs and bone marrow-derived dendritic cells (DCs) upon a pulse of 24 hours with or without OVA. (**H**) Quantification of activated OT-I CD8⁺ T cells after co-culture with bone marrow-derived DCs, OVA-pulsed bone marrow-derived DCs, CXCR4^{low} MKs, or CXCR4^{high} MKs. (**I**) Schema for antigen-specific T cell activation assay shown in (**J**). (**J**) Splenocytes from control or MK ablated mice seven days after *L. monocytogenes*-OVA₂₅₇₋₂₆₄ infection and seven DT injections were stimulated with OVA peptide *in vitro* for 4 hours, and antigen-specific activated T cells were quantified (*n* = 4 mice). *L.m.*-OVA, *L. monocytogenes*-OVA₂₅₇₋₂₆₄. (**K**) Schema for DT, *L. monocytogenes* administration, MK transfusing and bacterial burden determination shown in (**L**). (**L**) Bacterial burdens in the liver and spleen of *Pf4^{Cre}; Rosa26^{fs-iDTR}* mice without or with CXCR4^{low} or CXCR4^{high} MK transfused. Data represent mean ± s.e.m. Repeated-measures one-way ANOVA followed by Dunnett's test for multiple comparisons in (**F**), ## *p* < 0.001. Paired Student's *t*-test was performed to assess statistical significance (**G**), # *p* < 0.05, n.s., not significant. Two-tailed Student's *t*-test was performed to assess statistical significance except (**F**), * *p* < 0.05, ** *p* < 0.01, *** *p* < 0.001, n.s., not significant.

The following figure supplements are available for figure 3:

Figure 3-figure supplement 1. MK ablation influenced HSC and myeloid cell numbers.

Figure 3-figure supplement 2. CXCR4^{high} MKs induced B3Z T cell activation.

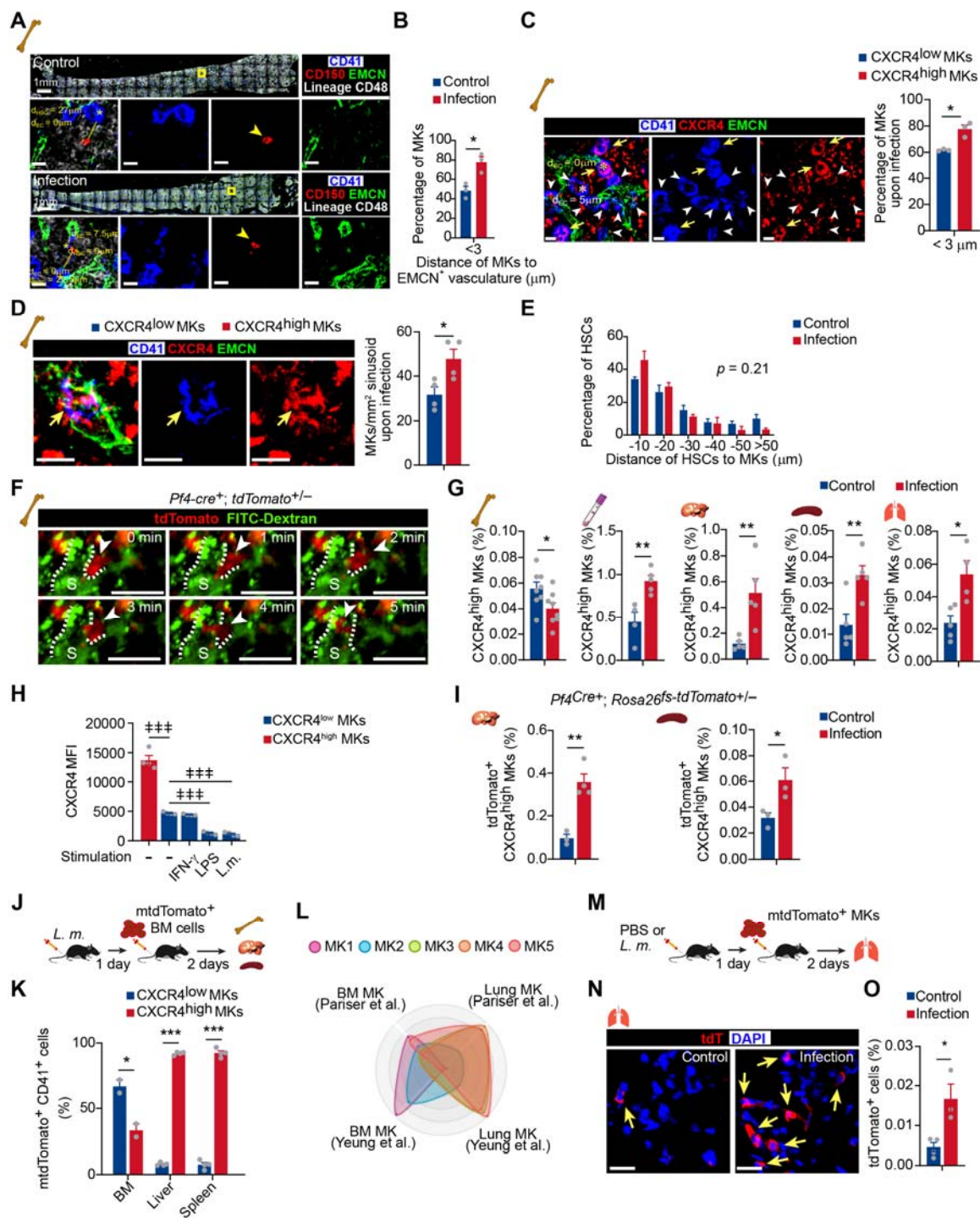


Figure 4. Bacterial infection stimulates the migration of CXCR4^{high} MKs

(A) Representative image of CD41 (blue), CD150 (red), EMCN (green) and lineage cells (white) in bone marrow from control mice or mice at three days after *L. monocytogenes*

infection. D_{HSC} and d_{EC} indicate the distance between the MK (blue, marked with an asterisk) and the closest HSC (red), endothelial cell (green), respectively. Yellow boxes indicate the locations of the magnified images. Arrowheads indicate HSCs. EMCN, endomucin; EC, endothelial cell. **(B)** Comparison of the distance between MKs to Ecs ($n = 119$ control and 103 infected MKs) in the bone marrow of control mice or mice at three days after *L. monocytogenes* infection. **(C)** Comparison of the distance between CXCR4^{low} or CXCR4^{high} MKs and endothelial cells (Ecs) in the bone marrow of mice three days after *L. monocytogenes* infection ($n = 68$ CXCR4^{low} and 78 CXCR4^{high} MKs). CD41 (blue), CXCR4 (red) and EMCN (green). Yellow arrows indicate CXCR4^{high} MKs, while white arrowheads indicate CXCR4^{low} MKs. **(D)** Representative immunofluorescent staining images (left) and quantification (right) of CXCR4 (red) labeled MKs (blue) egressed into sinusoids (green) upon infection ($n = 46$ CXCR4^{low} MKs and 69 CXCR4^{high} MKs in four biological replicates). Yellow arrows indicate CXCR4^{high} MKs. **(E)** Comparison of the distance between HSCs to MKs ($n = 96$ control and 127 infected HSCs, $p = 0.21$ by two-sample KS test) in the bone marrow of control mice or mice at three days after *L. monocytogenes* infection. **(F)** Visualization of MK migration (red, arrowhead) into sinusoids (green) by live imaging in the bone marrow of *Pf4*^{Cre+}; *Rosa26*^{fs-tdTomato+/-} mice 24 hours after *L. monocytogenes* infection (Movie S1). “S” indicates sinusoid and dashed lines demarcate the border of sinusoids. **(G)** Quantification of CXCR4^{high} MKs in bone marrow, peripheral blood, liver, spleen, and lung of control mice and mice three days after *L. monocytogenes* infection. **(H)** Quantification of CXCR4 levels on CXCR4^{low} MKs treated with IFN- γ , LPS or *L. monocytogenes* for 4 hours compared to CXCR4^{high} MKs. **(I)** Quantification of tdTomato⁺ CXCR4^{high} MKs in

the liver and spleen from control mice or mice three days after *L. monocytogenes* infection by flow cytometry. **(J)** Schema of mtdTomato⁺ bone marrow (from *R26R^{mTmG}* mice) cell perfusion in control and *L. monocytogenes* infected recipients. **(K)** The percentage of CXCR4^{high} mtdTomato⁺ MKs and CXCR4^{low} mtdTomato⁺ MKs in bone marrow, liver and spleen of control or infected recipients were analyzed two days after mtdTomato⁺ bone marrow cells were perfused. **(L)** Radar chart showing transcriptomic similarities of bone marrow MK subpopulations with reported BM and lung MK datasets (Pariser et al., 2021; Yeung et al., 2020). **(M)** Schema for transfer experiments using tdTomato⁺ MKs from *Pf4^{Cre+}; Rosa26^{fs-tdTomato+/-}* mice into control recipients or recipients one day following *L. monocytogenes* infection. **(N-O)** Representative images **(N)** and quantification by flow cytometry **(O)** of tdTomato⁺ MKs in the lung of control or infected recipients two days after cell perfusion (*n* = 3 mice). Arrows indicate tdTomato⁺ MKs in the lung. Scale bars without indicated, 20 μ m. Data represent mean \pm s.e.m. A two-sample KS test was performed to assess statistical significance in **(E)**. Repeated-measures one-way ANOVA followed by Dunnett's test for multiple comparisons in **(H)**, # *p* <0.01, ## *p* <0.001. Two-tailed Student's *t*-test was performed to assess statistical significance except **(E, H)**, * *p* <0.05, ** *p* <0.01, *** *p* <0.001, n.s., not significant.

The following figure supplements are available for figure 4:

Figure 4-figure supplement 1. The effects of association of MKs and blood vessels, HSC activation, and MK numbers in bone marrow upon bacterial infection.

Figure 4-figure supplement 2. scRNA-seq of MKs from mice upon bacterial infection.

Figure 4-figure supplement 3. CXCL12 expression upon bacterial infection.

Figure 4-figure supplement 4. Cell cycle and apoptosis of CXCR4^{high} MKs, and CXCR4^{low} MK numbers in different organs upon bacterial infection.

Figure 4-figure supplement 5. Immune gene expression in bone marrow and lung MKs.

Figure 4-figure supplement 6. Intravascular and extravascular tdTomato⁺ MKs in the lung after MK perfusion.

Figure 4-video 1. MK migration traced by ex vivo live imaging.

Figure 4-source data 1. Distance of HSCs to MKs in the bone marrow from control mice or mice three days after *L. monocytogenes* infection.

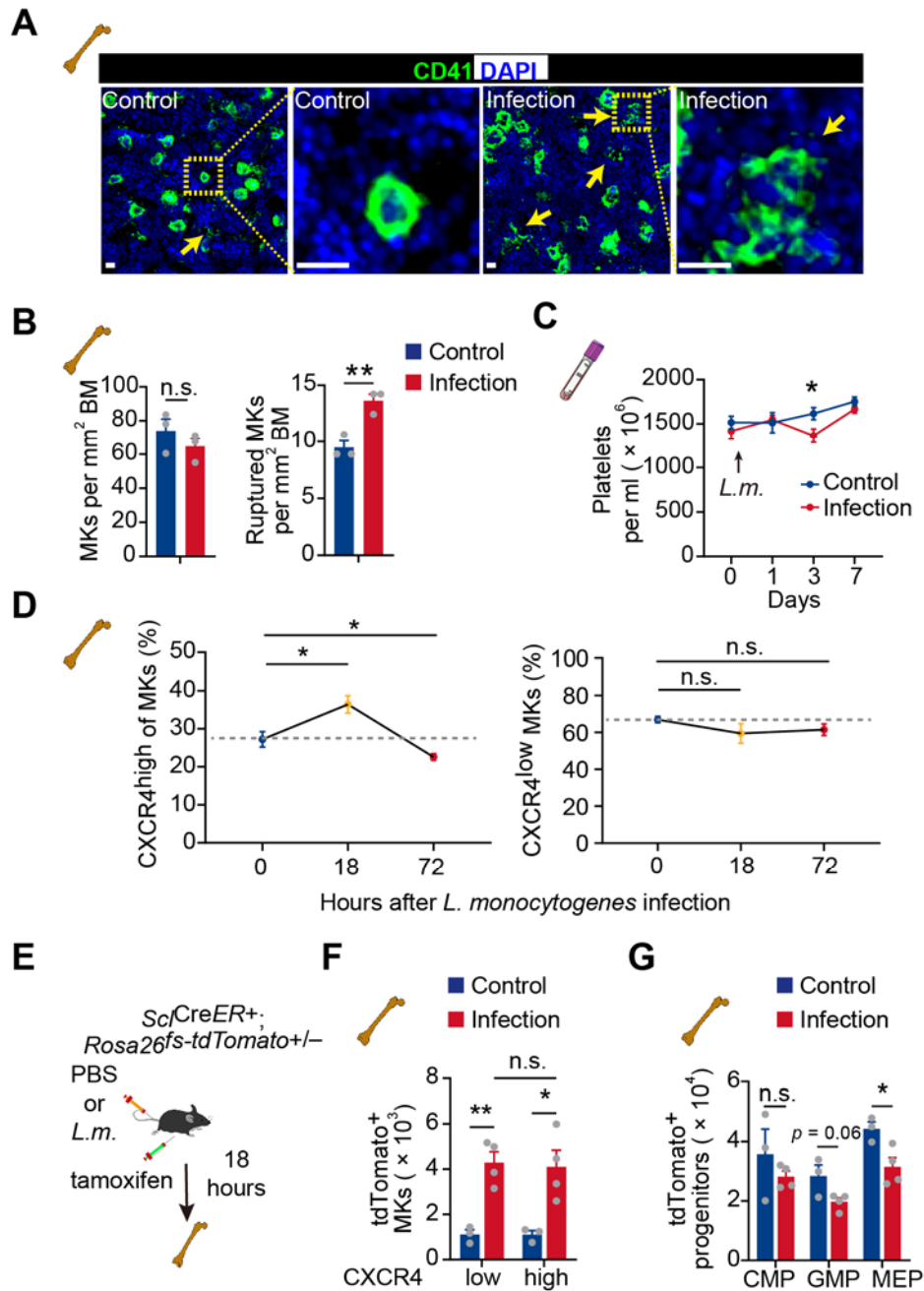


Figure 5. Acute inflammation induces emergency megakaryopoiesis of CXCR4^{high} MKs

(A-B) Representative images (A) and statistical analysis (B) of CD41 (green) and DAPI (blue) in bone marrow from control mice or mice three days after *L. monocytogenes*

infection. Arrows indicate ruptured MKs, yellow boxes indicate the locations of the magnified images. (C) Platelets in peripheral blood in control mice or mice after *L. monocytogenes* infection on indicated days. (D) The dynamics percentage of CXCR4^{high} MKs (left) or CXCR4^{low} MKs (right) in the bone marrow of *L. monocytogenes*-challenged mice within 72 hours of infection. (E) Schema for HSC lineage tracing upon *L. monocytogenes* infection using *Scl*^{CreER+}; *Rosa26*^{fs-tdTomato+/-} mice. (F-G) Cell numbers of tdTomato⁺ CXCR4^{low} MKs and tdTomato⁺ CXCR4^{high} MKs (F), and tdTomato⁺ progenitors (G) in the bone marrow of control and *L. monocytogenes* infected *Scl*^{CreER+}; *Rosa26*^{fs-tdTomato+/-} recipients 18 hours after *L. monocytogenes* infection and tamoxifen administration. CMP, common myeloid progenitor; GMP, granulocyte-monocyte progenitor; MEP, megakaryocyte-erythroid progenitor. Scale bars, 20 μ m. Data represent mean \pm s.e.m. Two-tailed Student's *t*-test was performed to assess statistical significance, * *p* < 0.05, ** *p* < 0.01, n.s., not significant.

Supplemental Figure Legends

Figure 1-figure supplement 1. Cell isolation, quality control and annotation of scRNA-seq data.

(A) Flow cytometry gating for isolation of MKs ($CD41^{+} FSC^{high}$) in bone marrow for scRNA-seq. (B) Quality control of scRNA-seq data. Violin plots showing the number of unique genes (gene number) before and after removing doublets, number of total unique molecular identifiers (UMI counts) and percentage of mitochondrial transcripts in single cells after removing doublets. Scatter plot showing the correlation between UMI counts and gene numbers. corr indicates Pearson correlation coefficient. (C-D) UMAP of 5368 bone marrow cells, colored by gene numbers (C) and by cluster identity indicated on the right (D). MK, megakaryocytes; Neu, neutrophils; M ϕ , macrophages; MP, myeloid progenitors; DC, dendritic cells; Mon, monocytes; B, B cells; T, T cells. (E) Heatmap of row-scaled signature gene expression in each cell type (top, color-coded by subpopulations). Columns denote cells; rows denote genes. Z score, row-scaled expression of the signature genes in each subpopulation. (F) Feature plots showing selected gene expression. (G) Violin plots showing the number of unique genes (gene number) of 1712 MKs.

Figure 1-figure supplement 2. Cell type identification by alignment with published scRNA-seq data.

(A) Radar charts showing cell similarities of our single cell dataset with the published bone marrow MK single cells (Pariser et al., 2021; Yeung et al., 2020), bone marrow immune cells and myeloid progenitor single cells (Almanzar et al., 2020; Fiona K. Hamey et al., 2021; Xie et al., 2020) using MetaNeighbor R package. (B) Comparison of our bone marrow scRNA-seq data with published bone marrow MK (Pariser et al., 2021; Yeung et al., 2020) and immune cell (Almanzar et al., 2020; Fiona K. Hamey et al., 2021; Xie et al., 2020) datasets. All cells were integrated by iMAP.py and projected on UMAP. (C) Column-scaled Euclidean distances between the centroid of each cluster. Z score, column-scaled Euclidean distance. MK, megakaryocytes; Neu, neutrophils; M ϕ , macrophages; MP, myeloid progenitors; DC, dendritic cells; Mon, monocytes; B, B cells; T, T cells.

Figure 1-figure supplement 3. Identification of MK subpopulations.

(A) Re-clustering of 1712 MKs from 5368 cells. (B) Violin plots showing MK marker gene expression (Aburima et al., 2021; Bernardes et al., 2020; Kanaji et al., 2005; Cuicui Liu et al., 2021; Machlus & Italiano, 2019; OZAKI et al., 2005; Shu Sun et al., 2021; Yeung et al., 2020) of MK1 to 5. Red lines indicate the median gene expression. (C) Projection of our datasets on reported MK (Pariser et al., 2021; Yeung et al., 2020) and immune cell (Fiona K. Hamey et al., 2021; Xie et al., 2020) scRNA-seq datasets by Symphony R package. MK, megakaryocytes; Neu, neutrophils; M ϕ , macrophages; MP, myeloid progenitors; DC, dendritic cells; Mon, monocytes; Bas, basophils; B, B cells; T, T cells; ABM, adult bone marrow. (D) MKs (MK1 to 5) and cell types projection based on similarities of our single cell transcriptional profiles and published MK (Pariser et al., 2021; Yeung et al., 2020) and immune cell datasets (Fiona K. Hamey et al., 2021; Xie et al., 2020) by scmap R package.

Figure 1-figure supplement 4. Enriched genes in MK1 to 4 and MK5.

(A) Volcano plot showing MK5 and MK1 to 4 enriched genes ($|\text{fold change}| > 1.4$, p value < 0.05). (B-C) Gene Ontology (GO) analysis showing MK5 enriched immune pathway genes and MK1 to 4 mainly enriched hemopoiesis and RNA processing pathway genes. (D-F) Gene set enrichment analysis (GSEA) evaluated enrichment of selected pathways in MK5 cells compared to other MK subpopulations (MK1 to 4).

Figure 1-figure supplement 5. MK5 interacts with immune cells and express signature genes of immune MKs.

(A) Dotplots of significant cytokine ligand (source) -receptor (target) interactions between MKs and immune cells discovered using CellChat. Color indicates communication probabilities, and bubble size indicates p value of the ligand-receptor pairs between MK subpopulations (source) and immune cells (target). (B) Selected signature gene expression in MK subpopulations.

Figure 1-figure supplement 6. Polyploidy, platelet generation ability and cell size of CXCR4^{low} and CXCR4^{high} MKs.

(A) Representative flow cytometry plots of gating strategy of CD41 and CXCR4 in the bone marrow of control mice and mice three days after *L. monocytogenes* infection. (B)

Relative expression of *Pf4*, *Vwf* and *Mpl* in CXCR4^{high} and CXCR4^{low} MKs by RT-qPCR. (C) Representative immunofluorescent staining image showing membranous CD41 staining typical of sorted bone marrow CXCR4^{high} MKs. (D) Sorted CXCR4^{low} and CXCR4^{high} MKs produced proplatelets *in vitro* on day five post cultured under 100 ng ml⁻¹ TPO. White arrowheads indicate proplatelet formation. (E) Polyploidy distribution of CXCR4^{low} MKs and CXCR4^{high} MKs (right). (F) Representative immunofluorescent staining images showing CD41 and CXCR4 expression of CXCR4^{low} and CXCR4^{high} MKs in the bone marrow. CD41, green; CXCR4, red; DAPI, blue. (G) Comparison of cell size between CXCR4^{low} MKs and CXCR4^{high} MKs on day three post cultured under 100 ng ml⁻¹ Thrombopoietin (TPO). (H) Median fluorescence intensity of CXCR4 in small and large sizes of MKs by flow cytometry. Scale bars, 20 μm. Data represent mean ± s.e.m in (B, D, E, H) or mean ± first and third quartiles in (G). Two-sample KS test was performed to assess statistical significance in (G). Two-tailed Student's *t*-test was performed to assess statistical significance in (B, D, E, H). * *p* < 0.05, ** *p* < 0.01, *** *p* < 0.001.

Figure 2-figure supplement 1. *L. monocytogenes* promote myelopoiesis and the association of myeloid cells and the CXCR4^{high} MK-blood vessel intersection.

(A-B) Representative immunofluorescent staining image (A) and statistical analysis (B) showing association of MKs (blue) and myeloid cells (green) in the bone marrow of control mice and mice three days after *L. monocytogenes* infection (*n* = 30 control and infected MKs). CD41, blue; CD11b, green. (C-D) Distance (C) and mean distance (D) of actual or randomly positioned myeloid cells to the closest CXCR4^{low} Mks and CXCR4^{high} MKs from mice without infection. (E-F) Representative images of MKs (blue), CXCR4 (red), vascular endothelial cells (green) and myeloid cells (white) (E), and statistical analysis (F) in bone marrow showing the distribution of myeloid cells to CXCR4^{low} or CXCR4^{high} MKs and vascular cells three days after *L. monocytogenes* infection. CD41, blue; CXCR4, red; EMCN, green; CD11b, white. Yellow arrows indicate CXCR4^{high} MKs and white arrowheads indicate CXCR4^{low} MKs (left) and two-dimensional probability distribution of distances from myeloid cells to CXCR4^{low} or CXCR4^{high} MKs and vascular cells (*n* = 104 CD11b⁺ cells; *p* = 0.04 by 2D KS test). Scale bars, 20 μm. Boxplots show medians, first and third quartiles in (B). Two-sample KS test was performed to assess statistical significance in (B, D). Two-dimensional-two-sample KS test was performed to assess statistical significance in (F).

Figure 2-figure supplement 2. CXCR4^{high} MKs promote myeloid cell phagocytosis and produce TNF α and IL-6.

(A-B) Quantification of phagocytosis abilities in neutrophils (A) and macrophages (B) without or with CXCR4^{low} MKs or CXCR4^{high} MKs as indicated. (C-E) TNF α and IL-6 protein levels in CXCR4^{low} and CXCR4^{high} MKs were shown by immunofluorescent staining (C-D) using sorted MKs, compared to their levels in sorted macrophages upon *L. monocytogenes* infection (E). Data represent mean \pm s.e.m in (A, B) and boxplots show medians, first and third quartiles in (C-E). Repeated-measures one-way ANOVA followed by Dunnett's test for multiple comparisons in (A, B), ‡ $p < 0.05$, # $p < 0.01$. Two-sample KS test was performed to assess statistical significance in (C-E).

Figure 3-figure supplement 1. MK ablation influenced HSC and myeloid cell numbers.

(A) Schema for diphtheria toxin (DT) and *L. monocytogenes* administration used for the experiments shown in (B-D). (B) Number of bone marrow hematopoietic stem and progenitor cells in *Pf4^{Cre+}; Rosa26^{fs-iDTR+/-}* mice compared to *Pf4^{Cre-}; Rosa26^{fs-iDTR+/-}* mice after *L. monocytogenes* infection and DT injection. (C-D) Gating strategies (C) and numbers (D) of myeloid cells in the bone marrow of *Pf4^{Cre-}; Rosa26^{fs-iDTR+/-}* mice after *L. monocytogenes* infection and DT injection. (D-E) Gating strategies of myeloid cells in the liver (D) and spleen (E) of *Pf4^{Cre-}; Rosa26^{fs-iDTR+/-}* mice at three days after *L. monocytogenes* infection. Neu, neutrophil; MF, macrophage; Mono, monocyte; DC, dendritic cell. Two-tailed Student's *t*-test was performed to assess statistical significance. * $p < 0.05$, ** $p < 0.01$, *** $p < 0.001$.

Figure 3-figure supplement 2. CXCR4^{high} MKs induced B3Z T cell activation.

The LacZ activity in B3Z T cells with or without co-culture as indicated. Ctrl indicates B3Z cells without MKs co-culture; bone marrow-derived DCs, CXCR4^{low} MKs and CXCR4^{high} MKs were pulsed with OVA for 24 hours. Two-tailed Student's *t*-test was performed to assess statistical significance, * $p < 0.05$.

Figure 4-figure supplement 1. The effects of association of MKs and blood vessels, HSC activation, and MK numbers in bone marrow upon bacterial infection.

(A) Bone marrow MKs (blue) and sinusoids (green) in control mice and mice three days after *L. monocytogenes* infection. CD41, blue; EMCN, green. Yellow arrows indicate MKs egressed into sinusoids. “S” indicates sinusoid and dashed lines demarcate the border of sinusoids. (B) HSC and progenitor cell number in the bone marrow of control mice and mice three days after *L. monocytogenes* infection. LT, long term; ST, short term; MPP, multipotential progenitor. (C-D) MK numbers (C) and CXCR4^{low} MK frequency (D) in the bone marrow of control mice and mice three days after *L. monocytogenes* infection ($n = 8$ mice). (E-F) Frequency of BrdU⁺ (E) and Annexin V⁺ (F) cells in CXCR4^{high} MKs from bone marrow of control mice or mice three days after *L. monocytogenes* infection ($n = 5$ mice). Scale bars, 20 μ m. Data represent mean \pm s.e.m. Two-tailed Student’s *t*-test was performed to assess statistical significance. * $p < 0.05$, n.s., not significant.

Figure 4-figure supplement 2. scRNA-seq of MKs from mice upon bacterial infection.

(A) Schematic depicting the strategy of scRNA-seq using bone marrow MKs from mice three days after *L. monocytogenes* infection. (B) Violin plots showing the number of unique genes (gene number) before and after removing doublets, number of total unique molecular identifiers (UMI counts) and percentage of mitochondrial transcripts in single cells after removing doublets. Scatter plot showing the correlation between UMI counts and gene numbers. corr indicates Pearson correlation coefficient. (C) UMAP of the combined 5 368 cells from control bone marrow and 4 276 cells from *L. monocytogenes* infection bone marrow, colored by cell types. Neu, neutrophil; MP, myeloid progenitor; Mon, monocytes; B, B cells; T, T cells. (D) UMAP of the combined 1 712 control MKs and 1 560 infection MKs in the bone marrow, colored by clusters. (E) Fraction of each MK subpopulation from control MKs or *L. monocytogenes* infection MKs. (F) Violin plot showing *Cxcr4* expression in each MK subpopulation of control and infection MKs.

Figure 4-figure supplement 3. CXCL12 expression upon bacterial infection.

(A-H) Relative expression of *Cxcl12* (A-D) and frequency of CXCL12^{DsRed} cells (E-H) in the bone marrow (A), lung (B), liver (C), and spleen (D) from control mice and mice three days after *L. monocytogenes* infection by RT-qPCR (A-D) and flow cytometry (E-H), respectively. Two-tailed Student’s *t*-test was performed to assess statistical significance. * $p < 0.05$, ** $p < 0.01$, *** $p < 0.001$.

Figure 4-figure supplement 4. Cell cycle and apoptosis of CXCR4^{high} MKs, and CXCR4^{low} MK numbers in different organs upon bacterial infection.

(A-B) Fraction of BrdU⁺ and Annexin V⁺ MKs in CXCR4^{high} MKs in the liver (A) and spleen (B) from control mice or mice three days after *L. monocytogenes* infection. (C) Quantification of CXCR4^{low} MKs in peripheral blood, liver, spleen, and lung of control mice and mice at three days after *L. monocytogenes* infection. (D) Quantification of CXCR4 levels on CXCR4^{high} MKs and CXCR4^{low} MKs treated with LPS or IFN-γ for 18 or 24 hours. (E-F) Representative images and quantification of mGFP⁺ MKs (green) in the liver (E) and spleen (F) from control mice or mice three days after *L. monocytogenes* infection (*n* = 4 and 7 mice, respectively). (G-H) Gating strategies for CXCR4^{high} MKs in the liver (G) and spleen (H). (I) Quantification of tdTomato⁺CXCR4^{low} MKs in the liver and spleen from control mice or mice three days after *L. monocytogenes* infection by flow cytometry. Data represent mean ± s.e.m. Two-tailed Student's *t*-test was performed to assess statistical significance except (D). * *p* < 0.05, ** *p* < 0.01, *** *p* < 0.001, n.s., not significant. Repeated-measures one-way ANOVA followed by Dunnett's test for multiple comparisons in (D), # *p* < 0.01, ## *p* < 0.01.

Figure 4-figure supplement 5. Comparison of immune gene expression in MK5 and lung MKs from control mice or mice upon bacterial infection.

(A) Gene set variation analysis (GSVA) of each MK subpopulation under control or *L. monocytogenes* infection, colored by row-scaled GSVA enrichment scores. (B) Antigen processing and presentation score of control MK5, infection MK5, and bone marrow and lung MKs from Yeung et al (Yeung et al., 2020). (C) Heatmap showing the row-scaled antigen processing and presentation gene expression of control and infection MK5 cells, comparing with bone marrow MK and lung MK from Yeung et al (Yeung et al., 2020). Data represent mean ± first and third quartiles in (B). Two-sample KS test was performed to assess statistical significance in (B).

Figure 4-figure supplement 6. Intravascular and extravascular tdTomato⁺ MKs in the lung after MK perfusion.

(A) Schema for transfer experiments using tdTomato⁺ MKs from *Pf4^{Cre+}; Rosa26^{fs-tdTomato+/-}* mice into recipients one day following *L. monocytogenes* infection. (B)

Transfused MKs (red) and sinusoids (green) in the lung of mice after *L. monocytogenes* infection as indicated in Figure 4M. DAPI, blue; EMCN, green; tdTomato, red. (C) Quantification of transfused intravascular and extravascular MKs in the lung. Data represent mean \pm s.e.m. Two-tailed Student's *t*-test was performed to assess statistical significance. *** $p < 0.001$.

Figure 4-video 1. MK migration traced by *ex vivo* live imaging.

MK (red, arrowhead) migrating into the bone marrow sinusoids (green, labeled by Dextran-FITC) by live imaging in the bone marrow of *Pf4^{Cre+}; Rosa26^{fs-tdTomato+/-}* mice 24 hours after *L. monocytogenes* infection.

1 Key resources table

Reagent type	Designation	Source	Identifier	Additional information
Antibody	anti-CD41a (mouse monoclonal)	eBioscience	Cat#17-0411-82 RRID:AB_1603237	FACS (1 ul per test)
Antibody	anti-CXCR4 (mouse monoclonal)	eBioscience	Cat#53-9991-80 RRID:AB_953573	FACS (1 ul per test)
Antibody	anti-CD11b (mouse monoclonal)	eBioscience	Cat#12-0112-82 RRID:AB_2734869	FACS (1 ul per test)
Antibody	anti-F4/80 (mouse monoclonal)	eBioscience	Cat#17-4801-80 RRID:AB_2784647	FACS (1 ul per test)
Antibody	anti-Gr-1 (mouse monoclonal)	Biolegend	Cat#108424 RRID:AB_2137485	FACS (1 ul per test)
Antibody	anti-Ly-6C (mouse monoclonal)	Biolegend	Cat#128022 RRID:AB_10639728	FACS (1 ul per test)
Antibody	anti-CD11c (mouse monoclonal)	eBioscience	Cat#12-0114-82 RRID:AB_465552	FACS (1 ul per test)
Antibody	anti-CD45.1 (mouse monoclonal)	eBioscience	Cat#15-0453-82 RRID:AB_468759	FACS (1 ul per test)
Antibody	anti-CD45.2 (mouse monoclonal)	Biolegend	Cat#109831 RRID:AB_10900256	FACS (1 ul per test)
Antibody	anti-CD4 (mouse monoclonal)	eBioscience	Cat#12-0041-82 RRID:AB_465506	FACS (1 ul per test)
Antibody	anti-CD8a (mouse monoclonal)	Biolegend	Cat#100707 RRID:AB_312746	FACS (1 ul per test)
Antibody	anti-IFN- γ (mouse monoclonal)	Biolegend	Cat#505813 RRID:AB_493312	FACS (1 ul per test)
Antibody	anti-IL-4 (mouse monoclonal)	Biolegend	Cat#504118 RRID:AB_10898116	FACS (1 ul per test)
Antibody	anti-CD34 (mouse monoclonal)	eBioscience	Cat#11-0341-82 RRID:AB_465021	FACS (1 ul per test)
Antibody	anti-Sca-1 (mouse monoclonal)	Biolegend	Cat#108114 RRID:AB_493596	FACS (1 ul per test)
Antibody	anti-c-Kit (mouse monoclonal)	Biolegend	Cat#105812 RRID:AB_313221	FACS (1 ul per test)
Antibody	anti-CD135 (mouse monoclonal)	Biolegend	Cat#135314 RRID:AB_2562339	FACS (1 ul per test)
Antibody	anti-CD3 ϵ (mouse monoclonal)	Biolegend	Cat#100310 RRID:AB_312675	FACS (1 ul per test)
Antibody	anti-B220 (mouse monoclonal)	Biolegend	Cat#103210 RRID:AB_312995	FACS (1 ul per test)
Antibody	anti-TER-119 (mouse monoclonal)	Biolegend	Cat#116210 RRID:AB_313711	FACS (1 ul per test)
Antibody	anti-IgM (mouse monoclonal)	eBioscience	Cat#15-5790-82 RRID:AB_494222	FACS (1 ul per test)

Antibody	anti-CD16/32 (mouse monoclonal)	Biologend	Cat#101333 RRID:AB_2563692	FACS (1 ul per test)
Antibody	anti-CD127 (mouse monoclonal)	Biologend	Cat#135021 RRID:AB_1937274	FACS (1 ul per test)
Antibody	anti-TNF α (mouse monoclonal)	Invitrogen	Cat#17-7321-81 RRID:AB_469507	FACS (1 ul per test) IF (1:100)
Antibody	anti-IL-6 (mouse monoclonal)	Biologend	Cat#504507 RRID:AB_10694868	FACS (1 ul per test) IF (1:100)
Antibody	anti-BrdU (mouse monoclonal)	eBioscience	Cat#11-5071-42 RRID:AB_11042627	FACS (1 ul per test)
Antibody	anti-Endomucin (mouse polyclonal)	R&D	Cat#AF4666	IF (1:100)
Antibody	anti-CD150 (mouse monoclonal)	Biologend	Cat#115908 RRID:AB_345278	IF (1:100)
Antibodies	anti-Lineage Panel (mouse monoclonal)	Biologend	Cat#133307 RRID:AB_11124348	IF (1:100)
Antibody	anti-Goat AF488 (goat polyclonal)	Invitrogen	Cat#A32814 RRID:AB_2762838	IF (1:1000)
Antibody	anti-TNF-alpha (mouse monoclonal)	Sino Biological	Cat#50349-R023	2 $\mu\text{g ml}^{-1}$
Antibody	anti-Rabbit AF488 (rabbit polyclonal)	Invitrogen	Cat#R37118 RRID:AB_2556546	IF (1:1000)
Antibody	anti-OVA257-264 (SIINFEKL) peptide bound to H-2K ^b (mouse monoclonal)	Invitrogen	Cat#17-5743-82 RRID: AB_1311286	FACS (1 ul per test)
Antibody	anti-IL-2 (mouse monoclonal)	eBioscience	Cat#25-7021-80 RRID: AB_1235007	FACS (1 ul per test)
Chemical compound, drug	Diphtheria toxin (DT)	Sigma-Aldrich	Cat#D0564-1MG	40 $\mu\text{g kg}^{-1}$ body mass
Chemical compound, drug	BrdU (5-Bromo-2'-Deoxyuridine)	Sigma-Aldrich	Cat#B5002-250mg	125 mg kg^{-1} body mass
Chemical compound, drug	CFSE (5-Carboxyfluorescein, Succinimidyl Ester)	Invitrogen	Cat#C2210	2.5 μM
Chemical compound, drug	GM-CSF	Abbkine	Cat#PRP2116	10 ng ml^{-1}
Chemical compound, drug	IL-4	novoprotein	Cat#CK15	10 ng ml^{-1}
Chemical compound, drug	Tamoxifen	Sigma-Aldrich	Cat#T5648	20 mg ml^{-1} corn oil

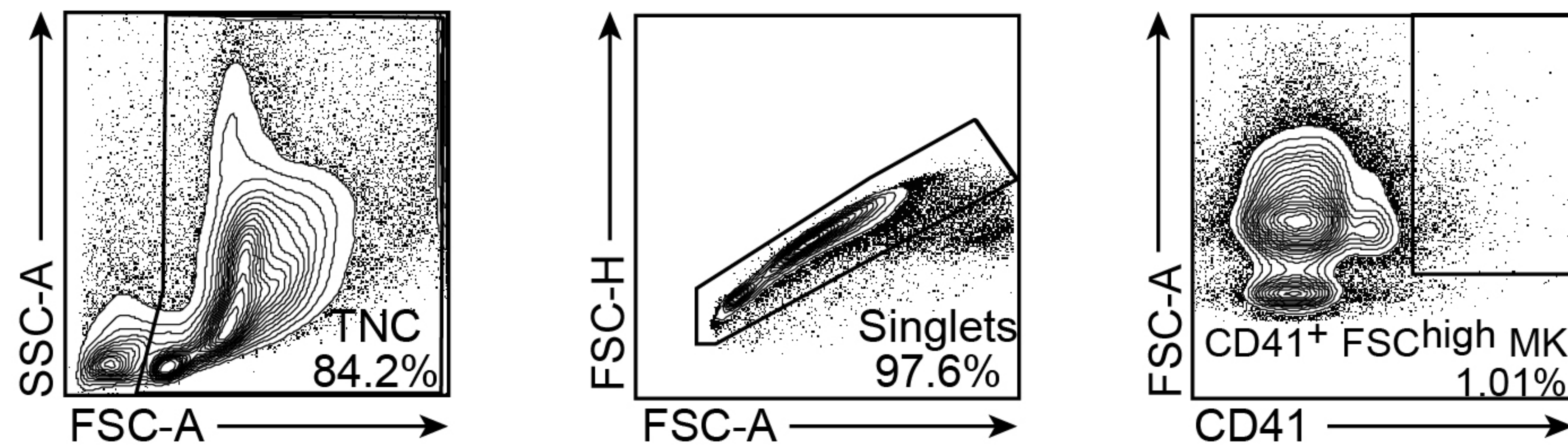
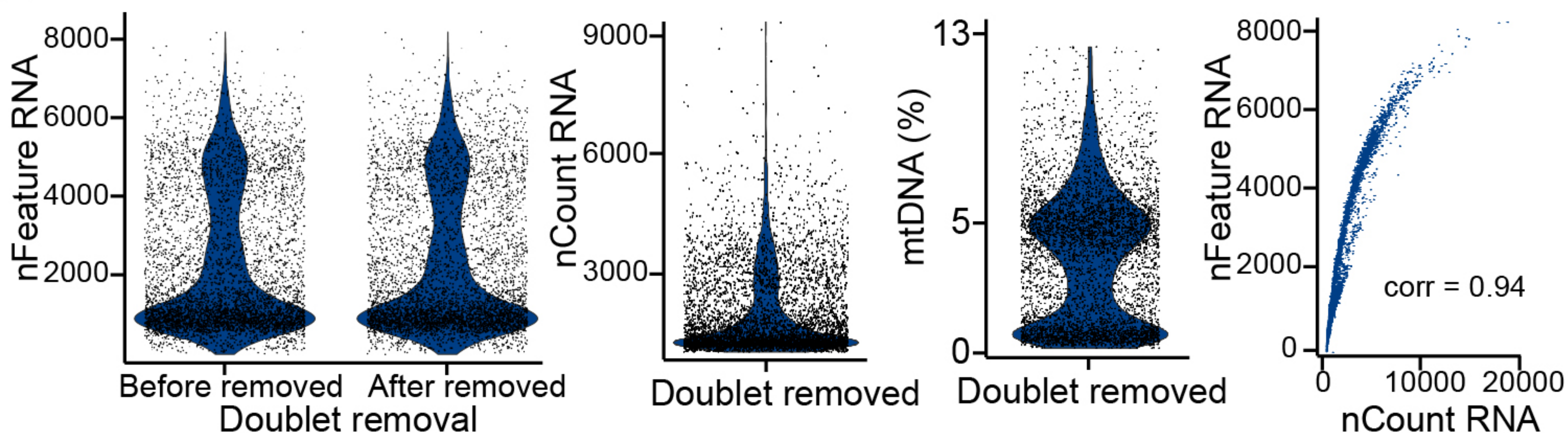
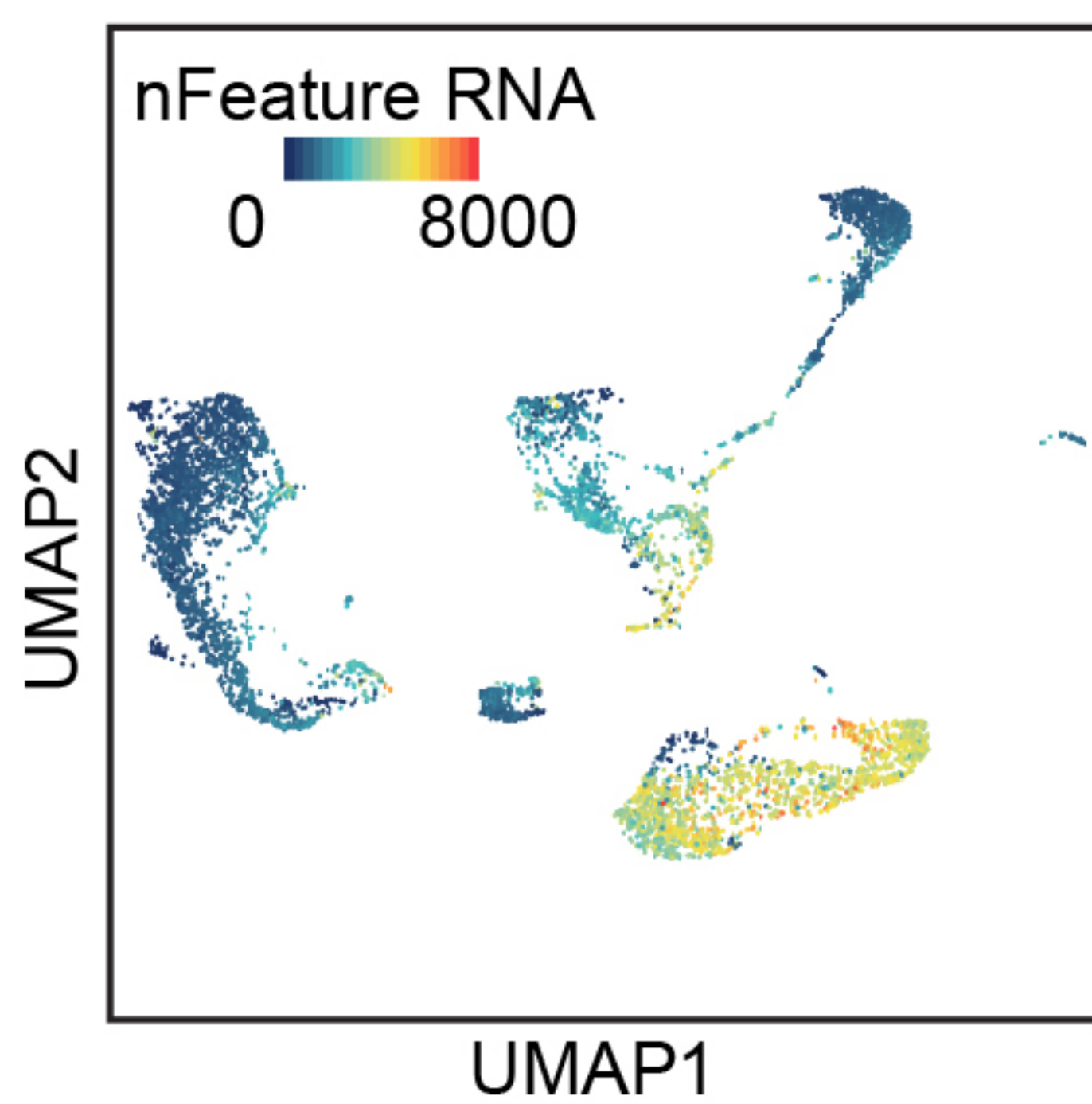
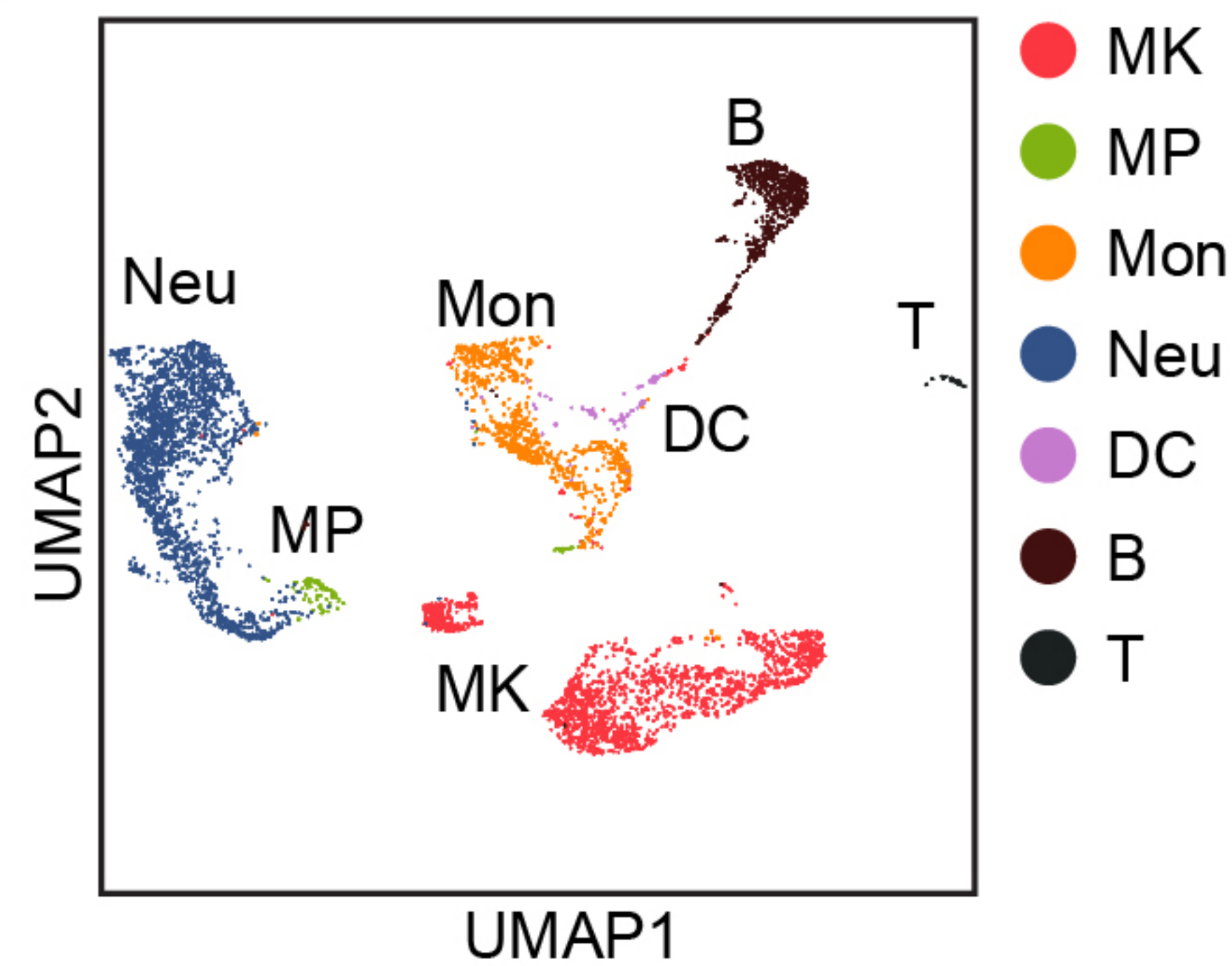
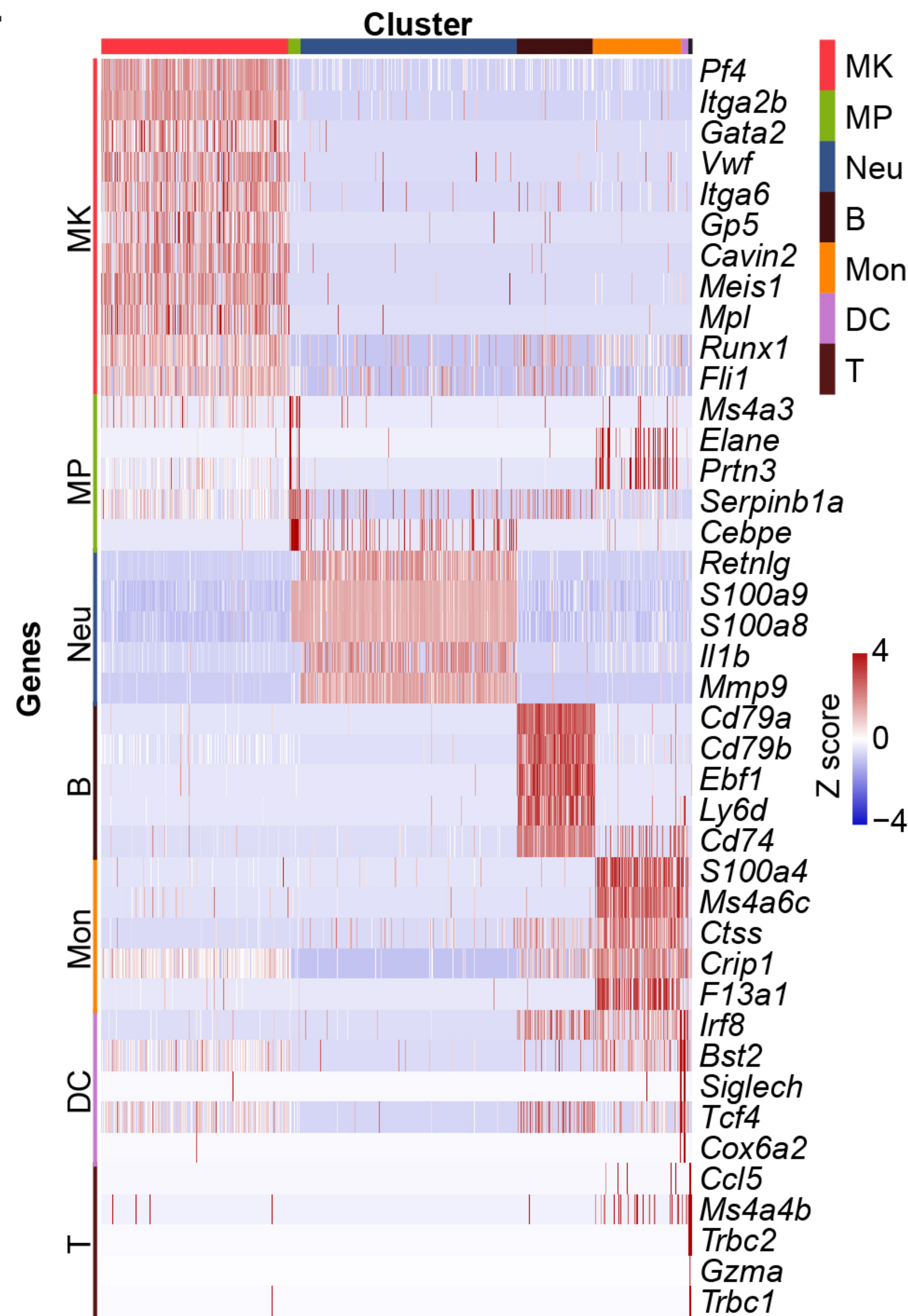
Commercial kit	Chromium Single Cell 3' GEM, Library & Gel Bead Kit v3	10x Genomics	PN-1000075	
Commercial kit	Chromium Chip B Single Cell Kit	10x Genomics	PN-1000074	
Cell line (Mus musculus)	NCTC clone 929	ATCC	CCL-1 RRID: CVCL_0462	
Cell line (Mus musculus)	B3Z hybridoma CD8 T cell	Dr. Nilabh Shastri		
Deposited data	scRNA sequencing data (raw and processed data)	This paper	GEO: GSE168224	
Genetic reagent (Mus musculus)	C57BL/6J	Shanghai Model Organisms	NA	
Genetic reagent (Mus musculus)	Tg(Pf4-icre)Q3Rsko/J (<i>Pf4^{Cre}</i>)	Jackson Laboratory	Stock No: 008535	
Genetic reagent (Mus musculus)	Gt(ROSA)26Sortm1(HBEGF)Awai/J (<i>Rosa26^{fs-iDTR}</i>)	Jackson Laboratory	Stock No: 007900	
Genetic reagent (Mus musculus)	Gt(ROSA)26Sortm4(ACTB-tdTomato,-EGFP)Luo/J (<i>Rosa26^{fs-mTmG}</i>)	Jackson Laboratory	Stock No: 007576	
Genetic reagent (Mus musculus)	Gt(ROSA)26Sortm9(CAG-tdTomato)Hze/J (<i>Rosa26^{fs-tdTomato}</i>)	Jackson Laboratory	Stock No: 007905	
Genetic reagent (Mus musculus)	<i>Scf^{CreER}</i> mice	J. R. Göthert	Göthert et al., 2005	

)				
Genetic reagent (Mus musculus)	Cxcl12tm2.1Sjm/J (<i>CXCL12^{fs-DsRed}</i>)	Jackson Laboratory	Stock No: 022458	
Genetic reagent (Mus musculus)	C57BL/6-Tg(TcraTcrb)1100 Mjb/J (<i>OT-I</i>)	Jackson Laboratory	Stock No: 003831	
Strain, strain background (L. monocytogenes)	10403S	Bishop and Hinrichs	Bishop and Hinrichs, 1987	
Software, algorithm	Cell ranger_3.0.2	10x Genomics	tenx RRID: SCR_01695	
Software, algorithm	R_3.6.3	CRAN (R_3.6.3)	NA	
Software, algorithm	Seurat_3.0.2	CRAN (R_3.6.3)	Seurat RRID: SCR_016341	
Software, algorithm	ggplot2_3.2.0	CRAN (R_3.6.3)	ggplot2 RRID:SCR_014601	
Software, algorithm	clusterProfiler_3.12.0	Bioconductor	clusterProfiler RRID: SCR_016884	
Software, algorithm	pheatmap_1.0.12	CRAN (R_3.6.3)	pheatmap RRID:SCR_016418	
Software, algorithm	CellPhoneDB_2.1.7	https://github.com/Teichlab/cellphonedb	CellPhoneDB RRID:SCR_017054	
Software, algorithm	CellChat_1.1.3	https://github.com/sqjin/CellChat	CellChat	
Software, algorithm	symphony_1.0	https://github.com/immunogenomics/symphony	symphony	
Software, algorithm	MetaNeighbor_1.10.0	https://github.com/maggiemagiecrow/MetaNeighbor	MetaNeighbor RRID:SCR_016727	
Software,	iMAP_1.0.0	https://github	iMAP	

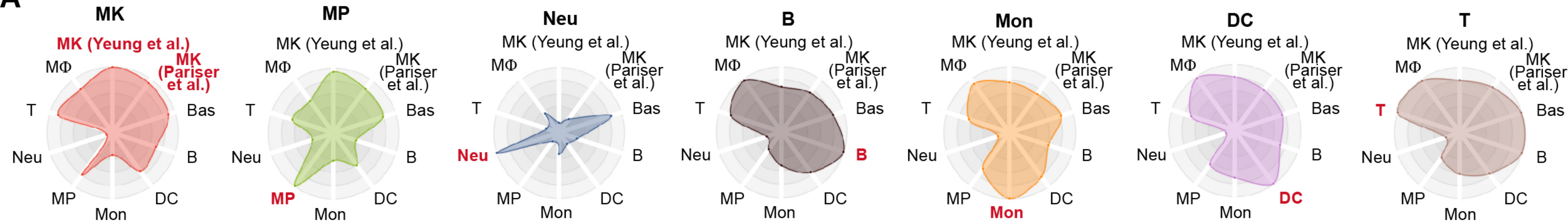
algorithm		b.com/Svvo rd/iMAP		
Software, algorithm	scmap_ 1.16.0	Bioconduct or	Scmap RRID:SCR_017338	
Software, algorithm	enrichplot_1.4.0	Bioconduct or	enrichplot	
Software, algorithm	Imaris_8.4	Bitplane	Imaris RRID:SCR_007370	
Software, algorithm	FlowJo_10	BD Bioscience	FlowJo RRID:SCR_008520	
Software, algorithm	ImageJ_ 1.8.0	National Institutes of Health	ImageJ RRID:SCR_003070	
Other	DAPI (4',6- Diamidino-2- Phenylindole, Dihydrochloride)	Thermo Fisher	Cat#D1306	IF (0.5 µg/mL)
Other	Corn oil	Sigma- Aldrich	Cat#PHR2897	Tamoxifen dissolution
Other	Lymphocyte Separation Medium	TBD Science	Cat#LTS1077	Liver cell isolation

2

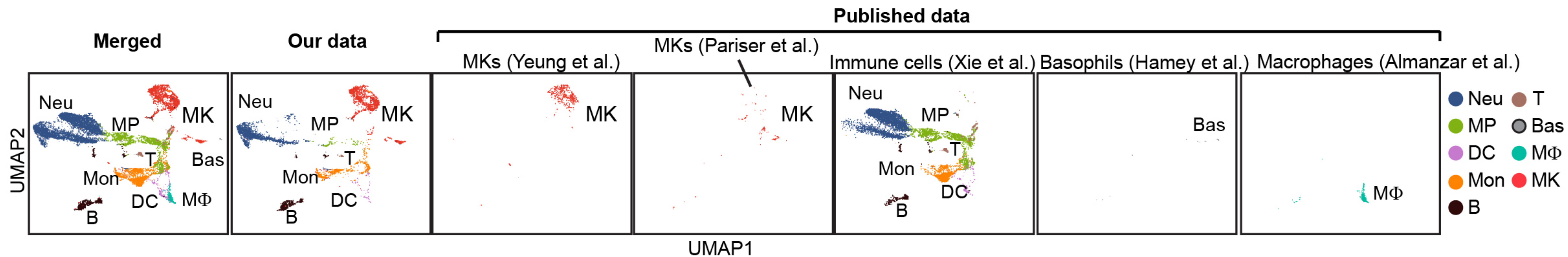
3

A**B****C****D****E**

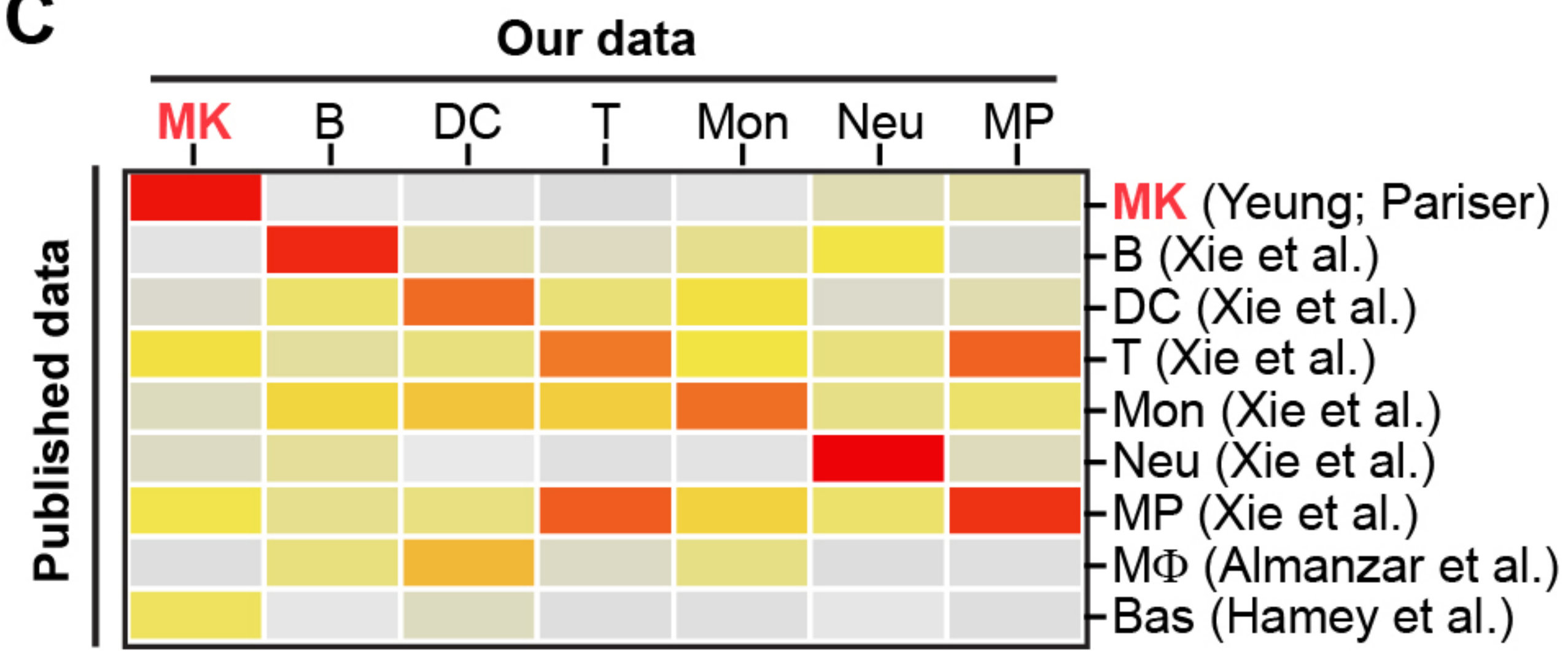
A



B



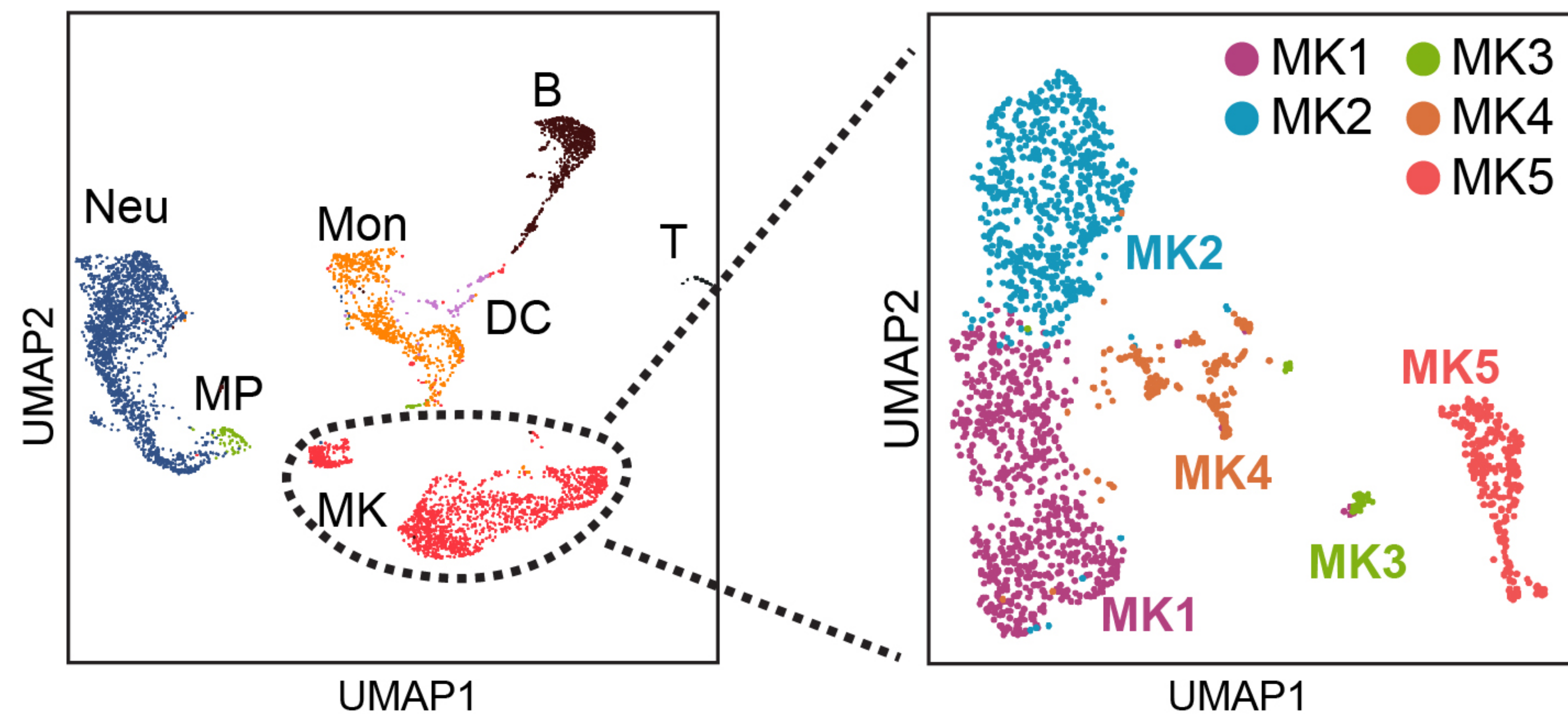
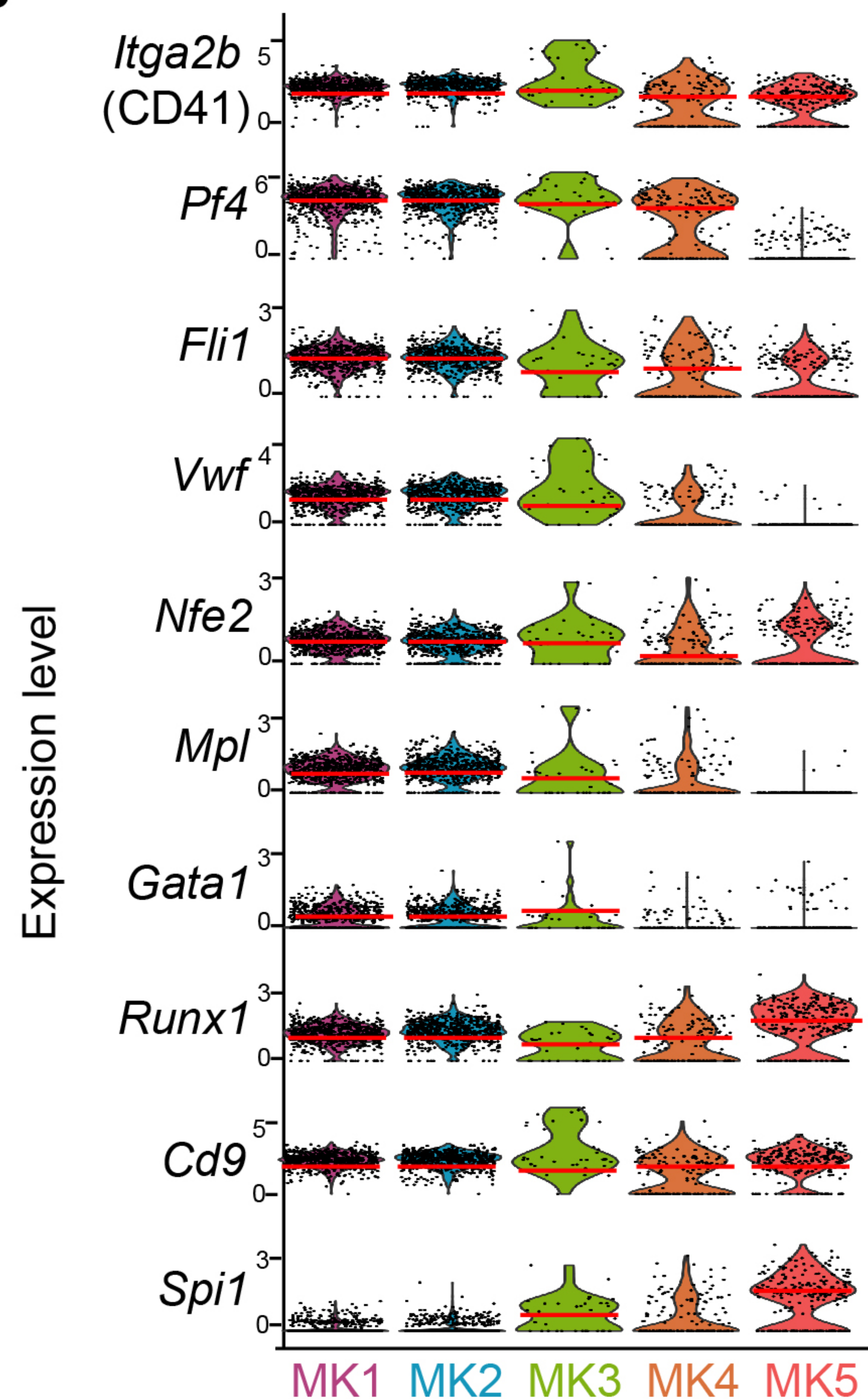
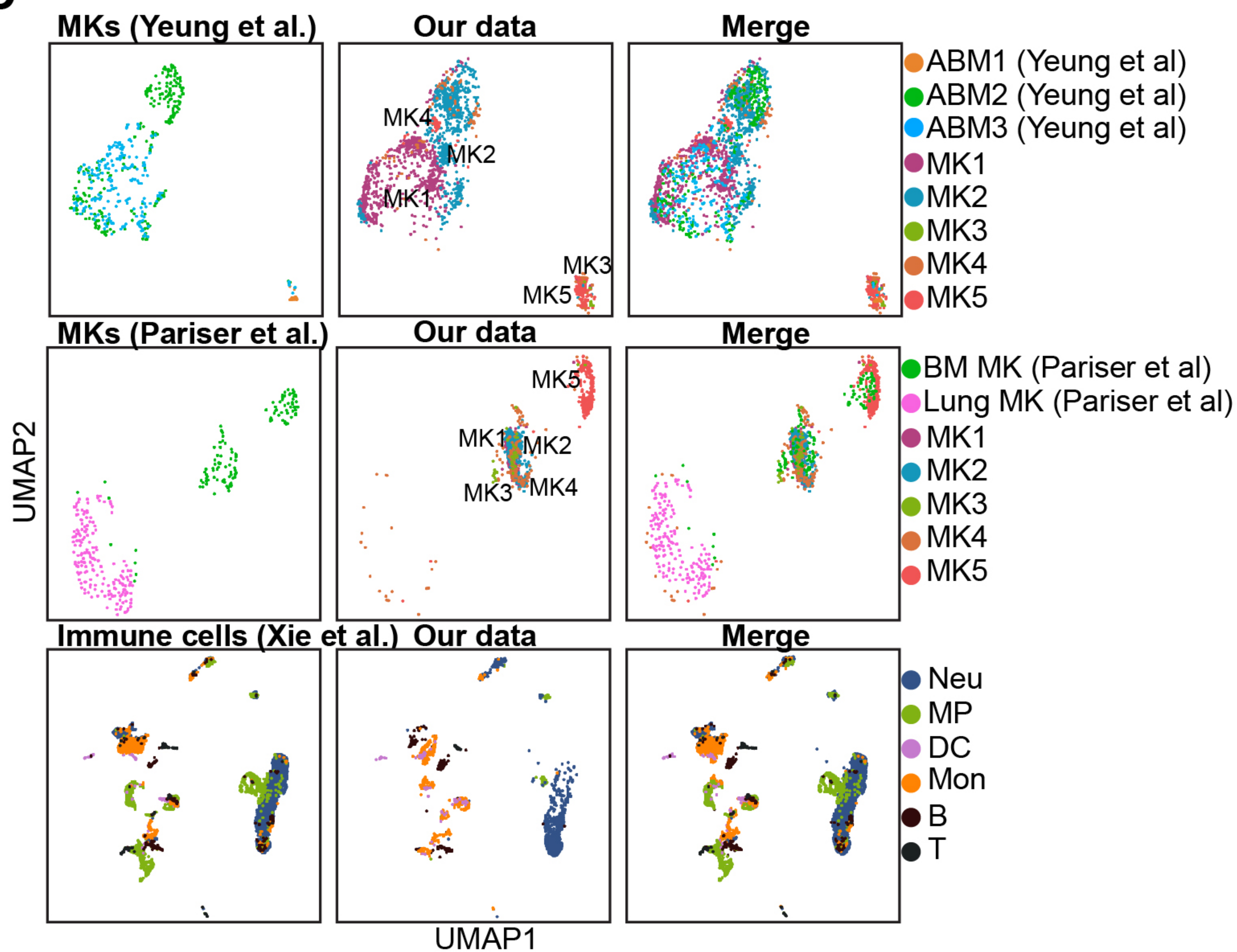
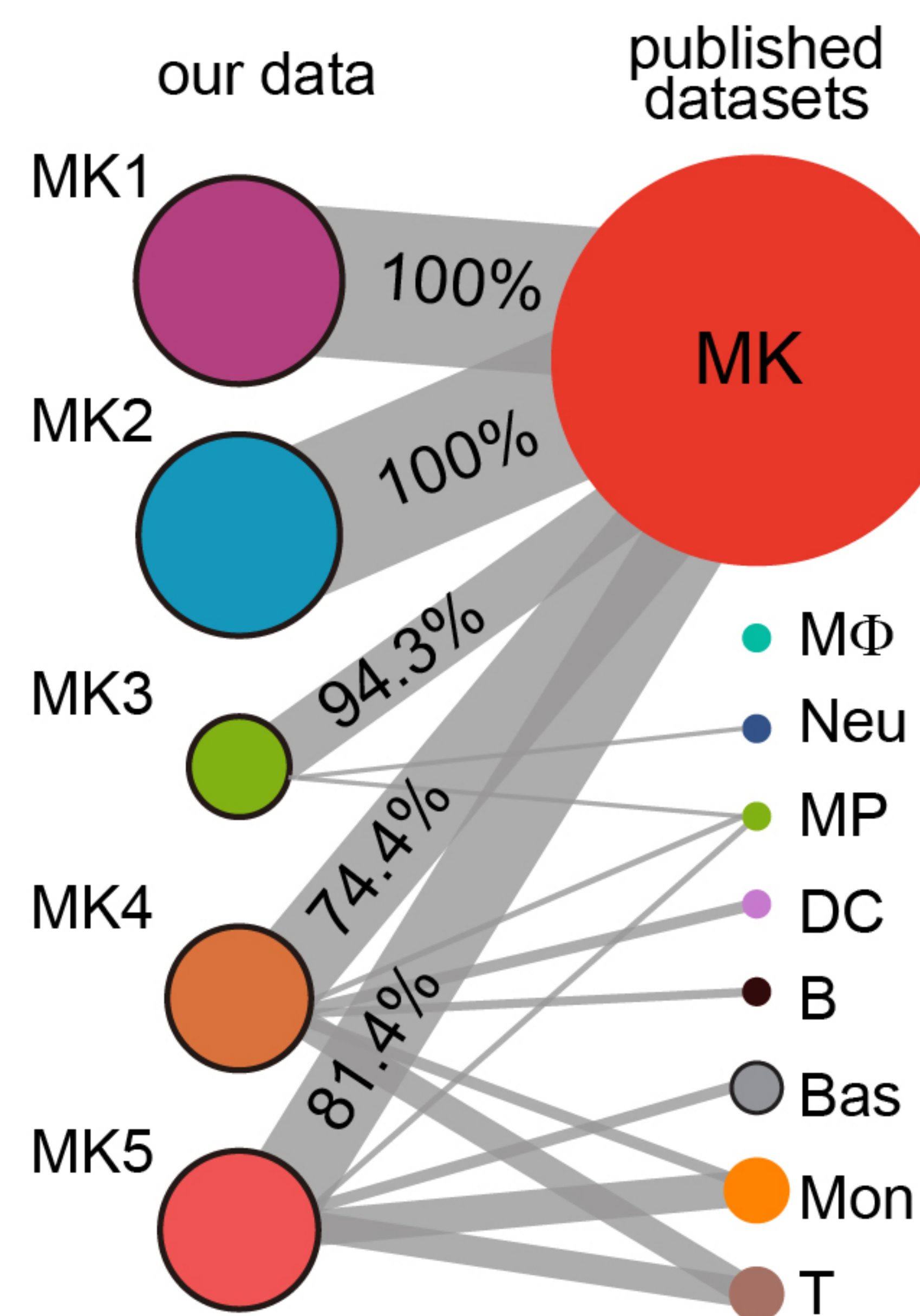
C



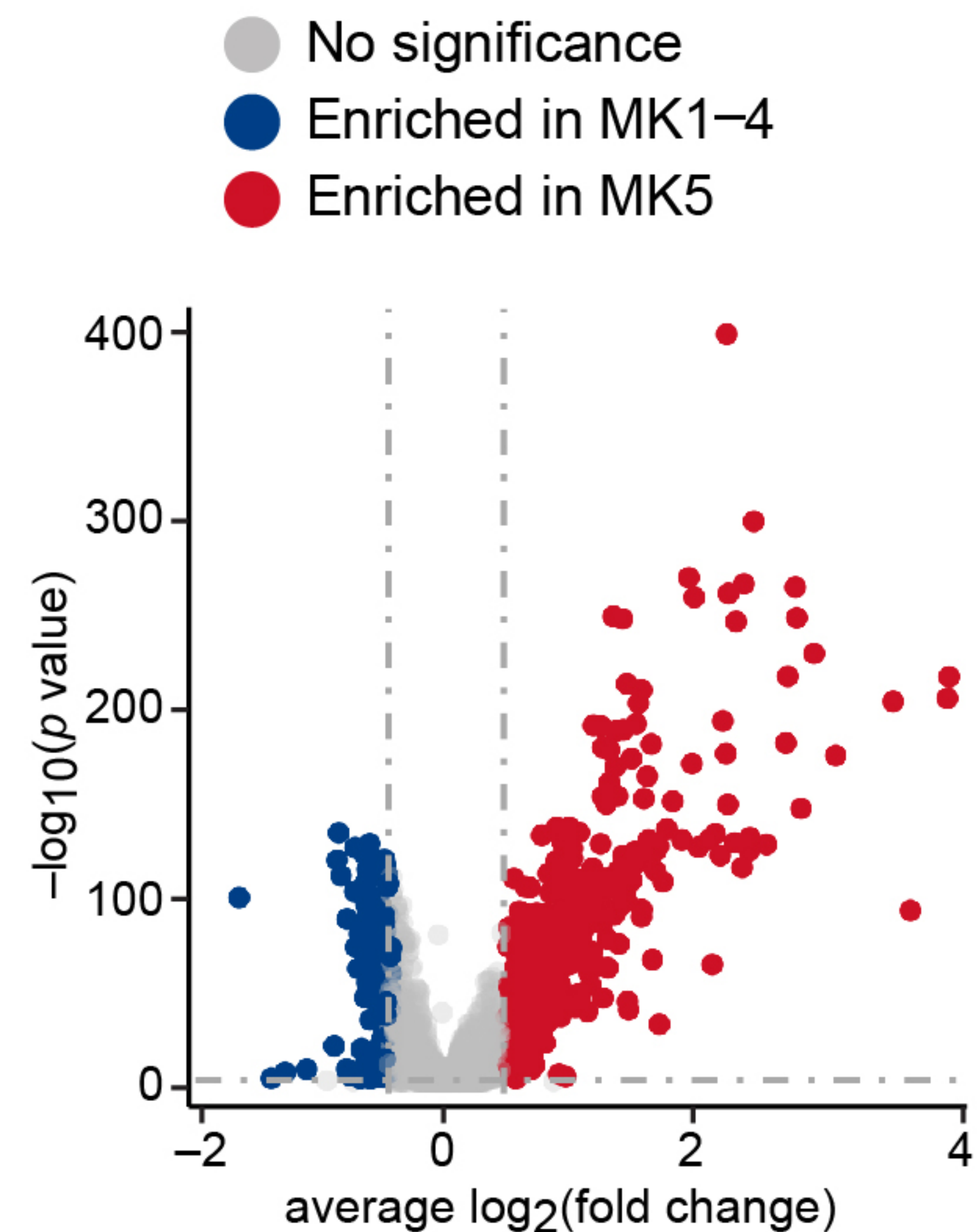
Euclidean Distance
between clusters

Z score

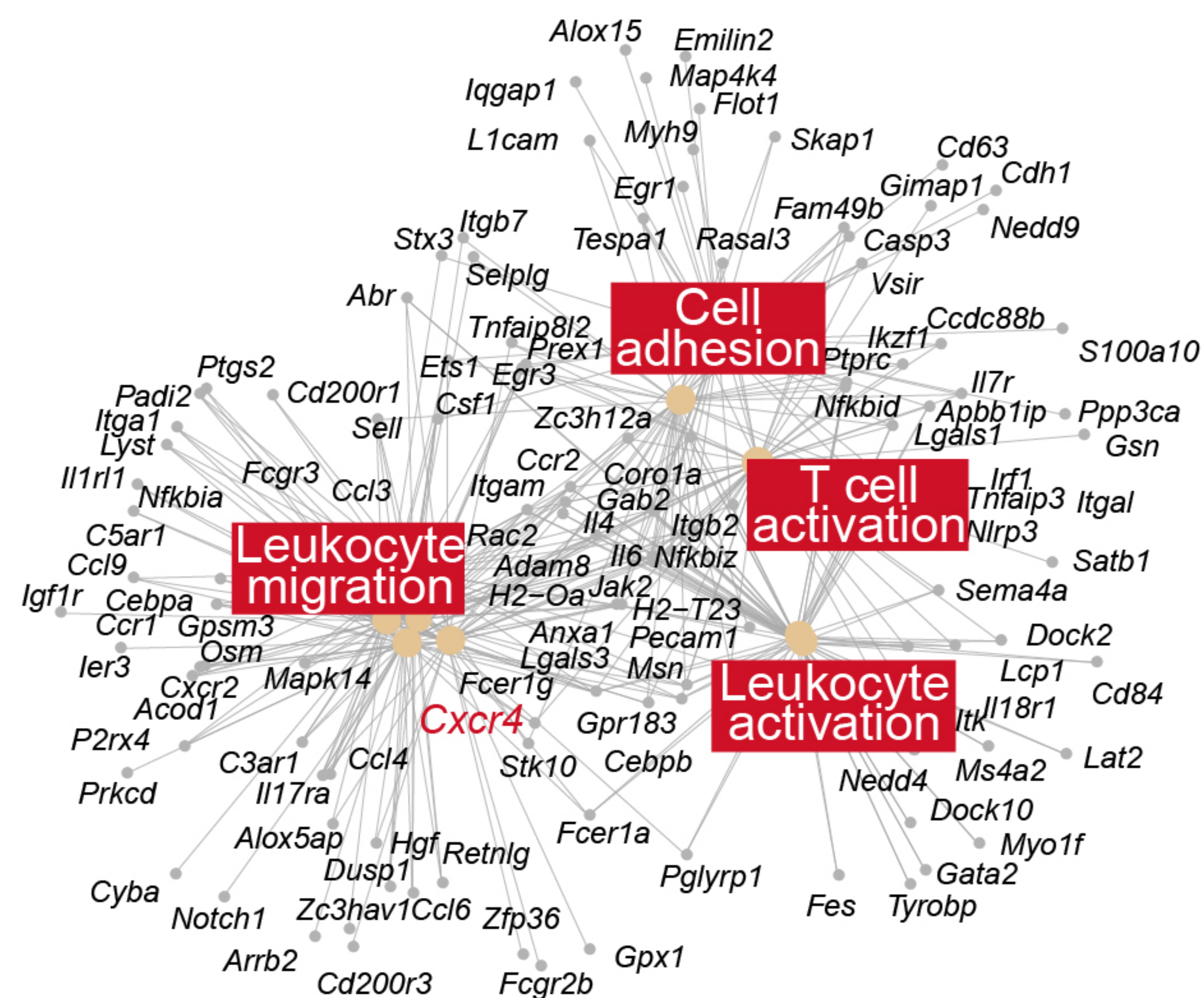


A**B****C****D**

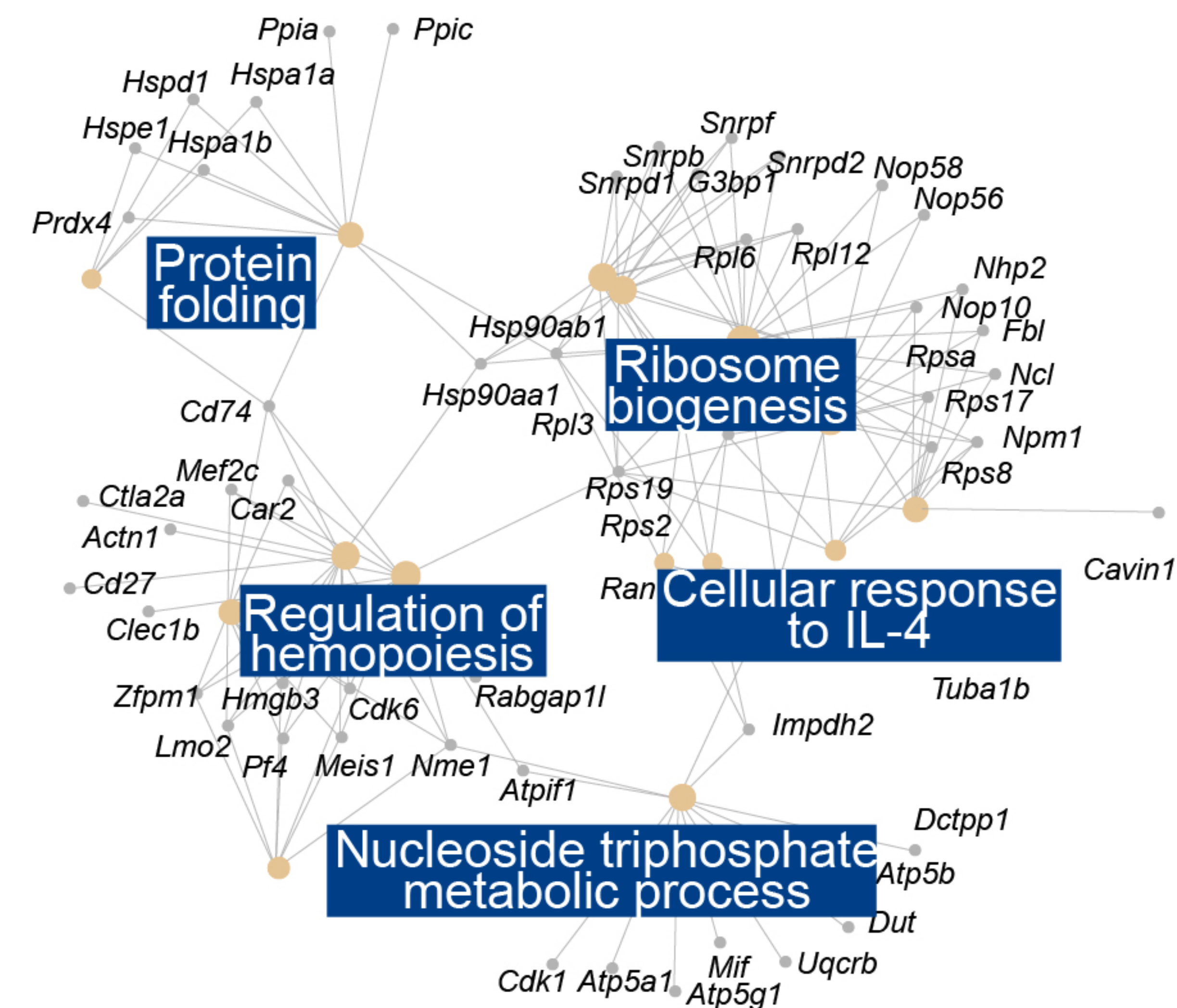
A



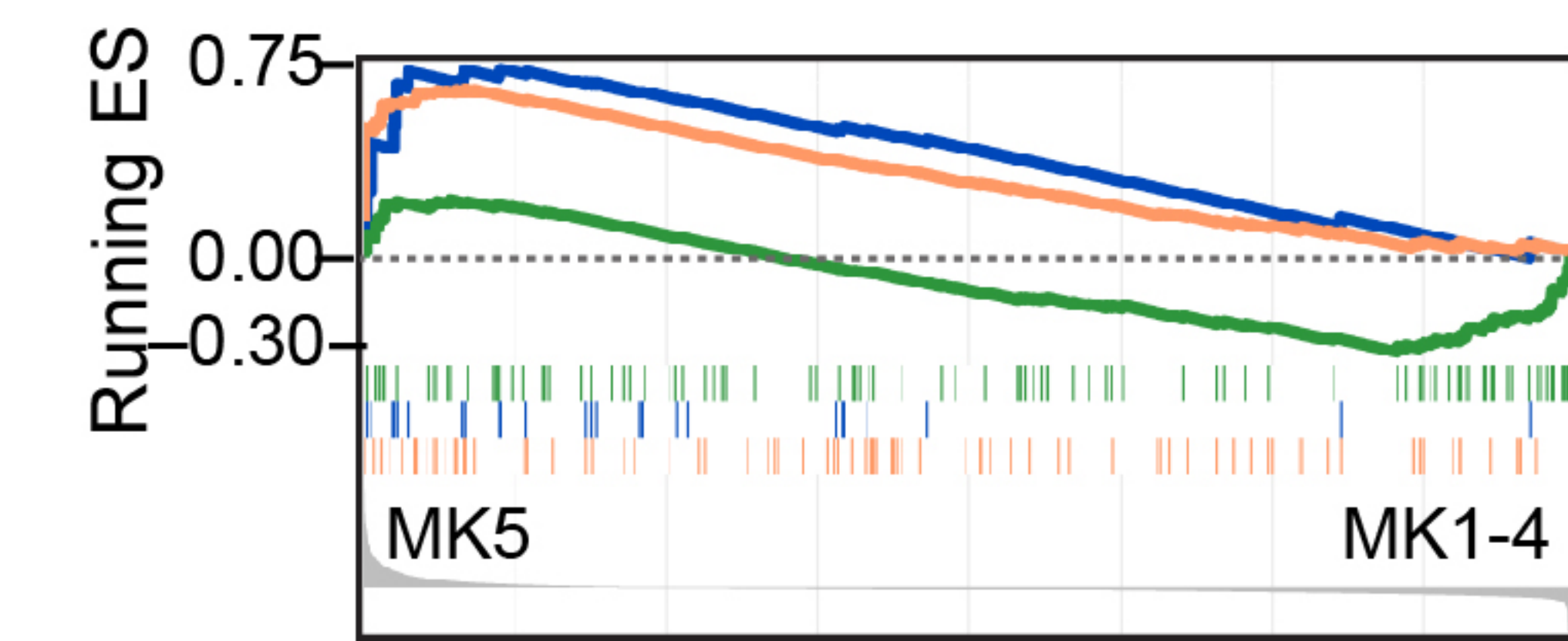
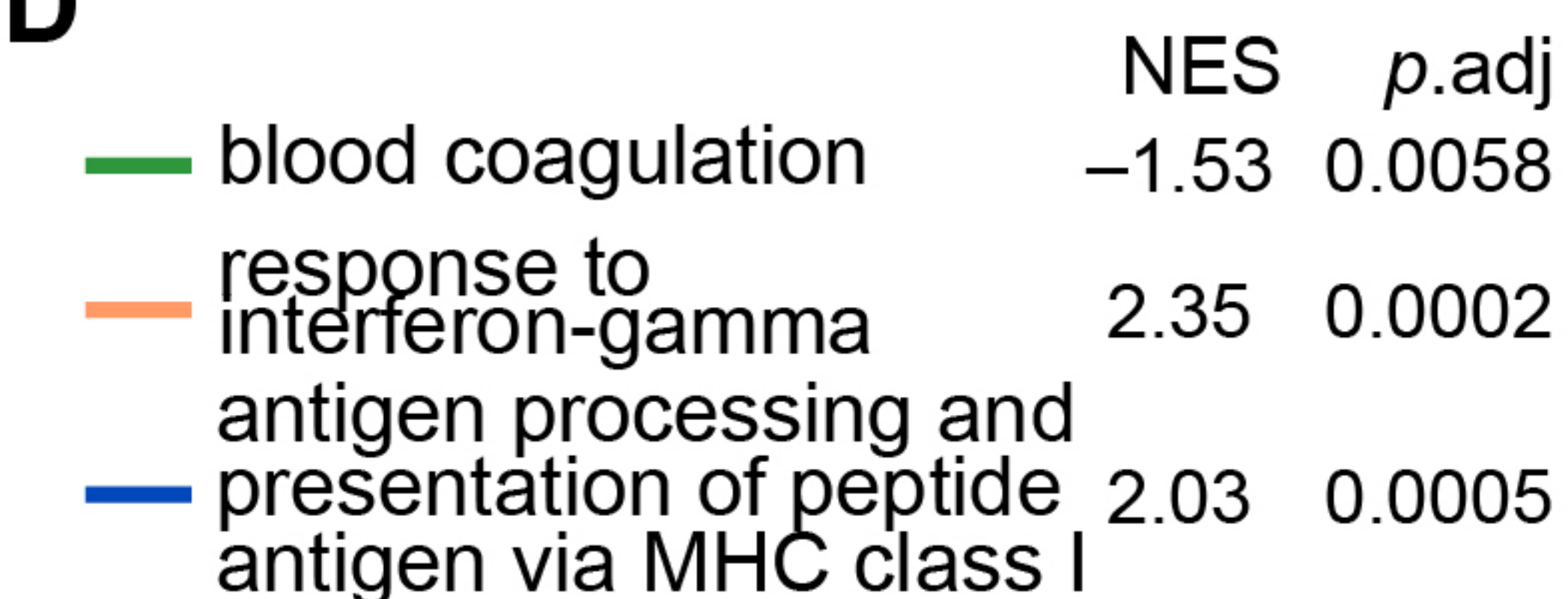
B



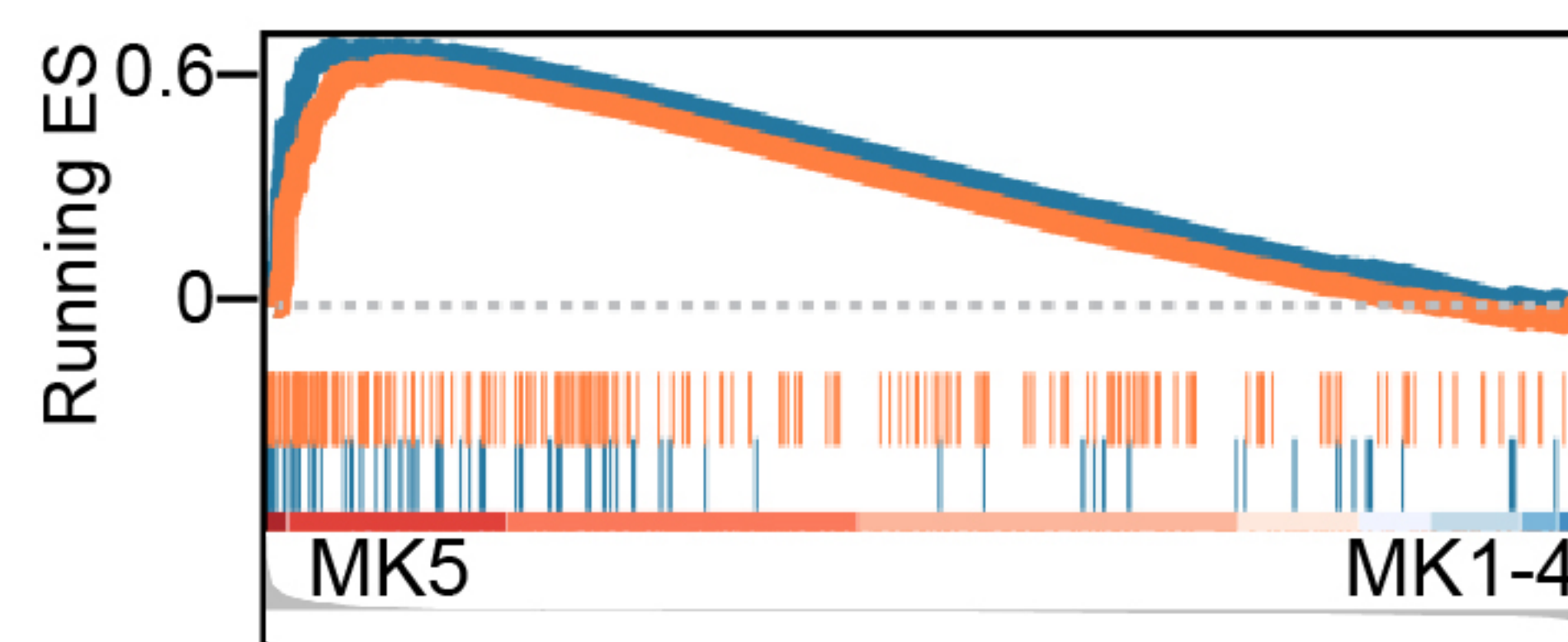
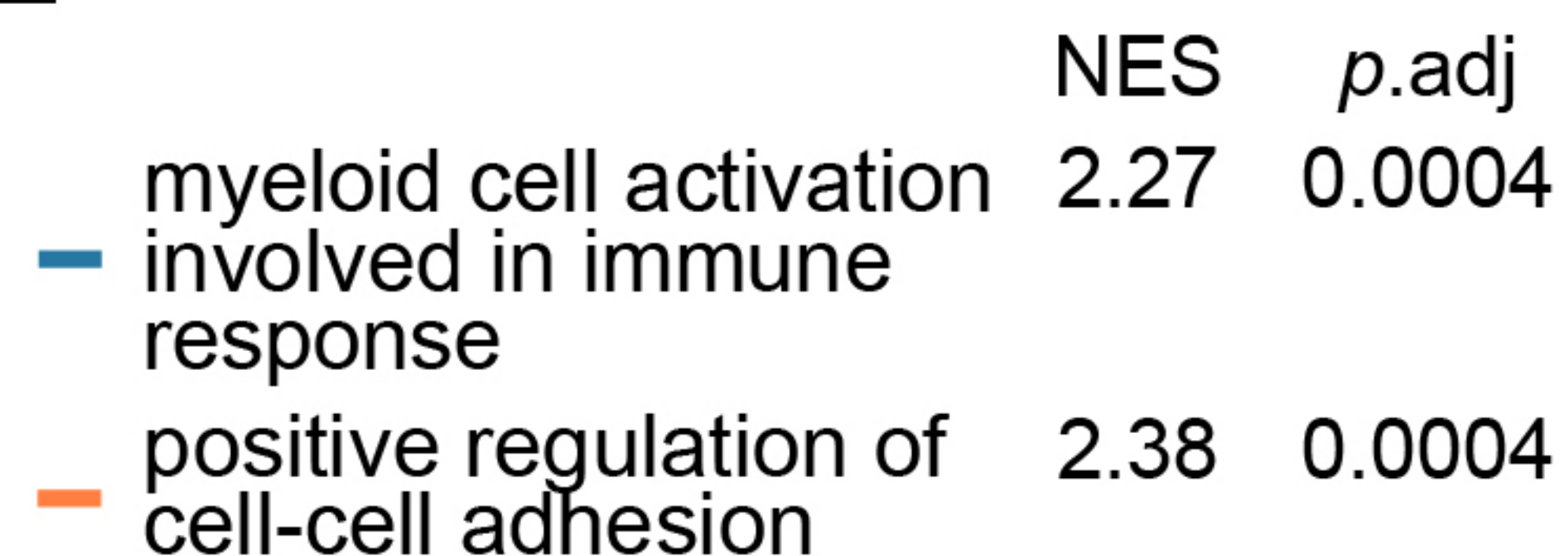
C



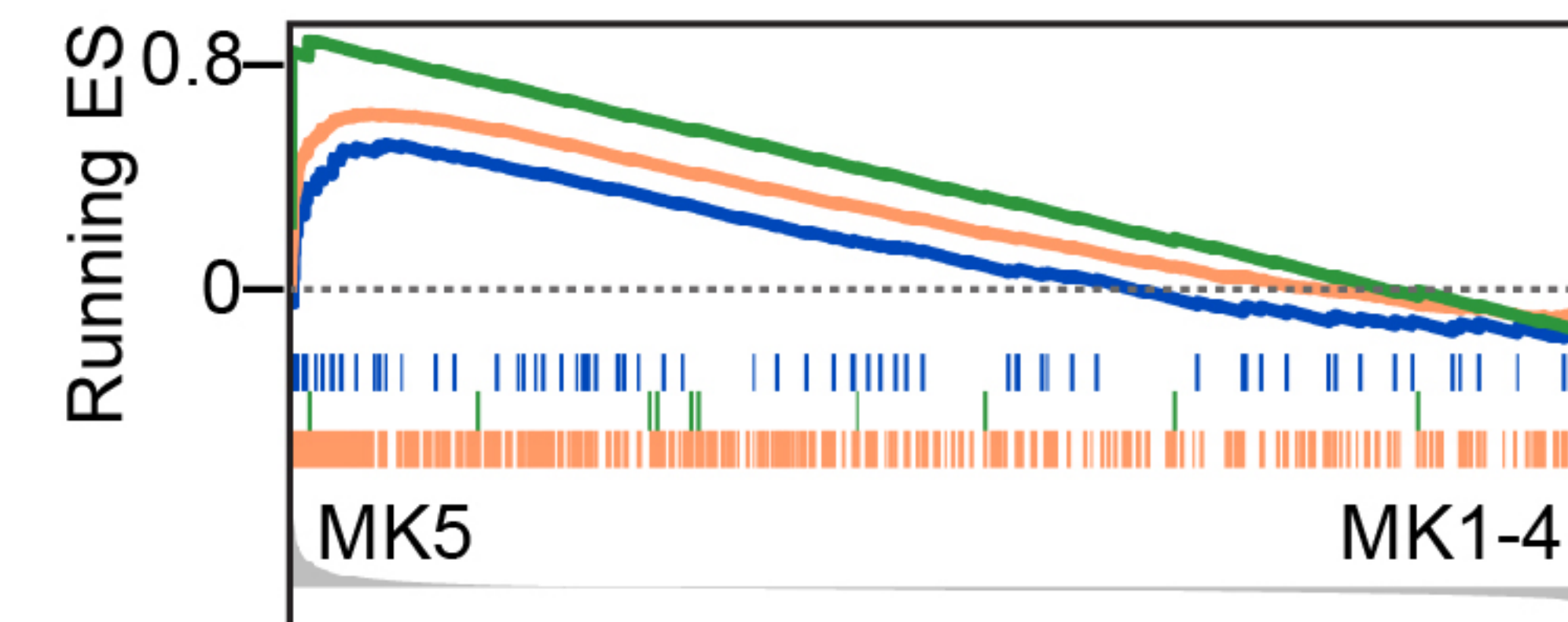
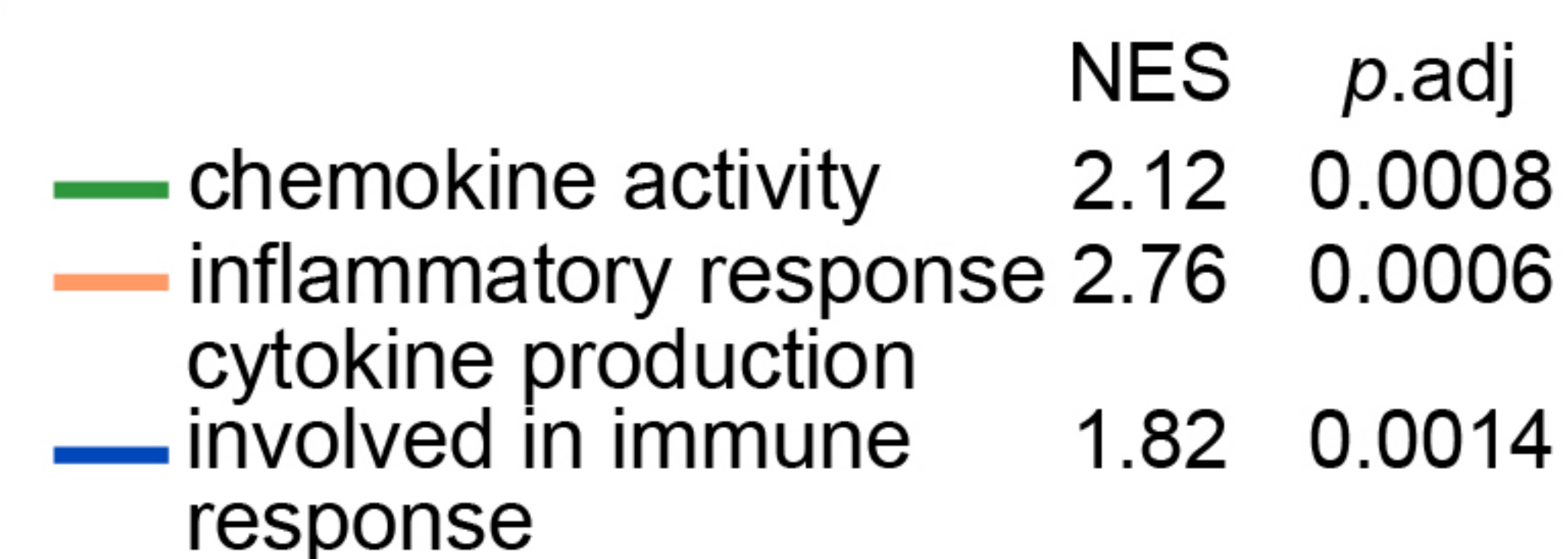
D

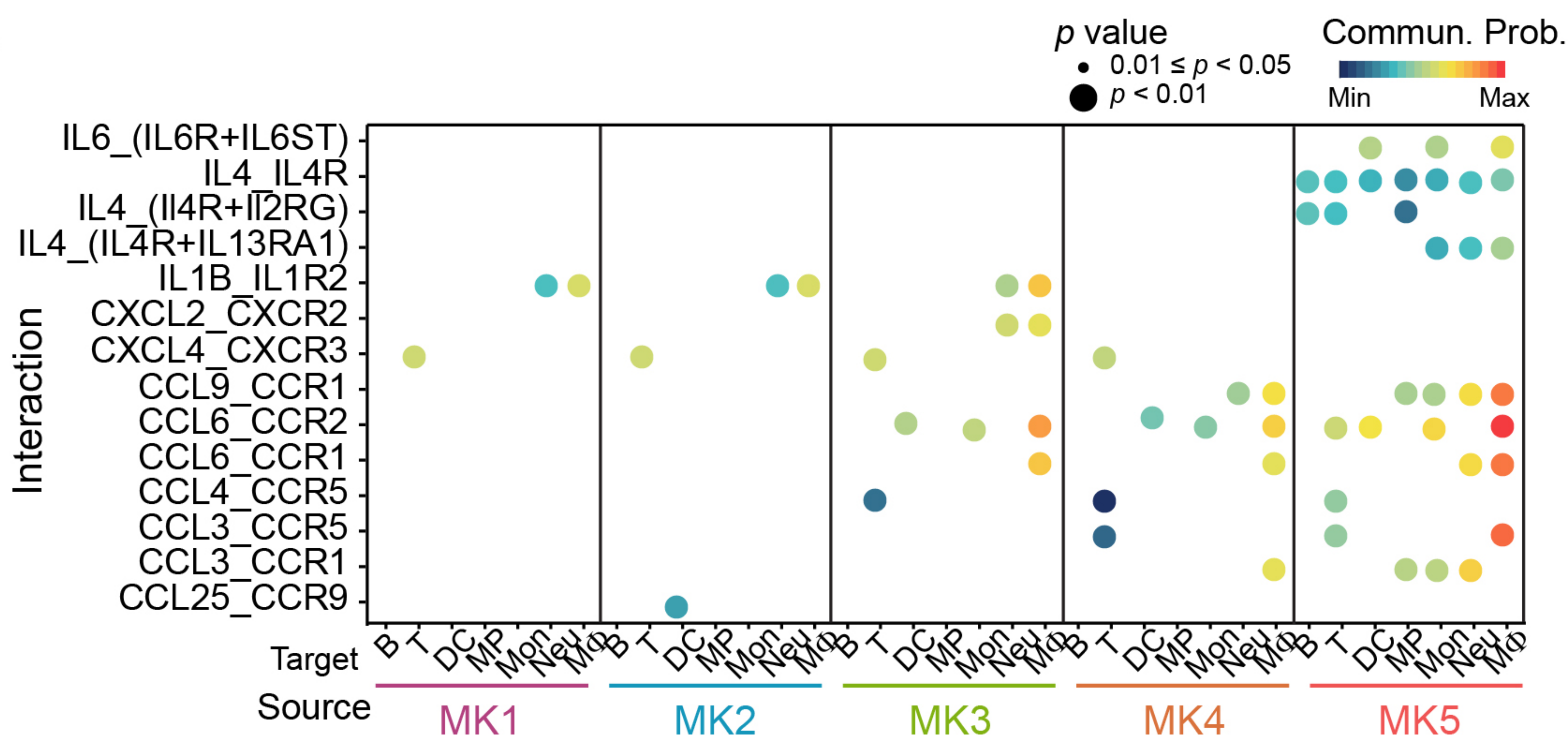
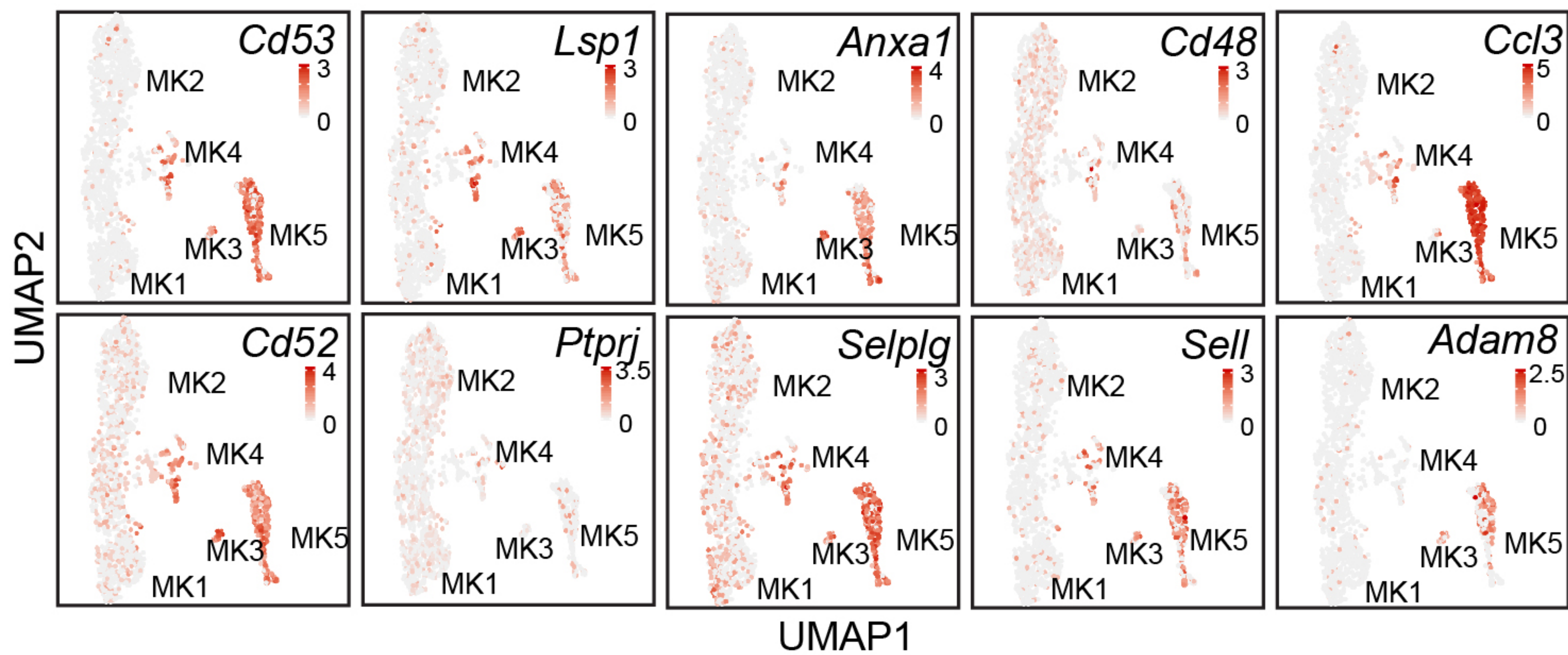


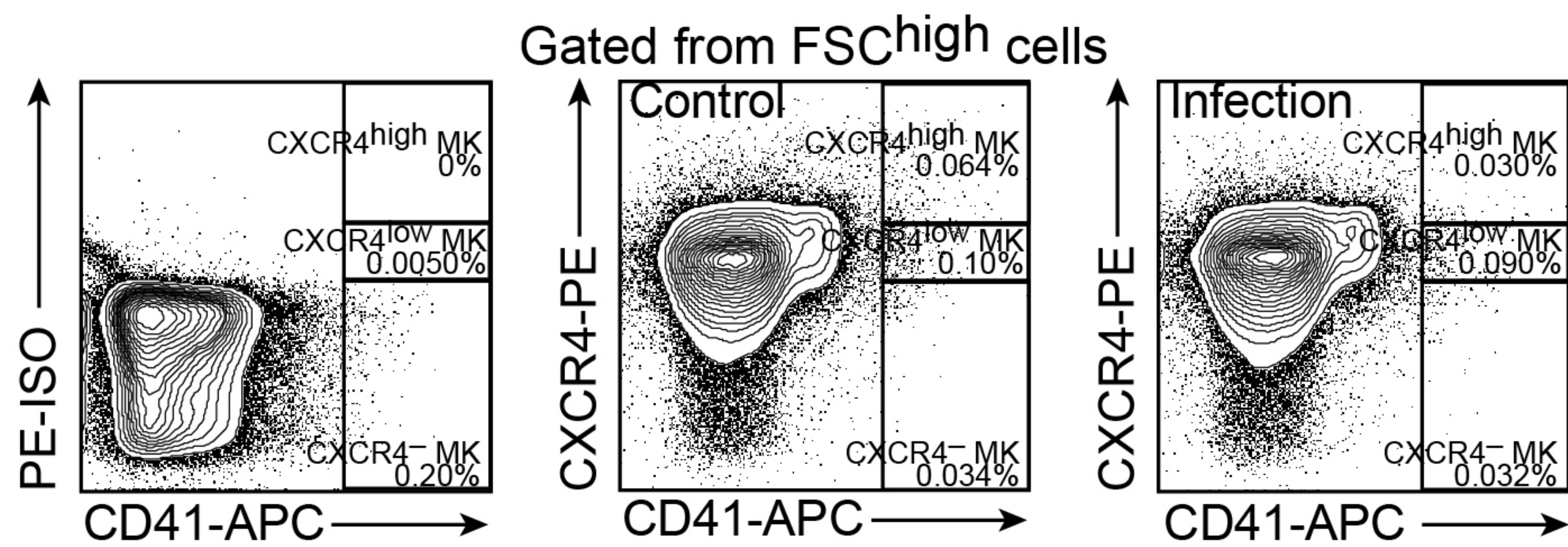
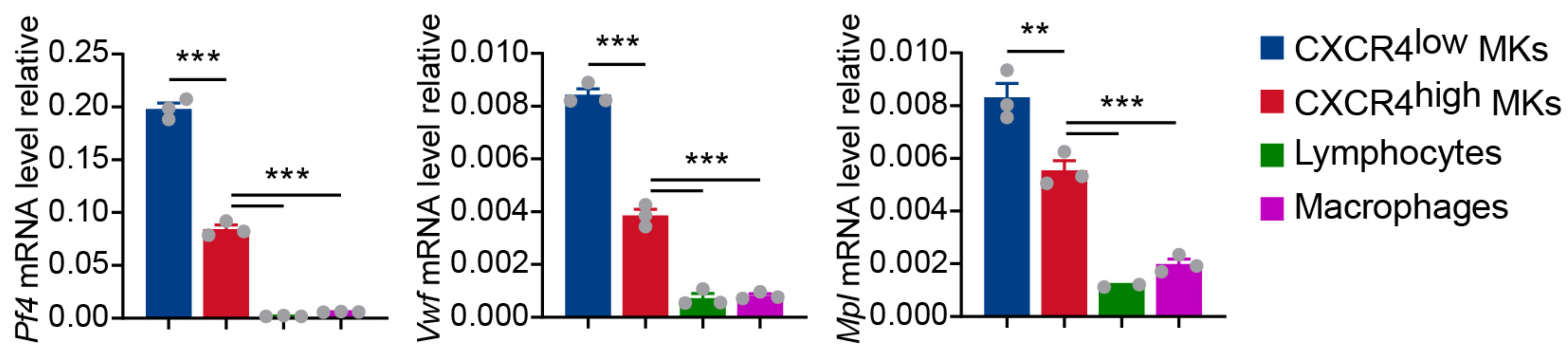
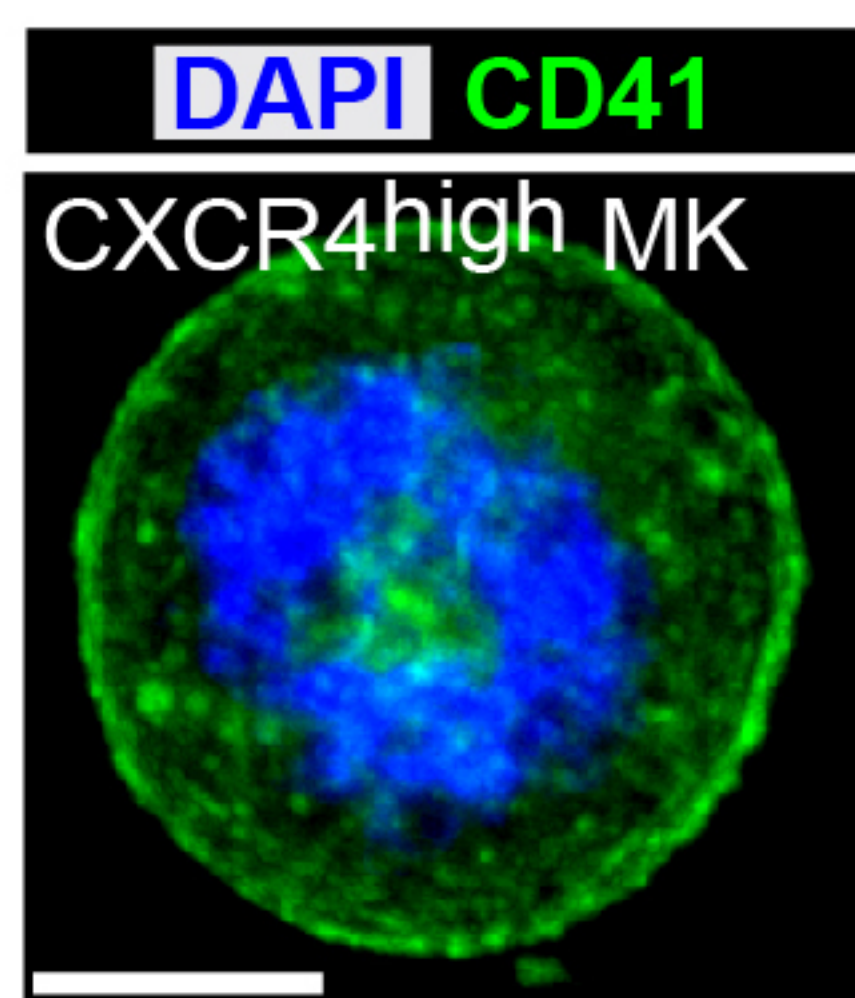
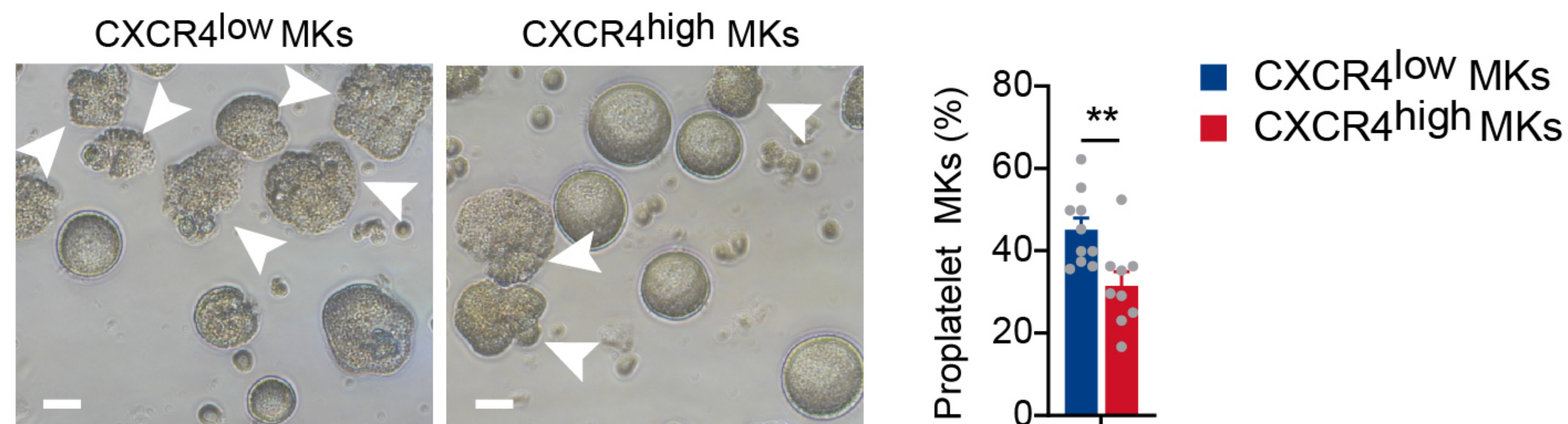
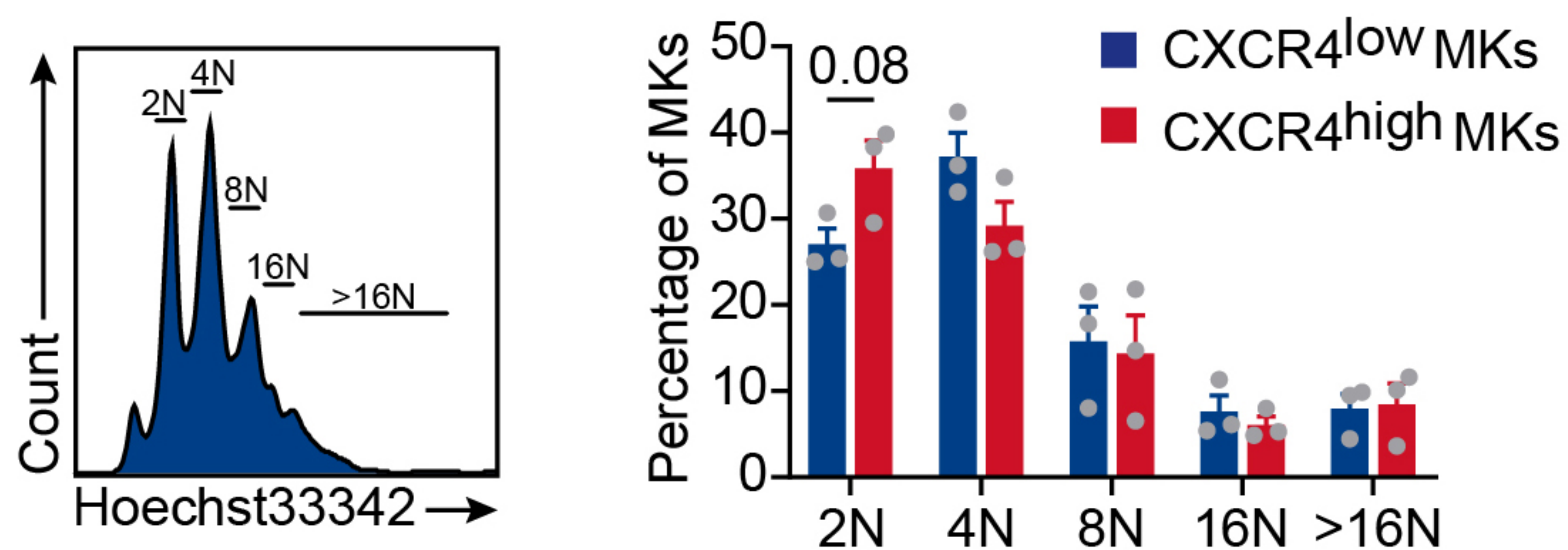
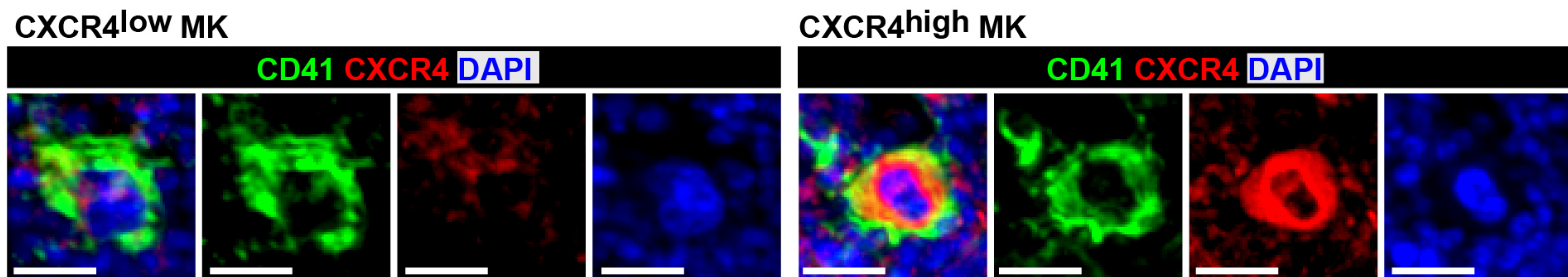
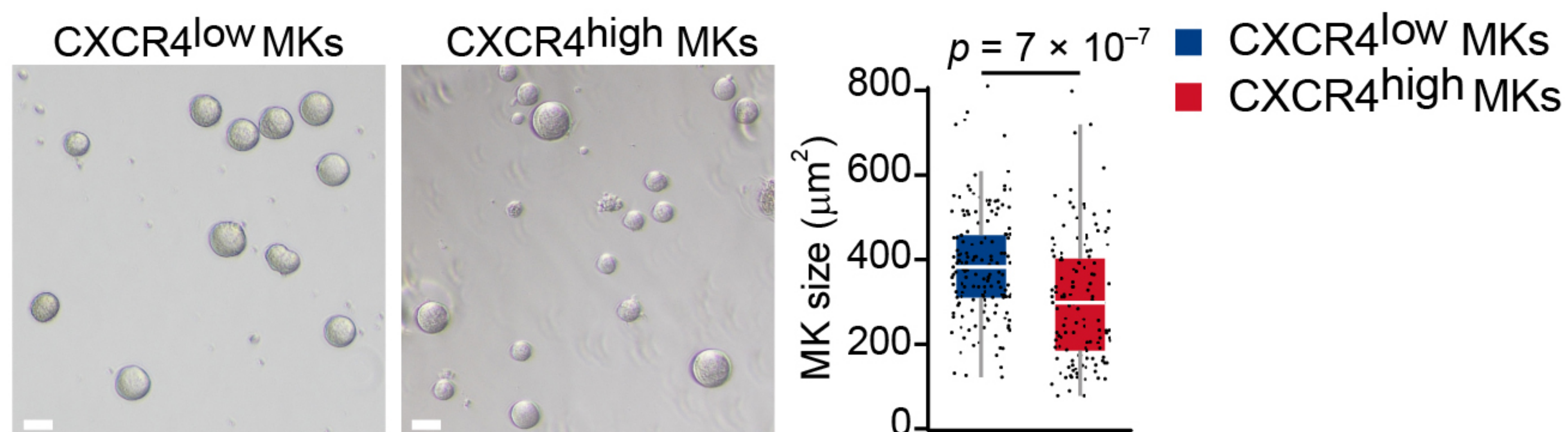
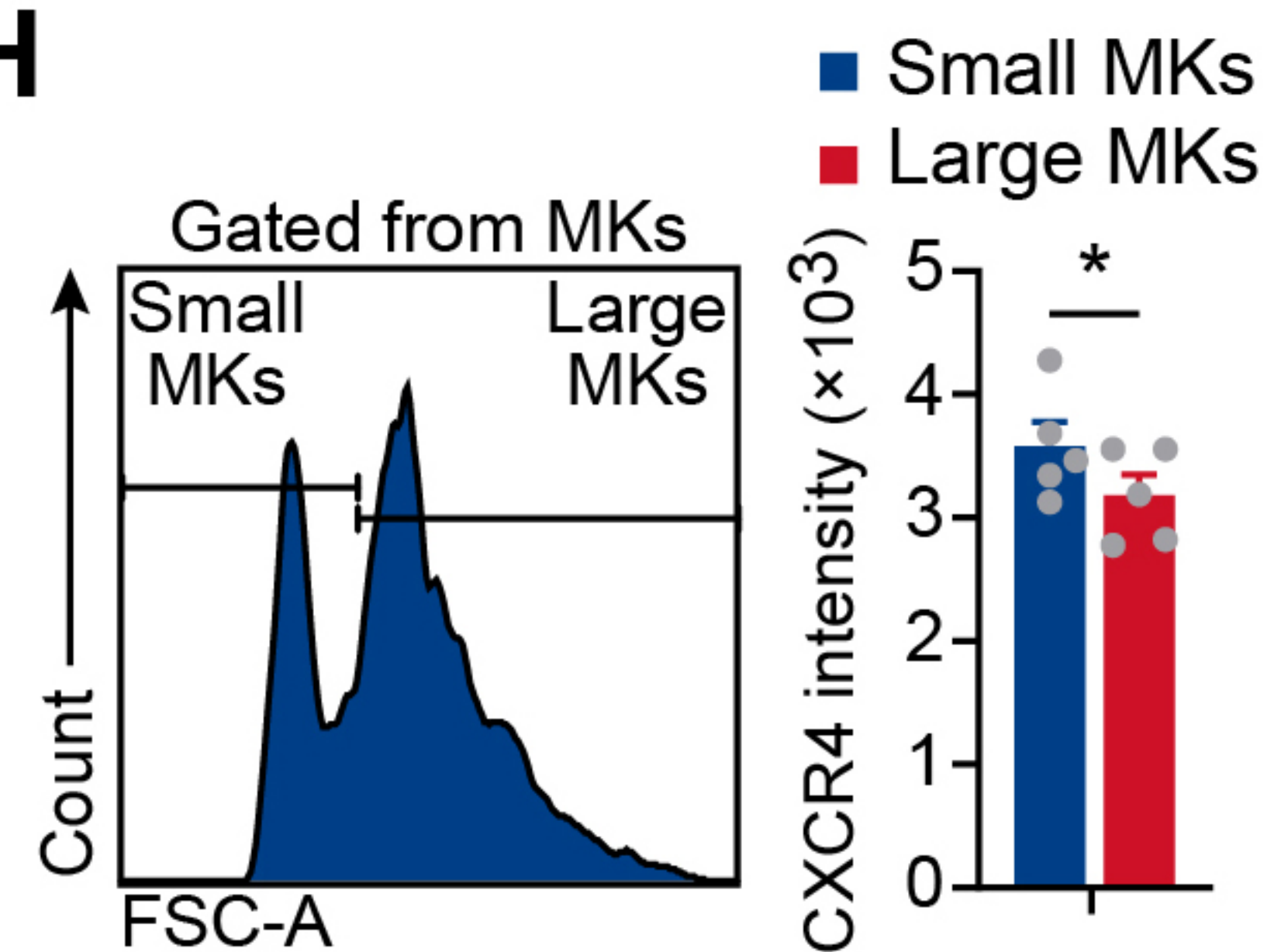
E

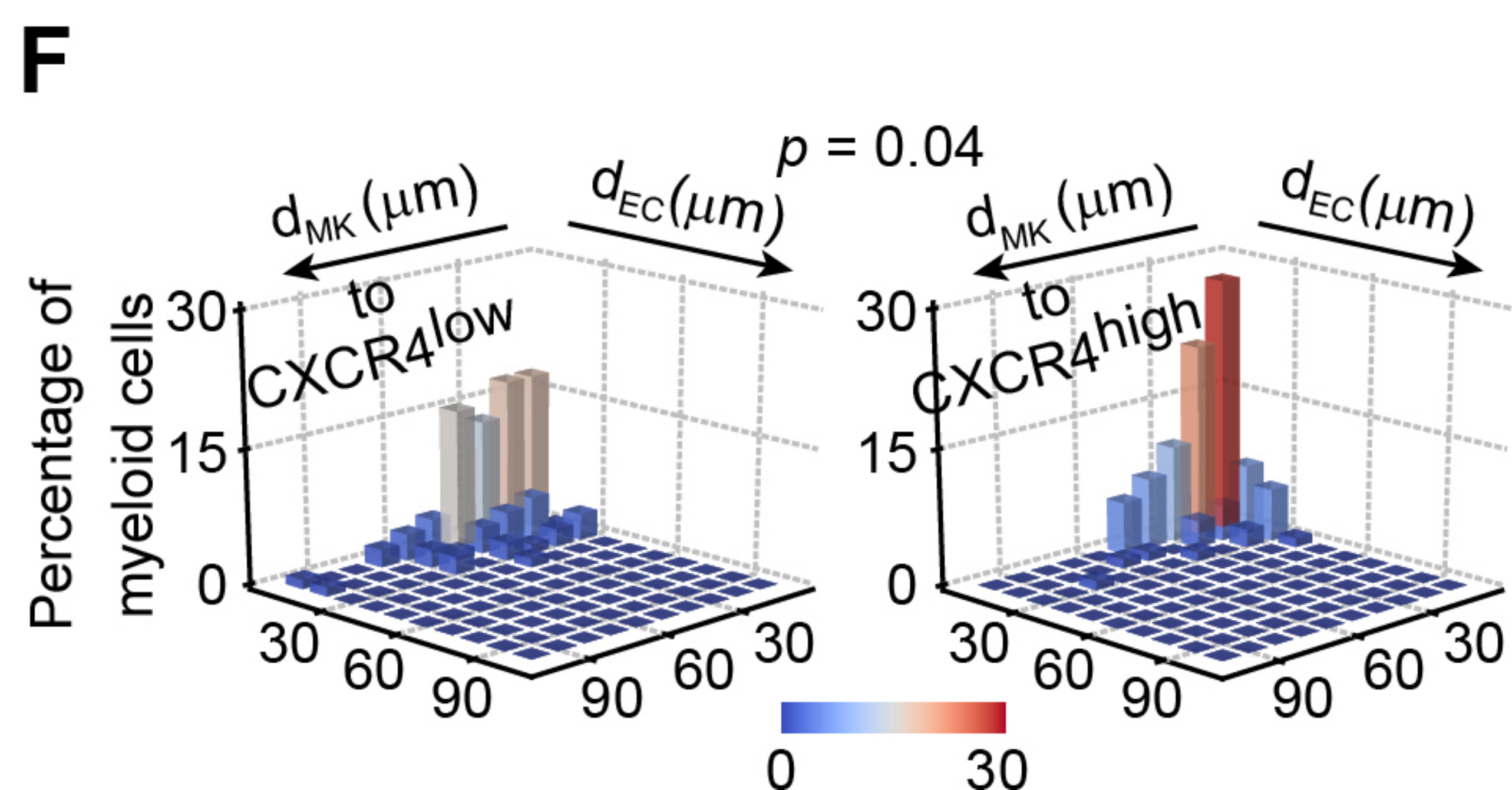
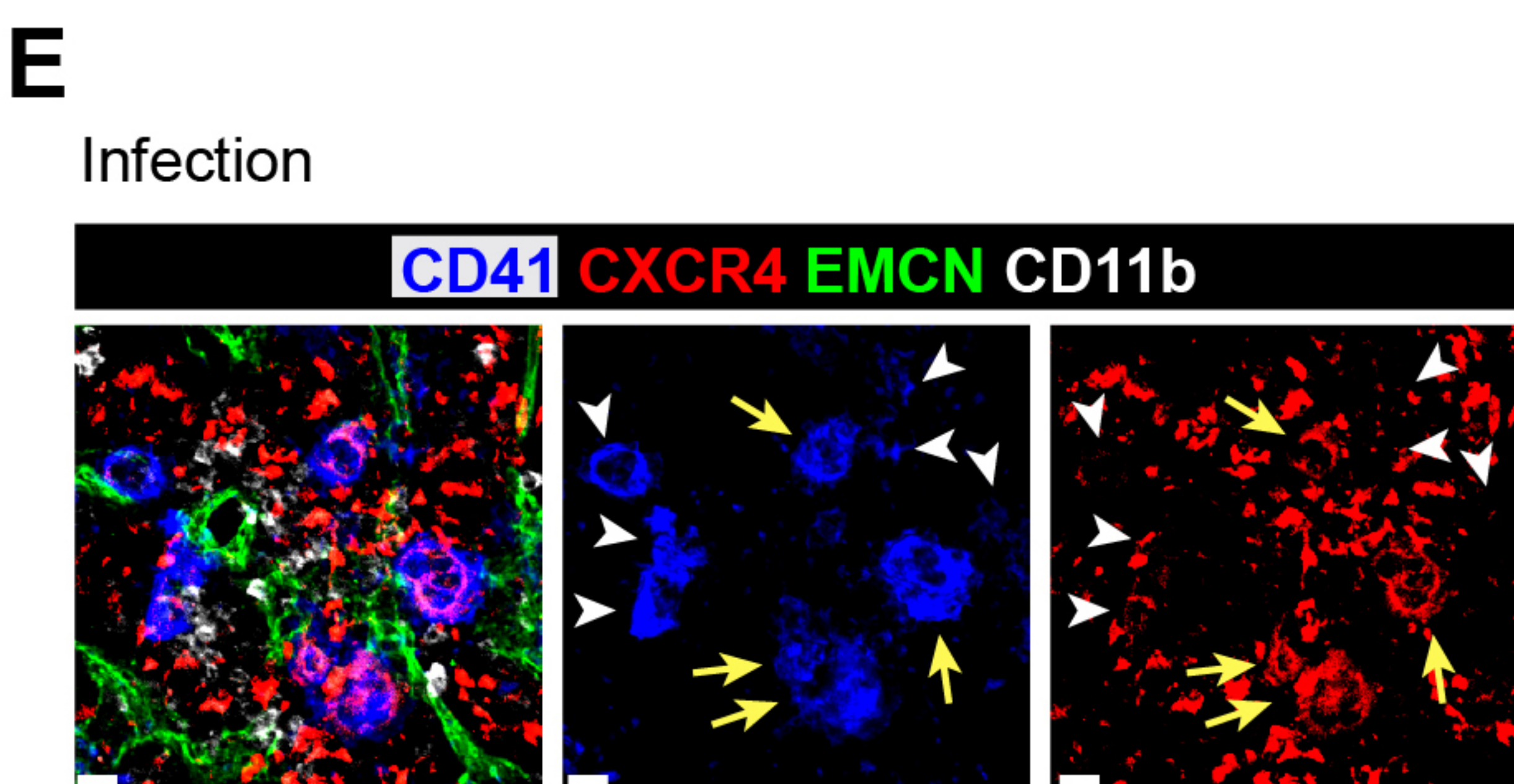
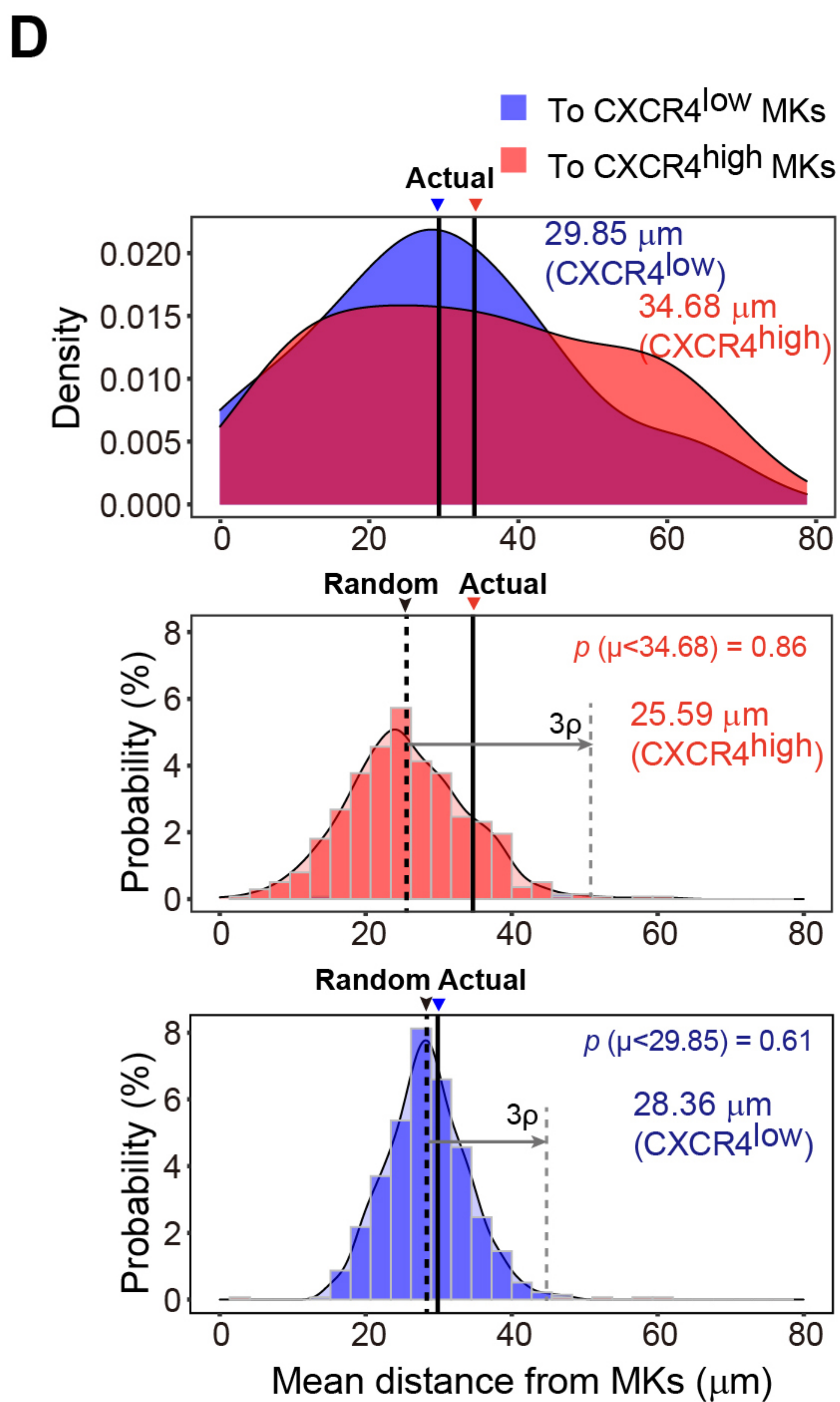
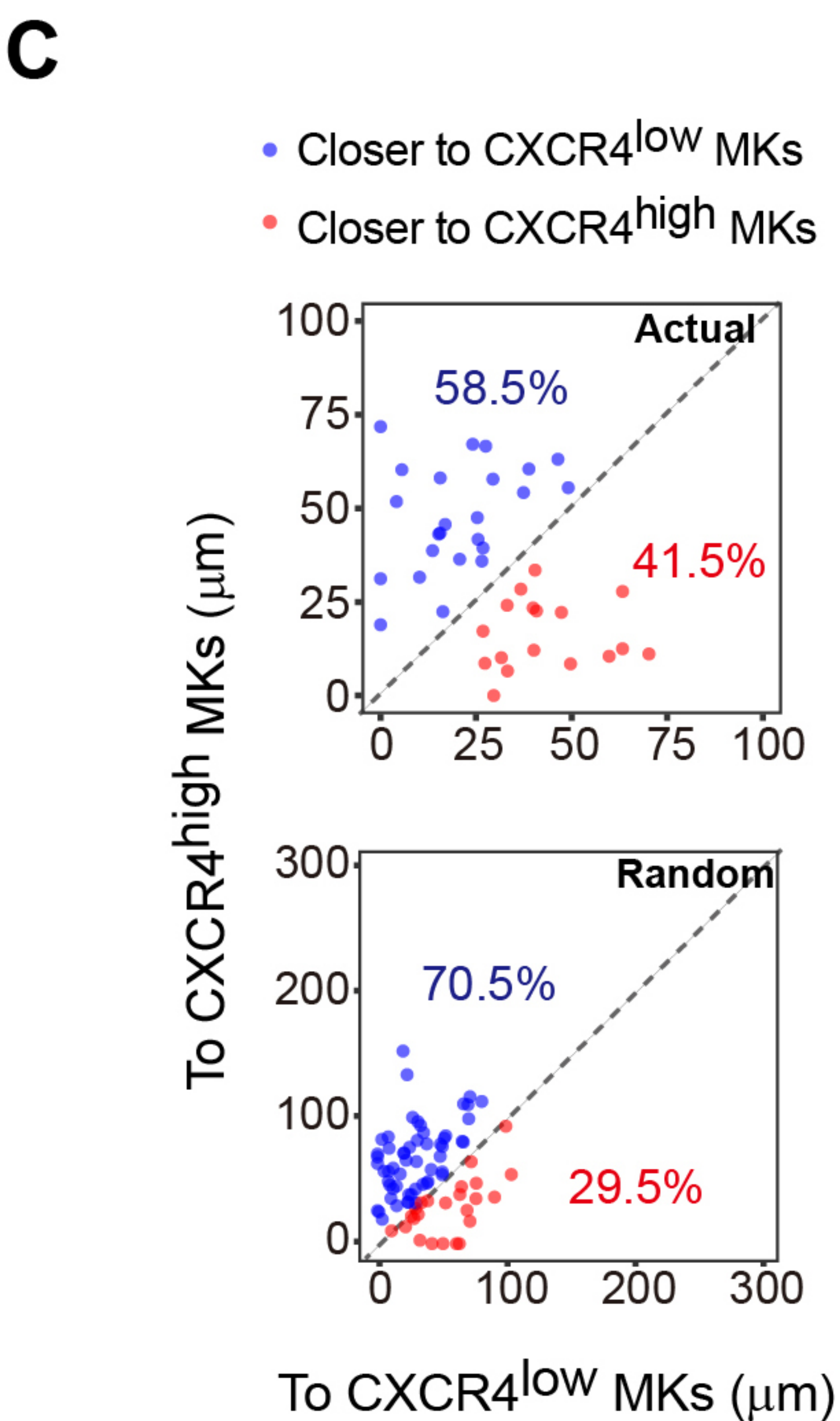
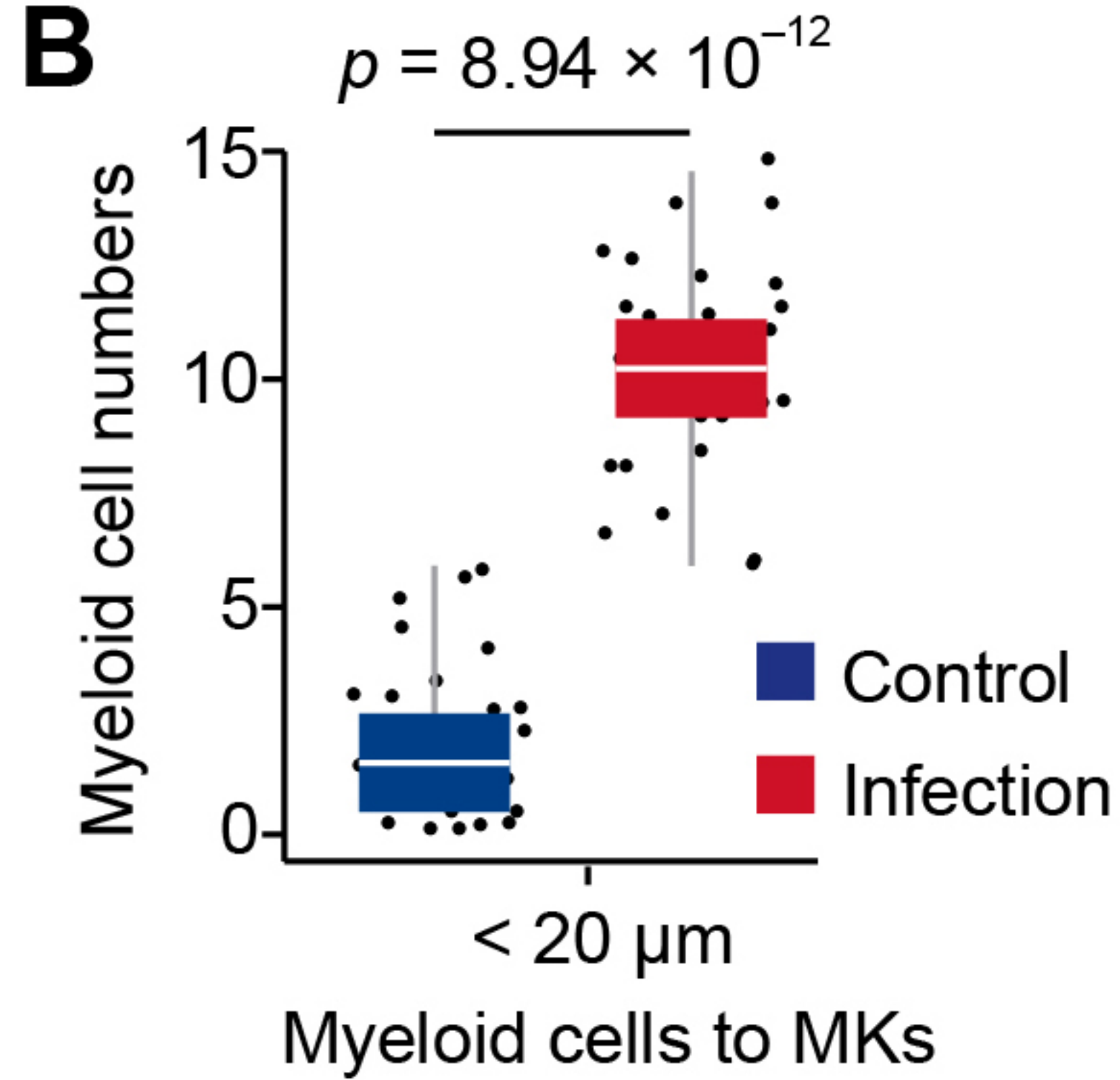
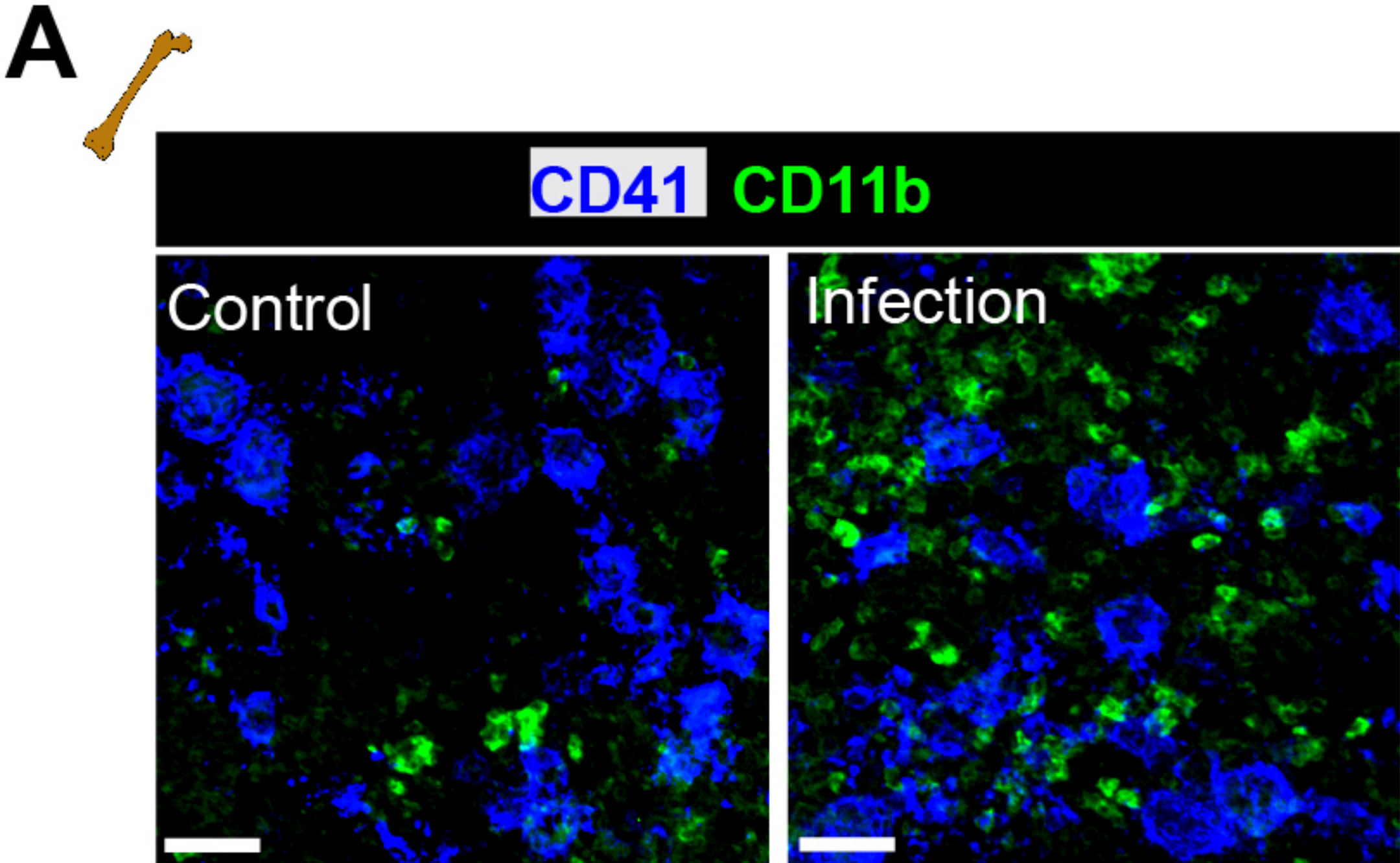


F



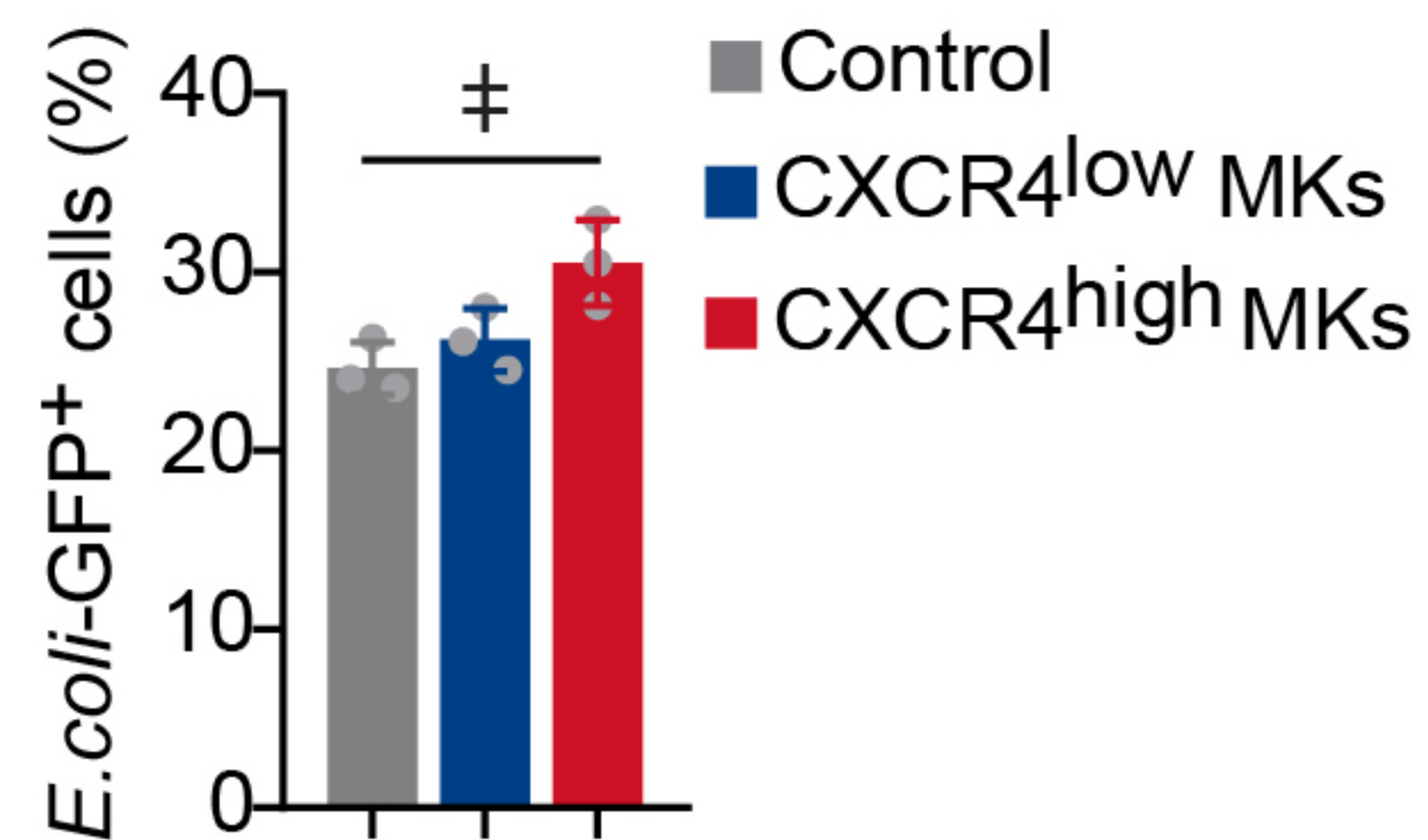
A**B**

A**B****C****D****E****F****G****H**

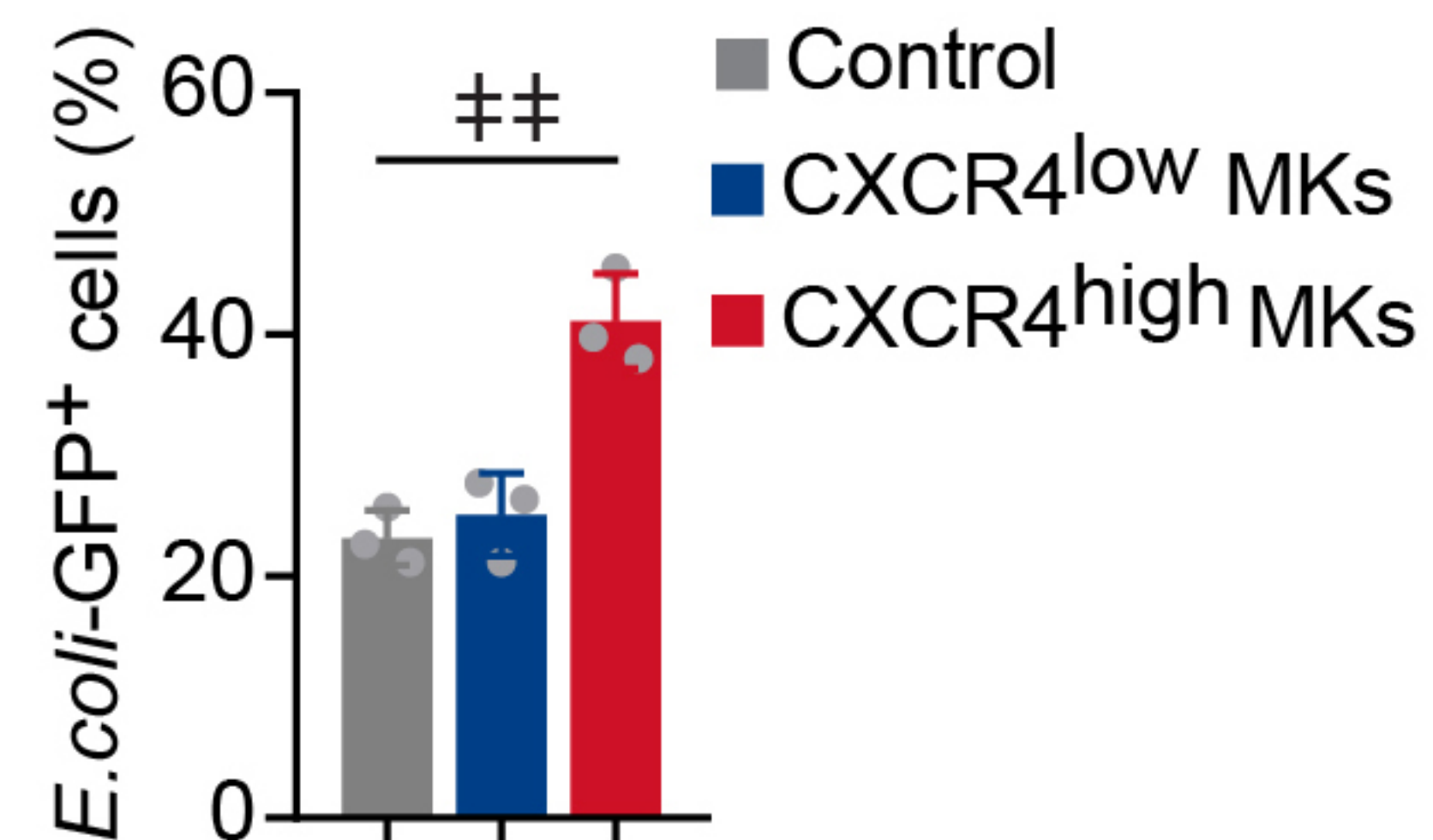
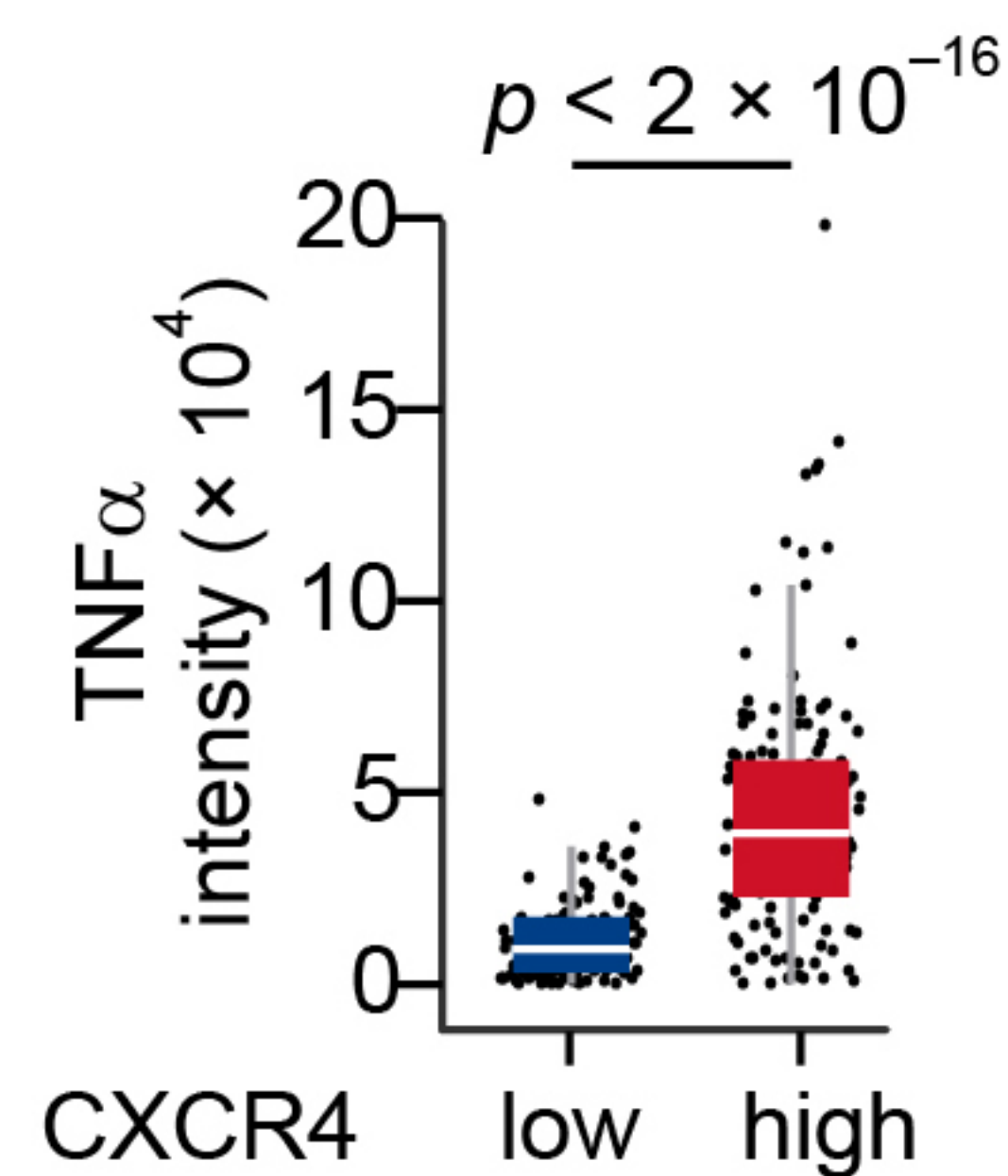
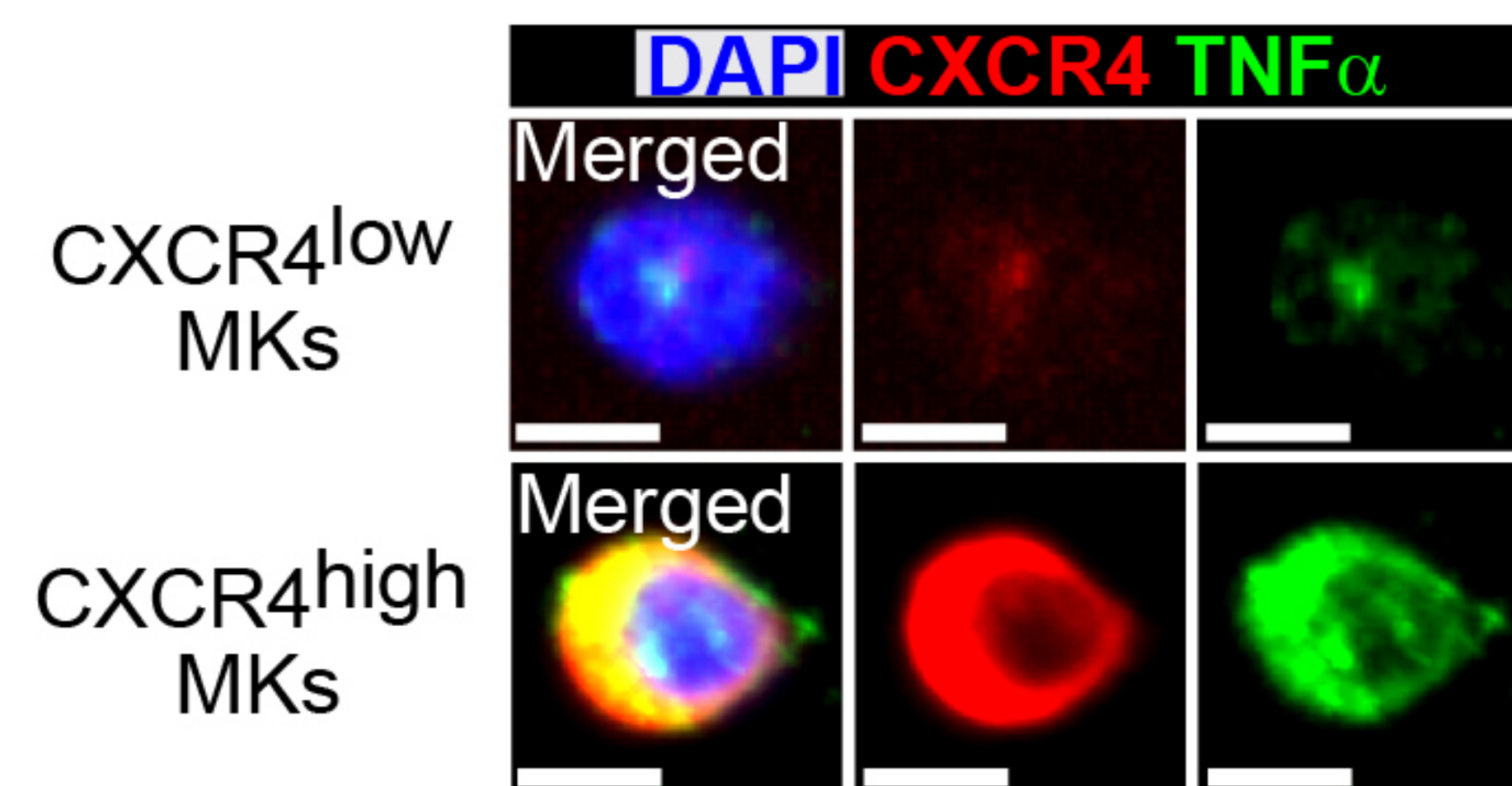
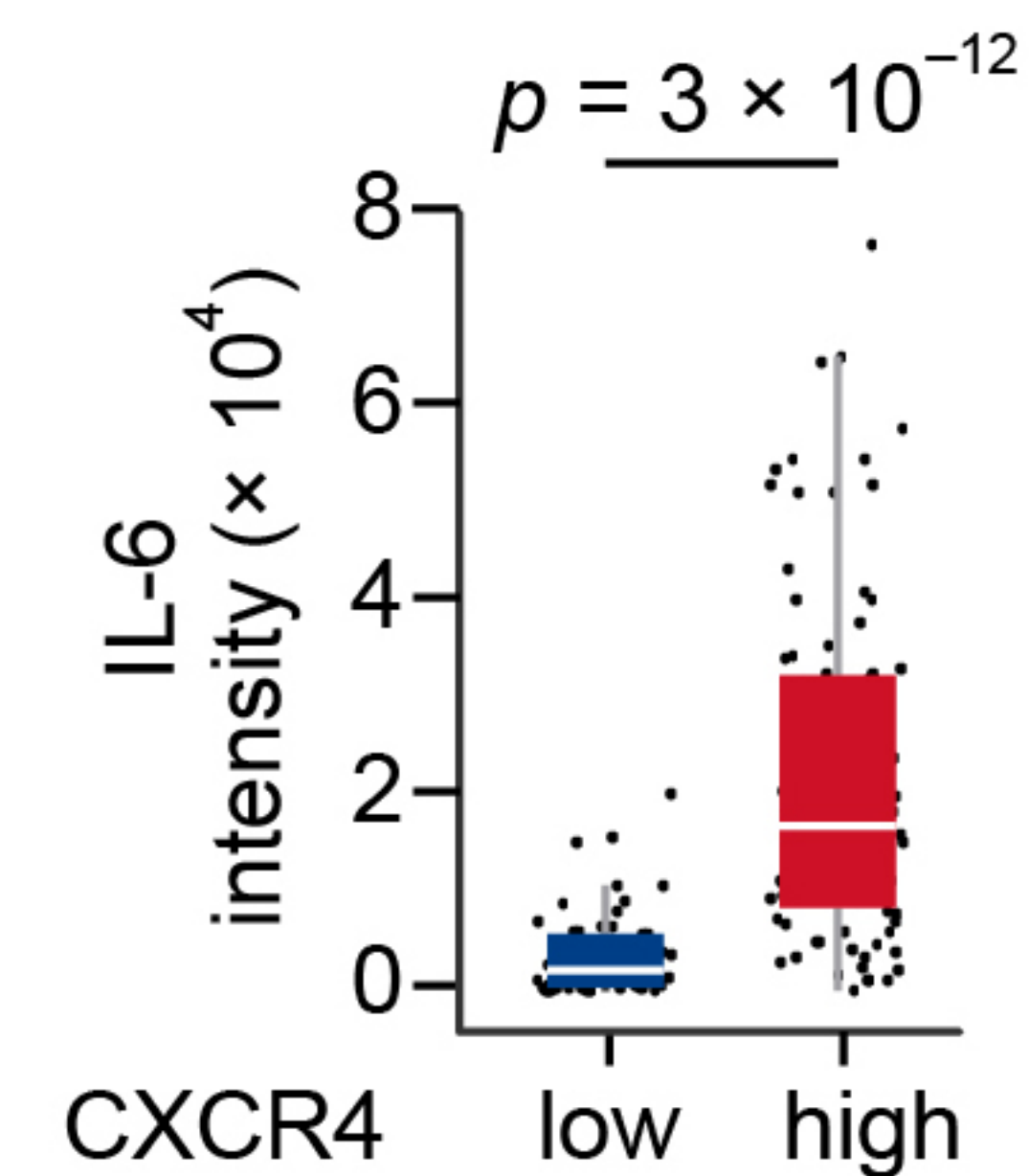
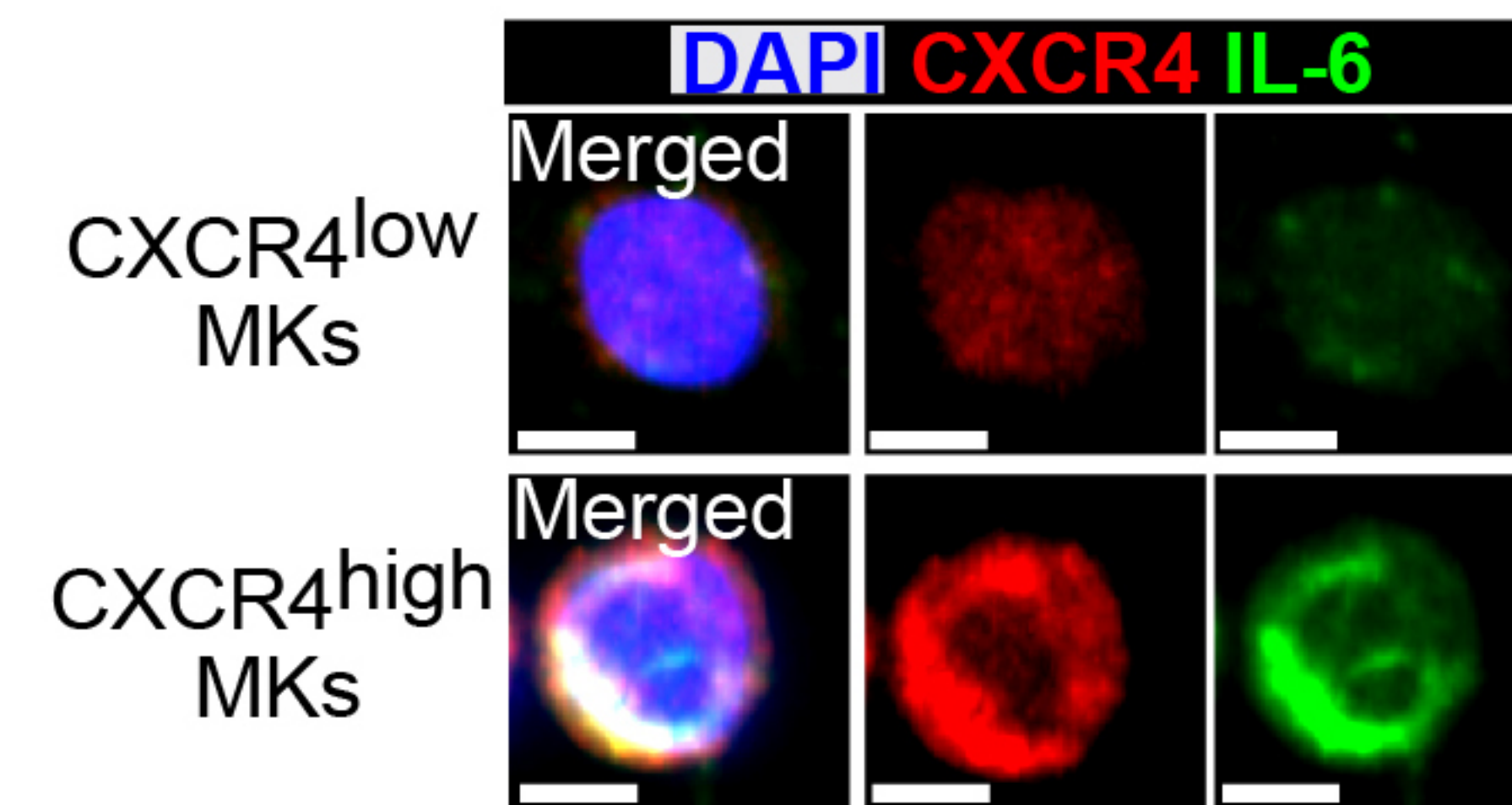
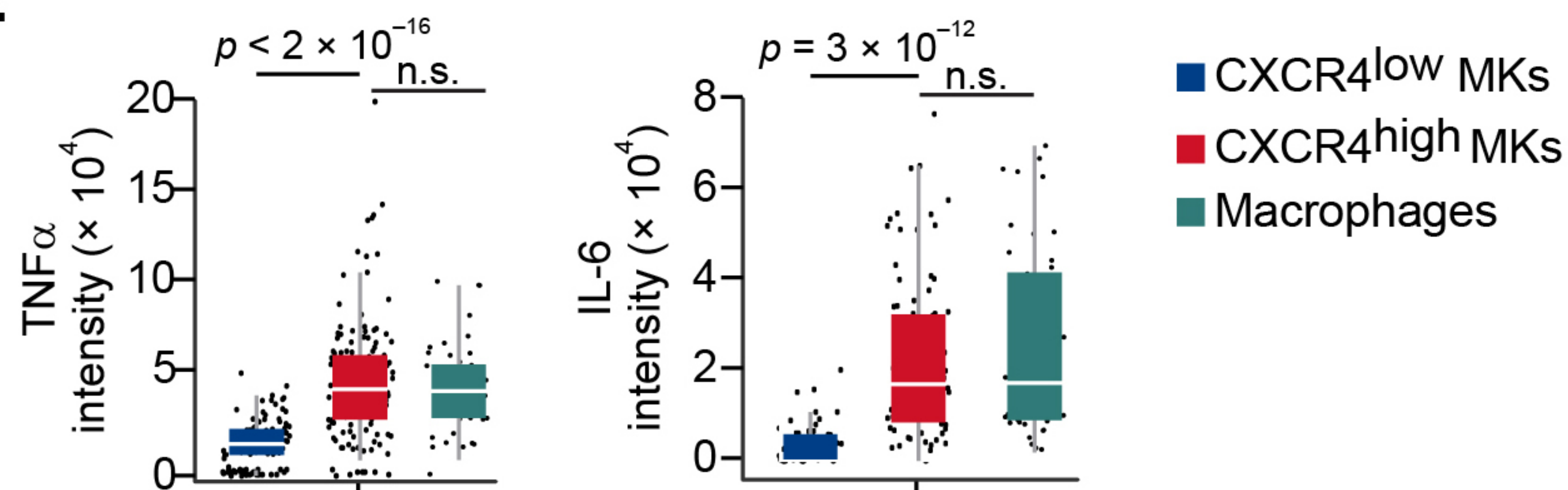


A

Neutrophil

**B**

Macrophage

**C****D****E**

A

Pf4Cre^{-/-}
Rosa26^{fls-iDTR}+/-

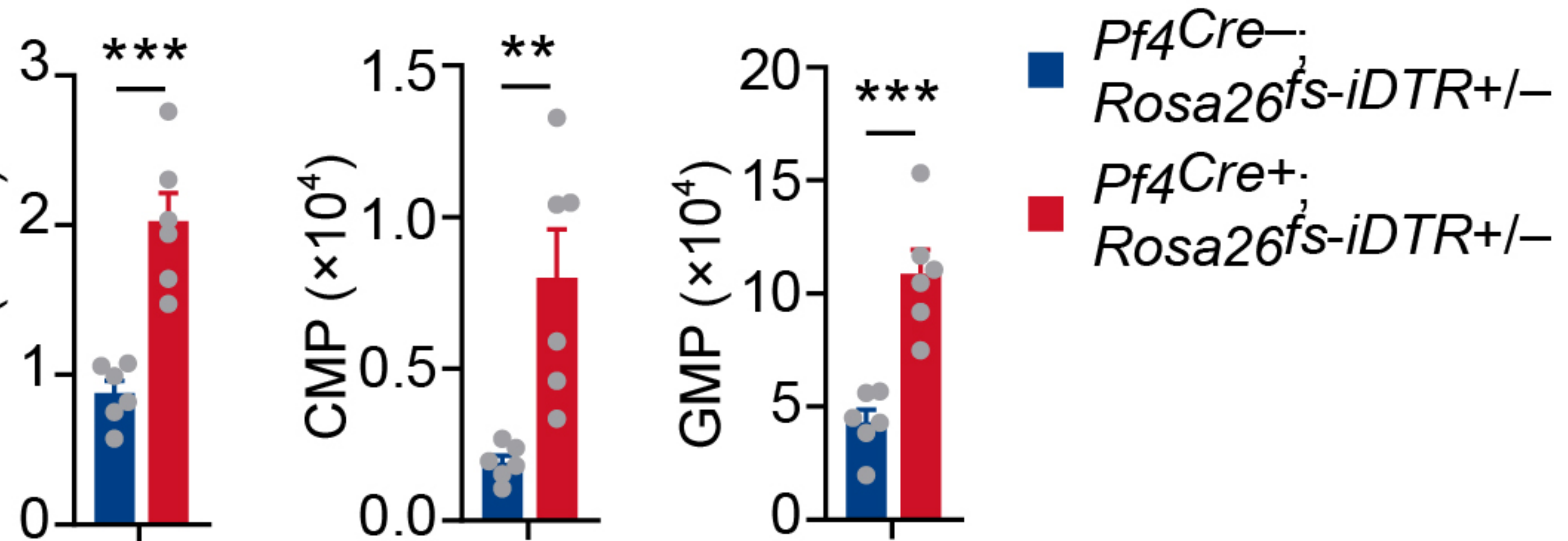
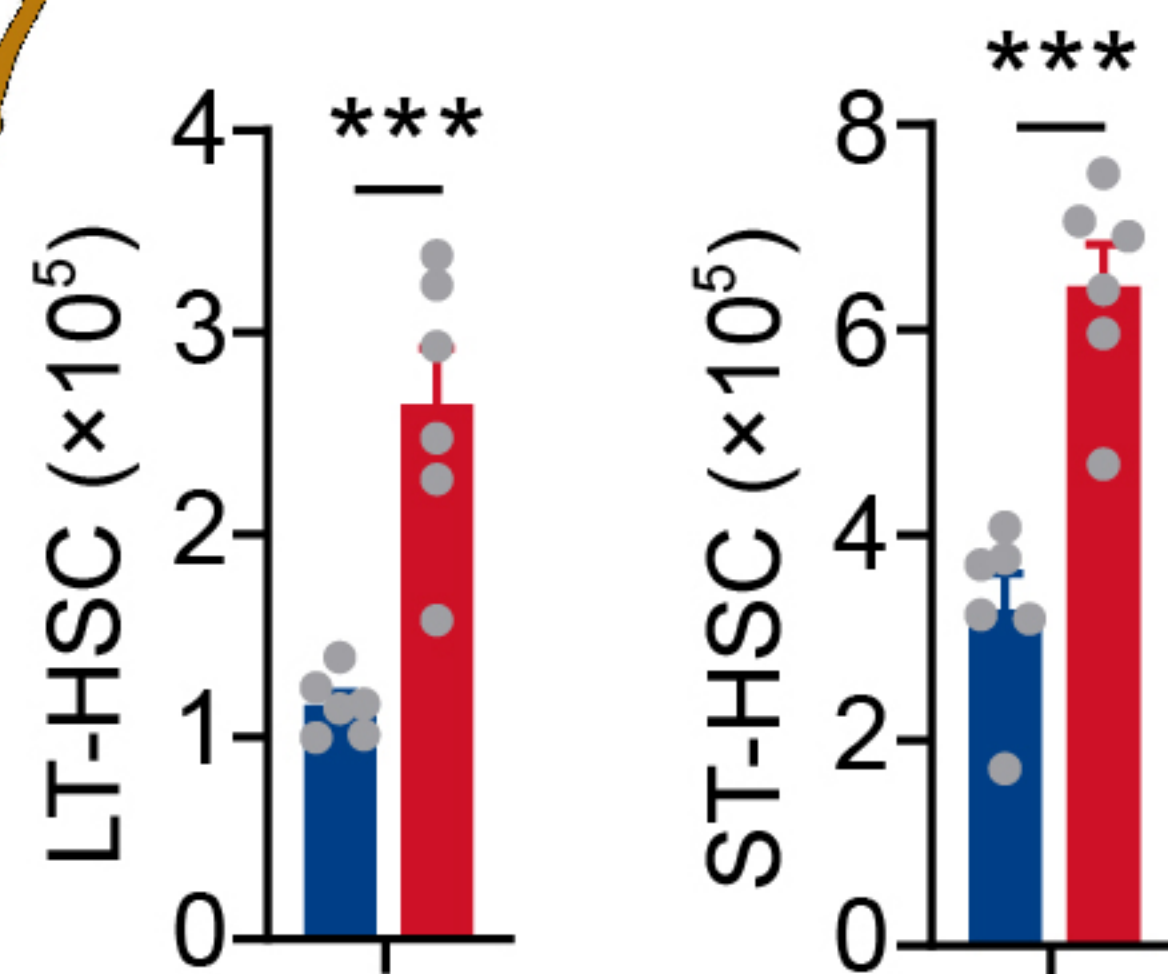
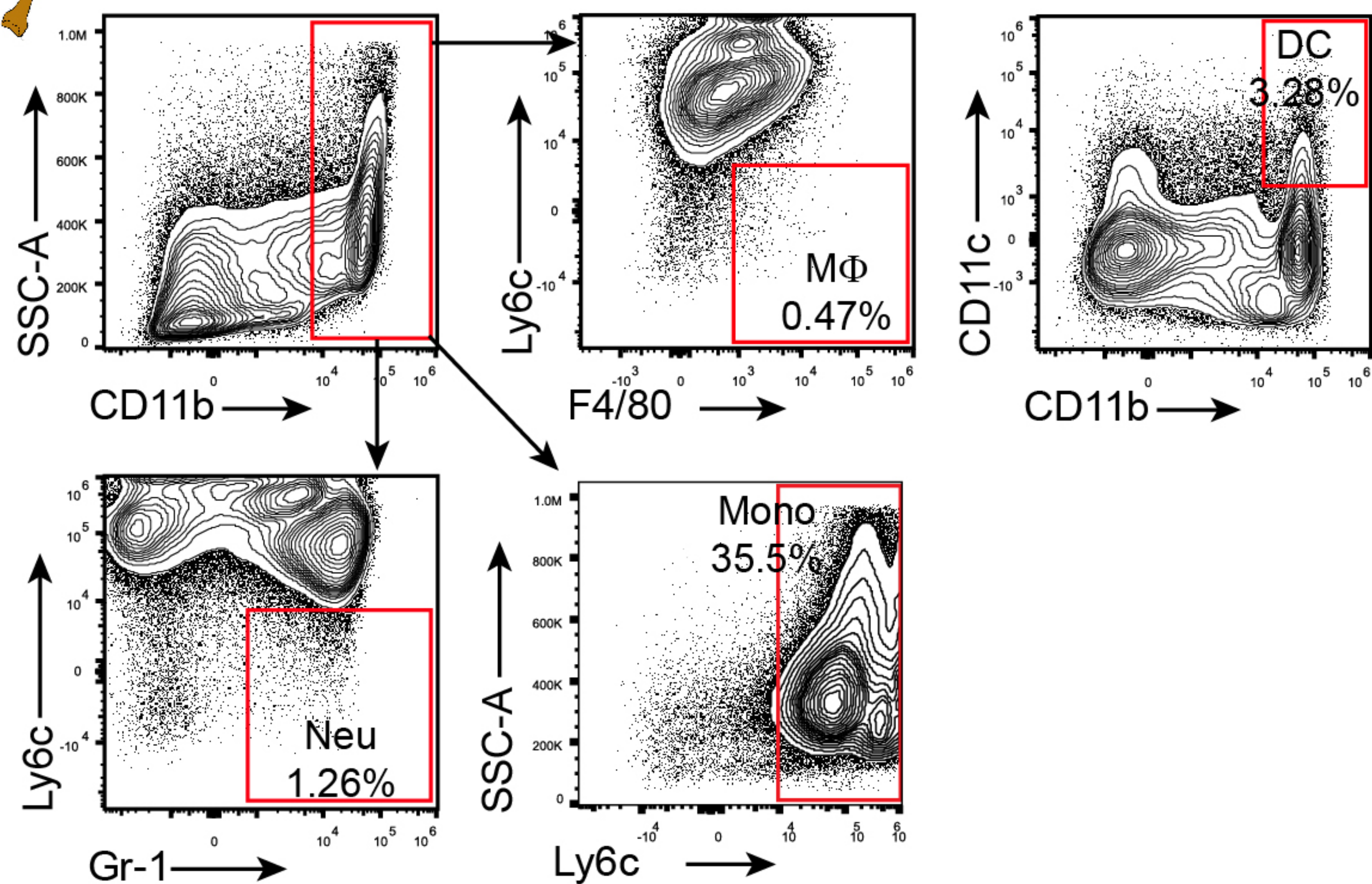
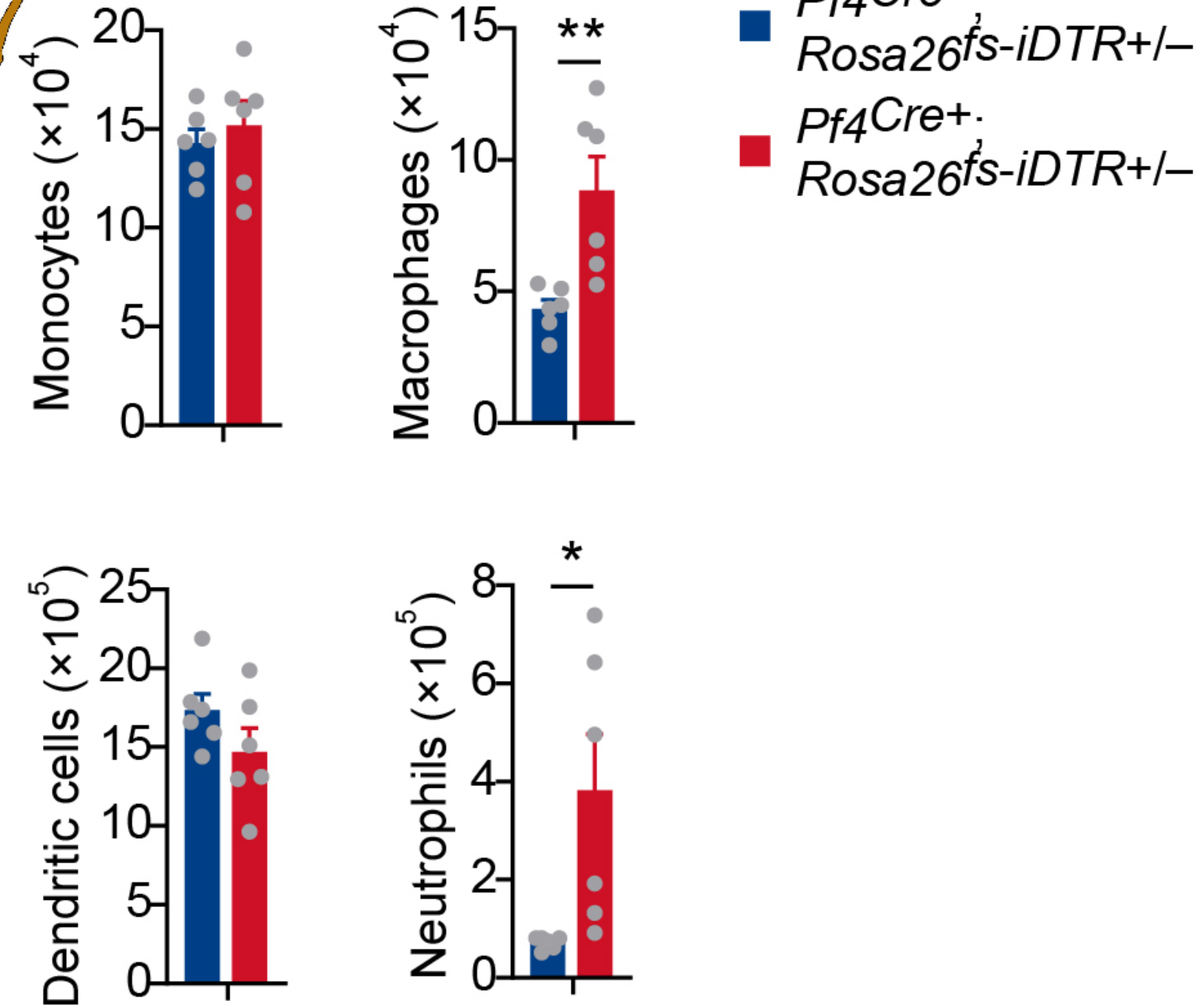
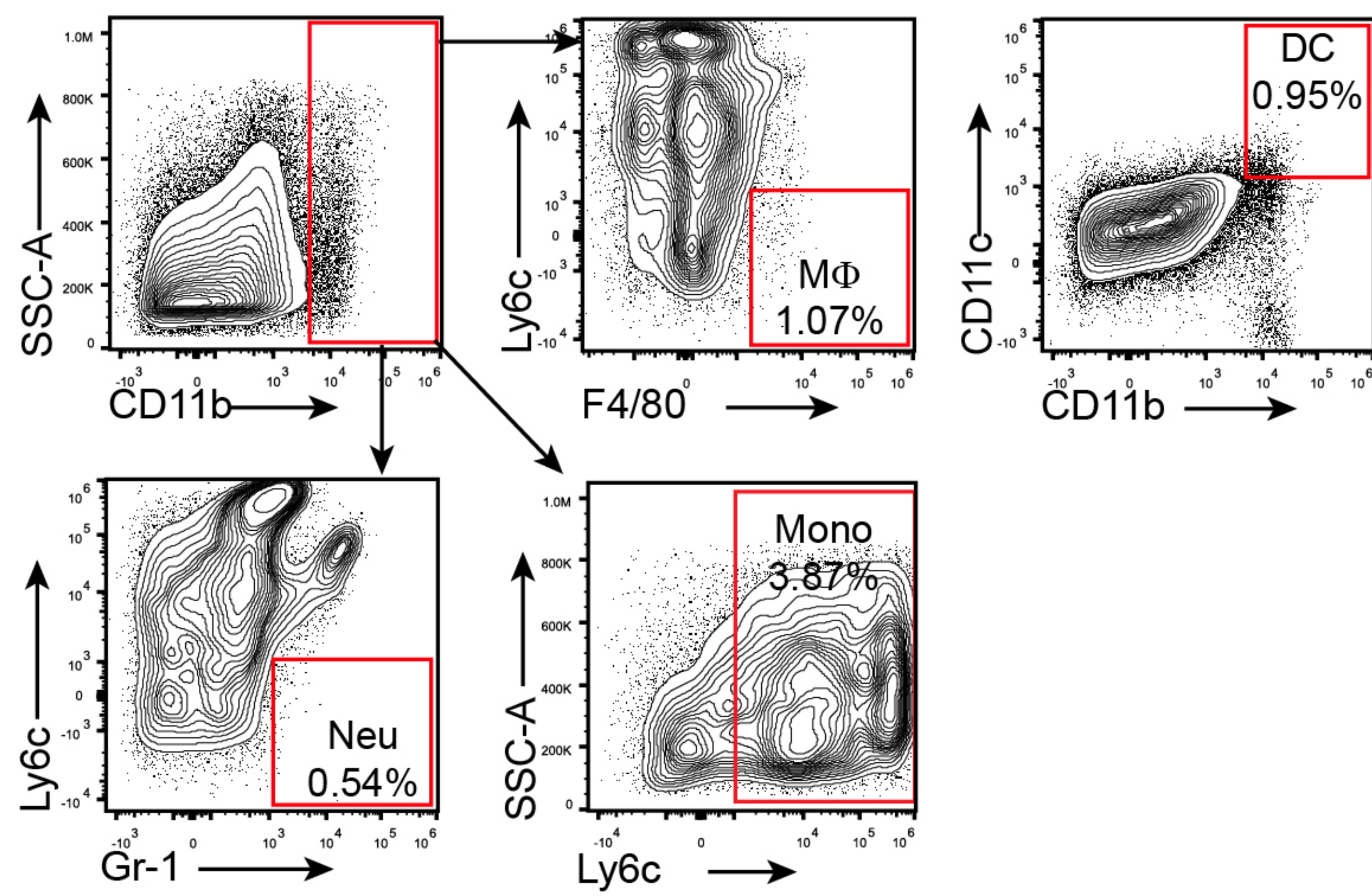
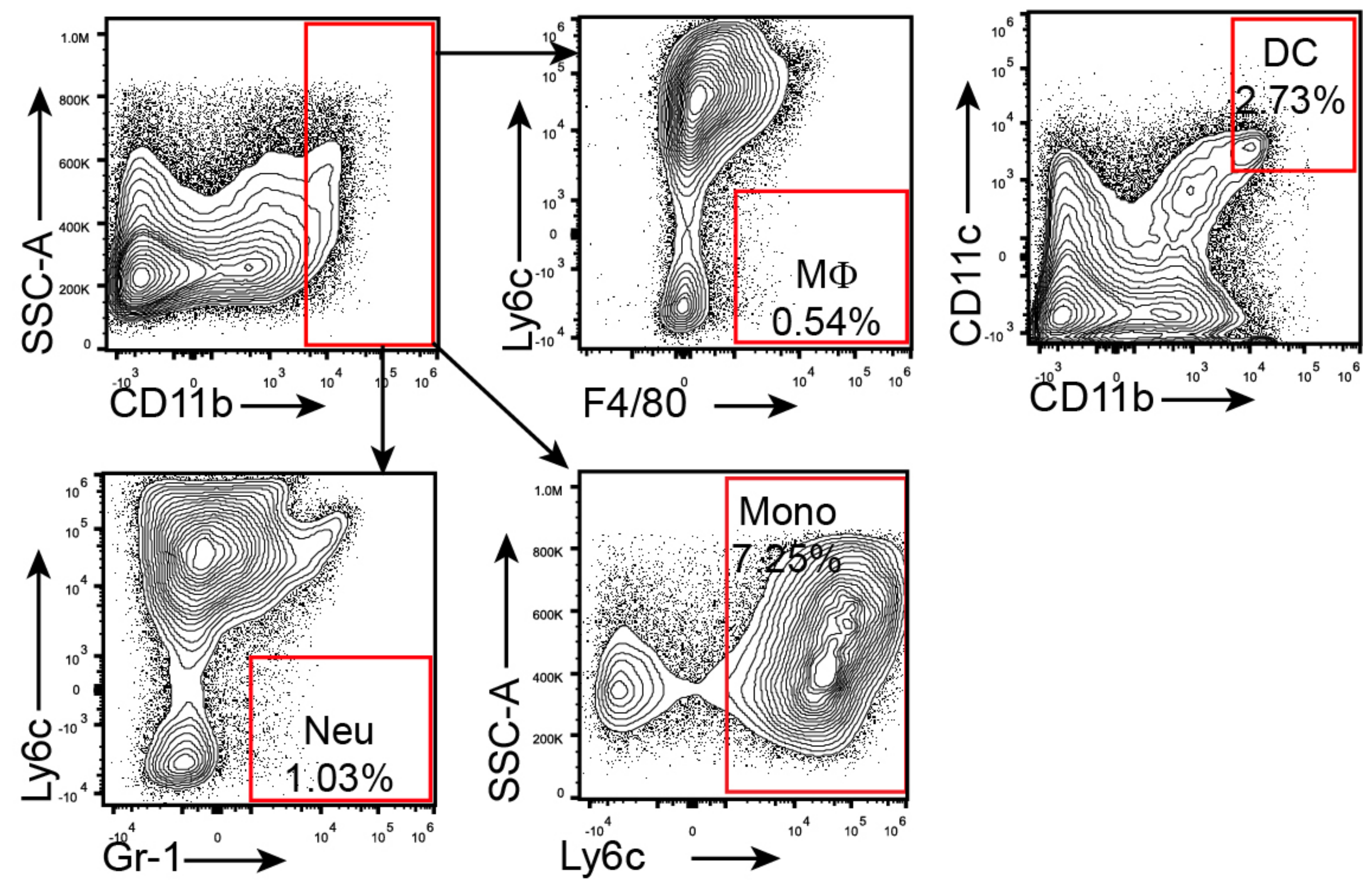


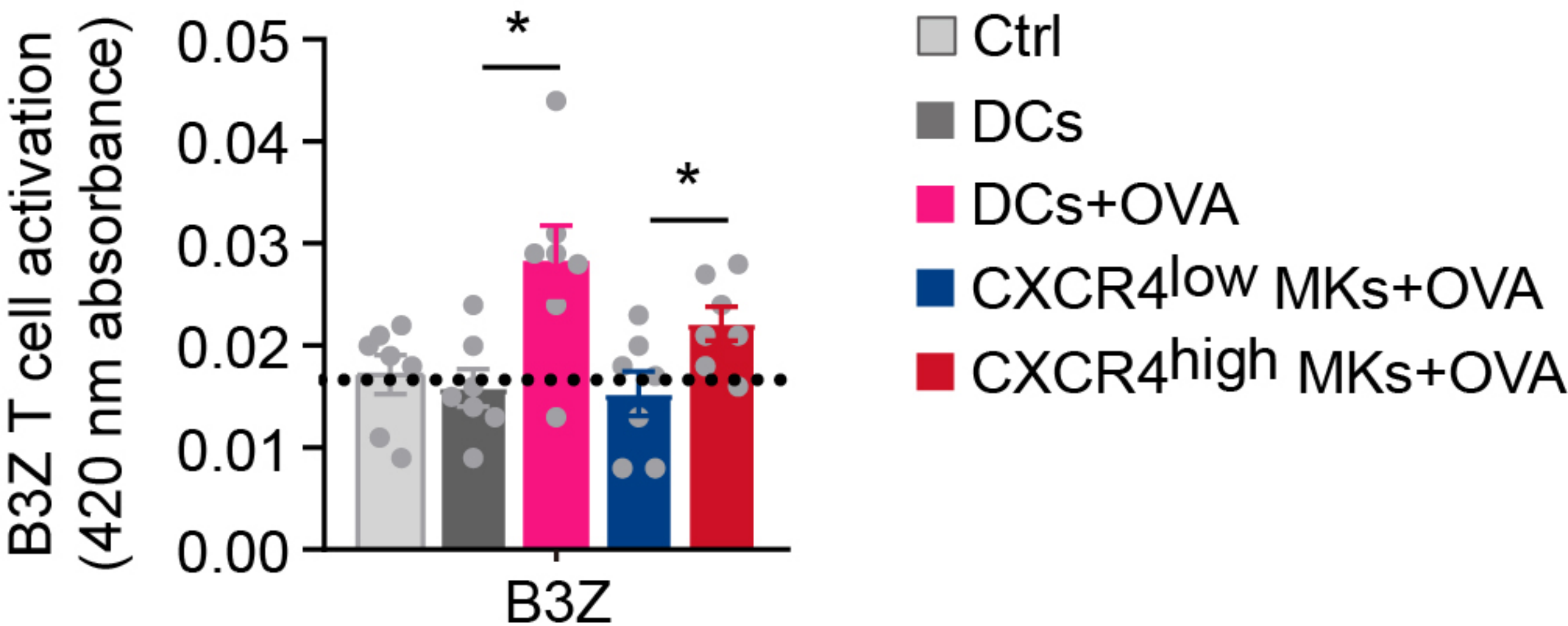
DT
0 1 2 3 4 days

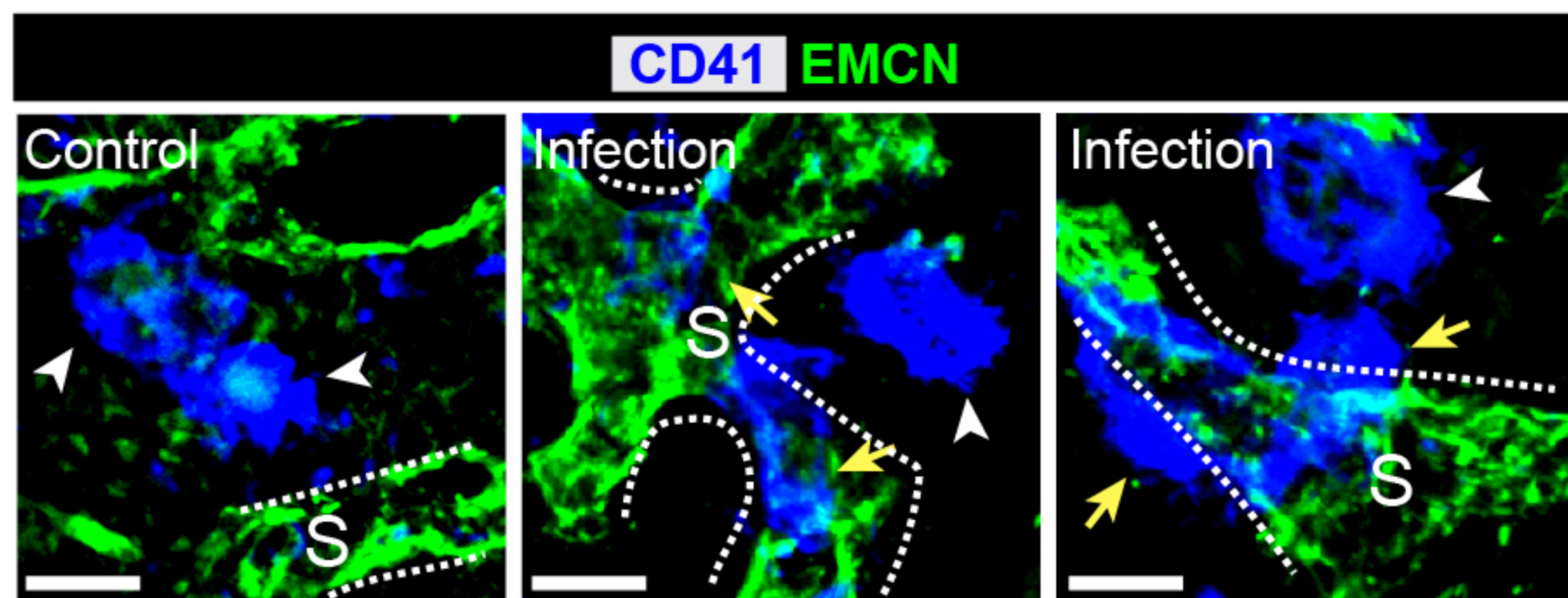
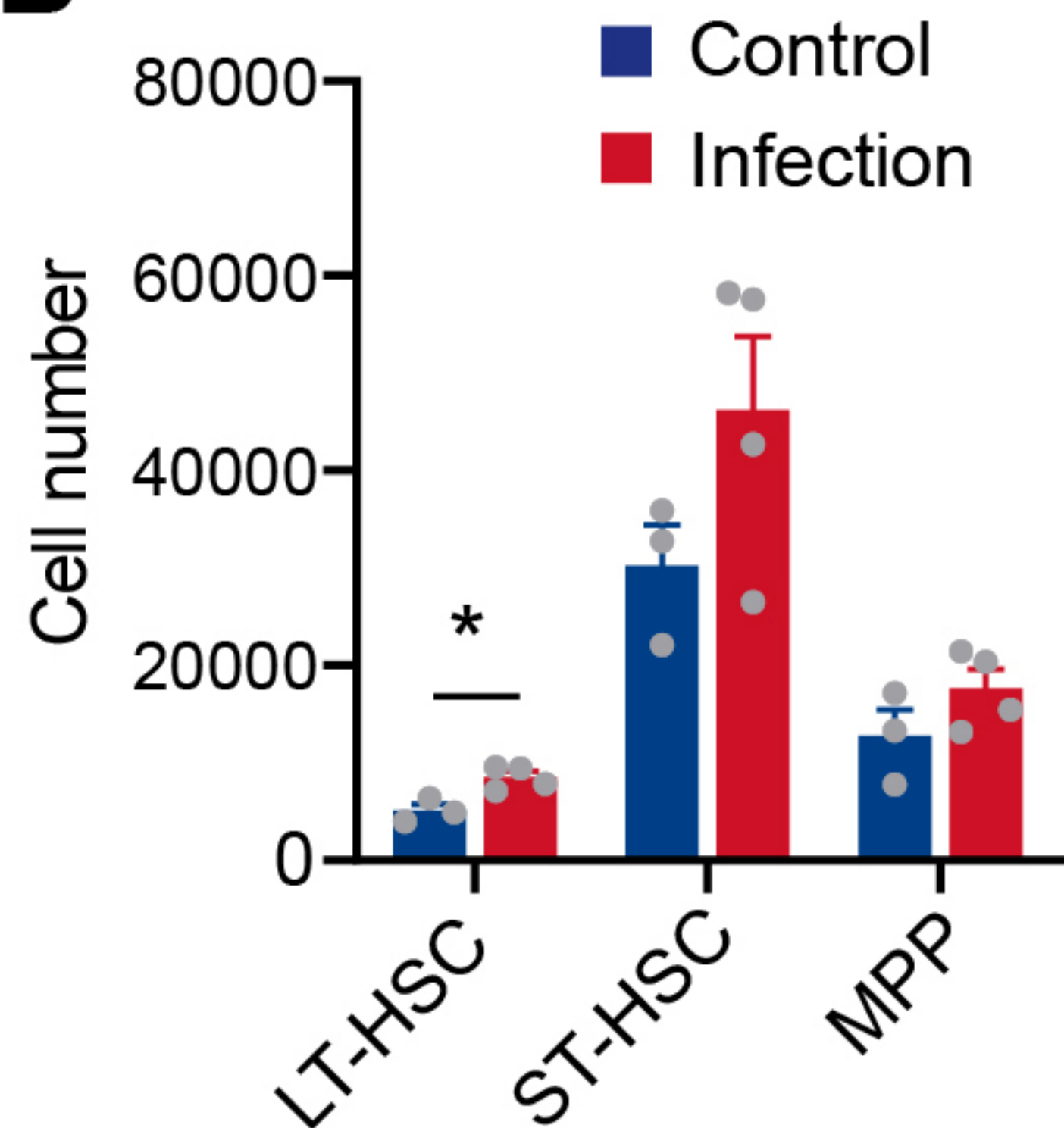
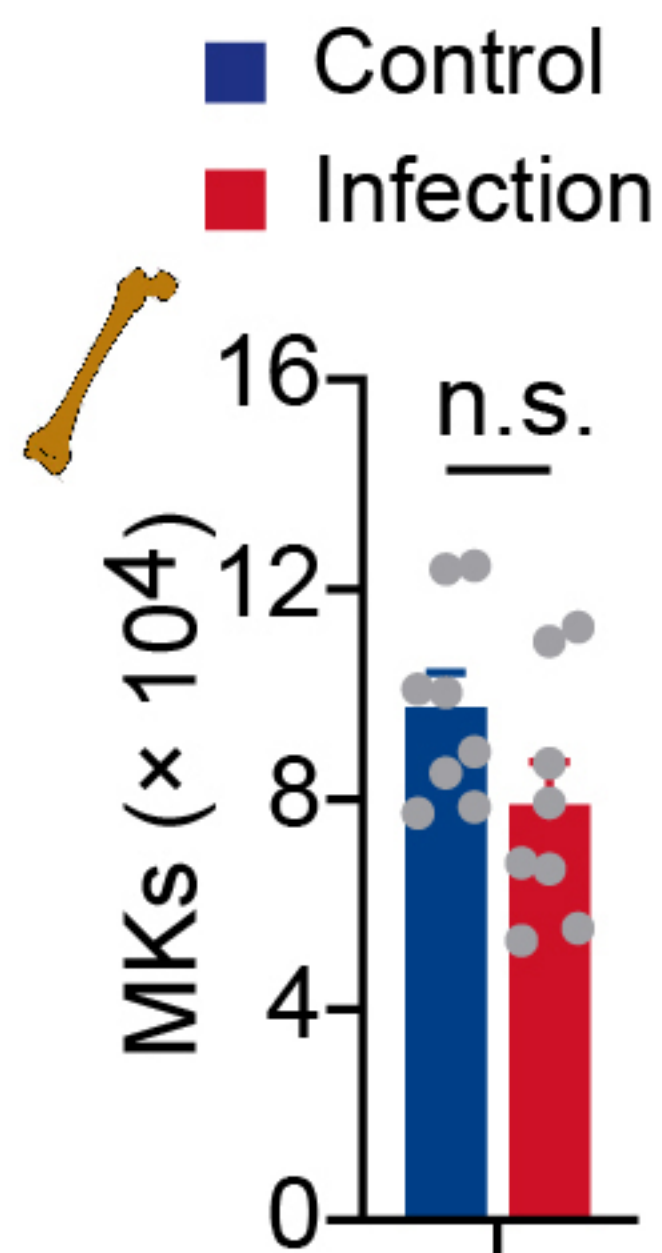
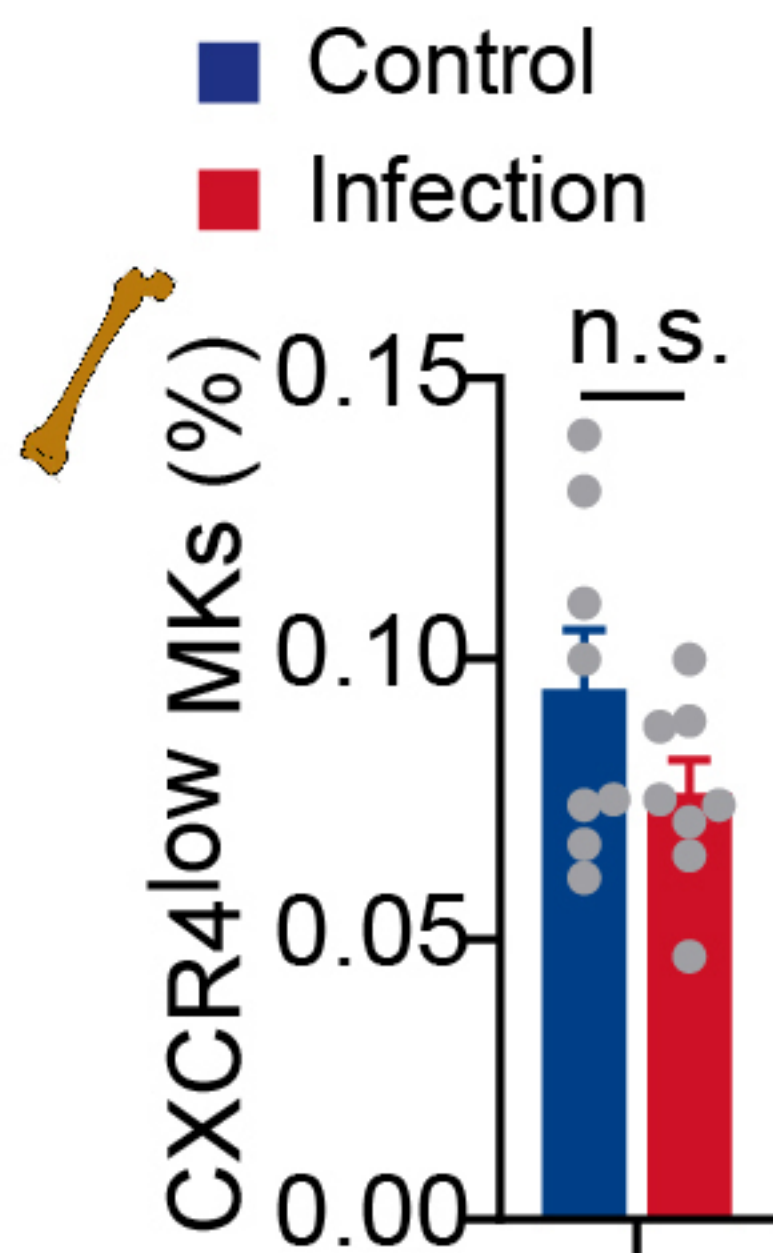
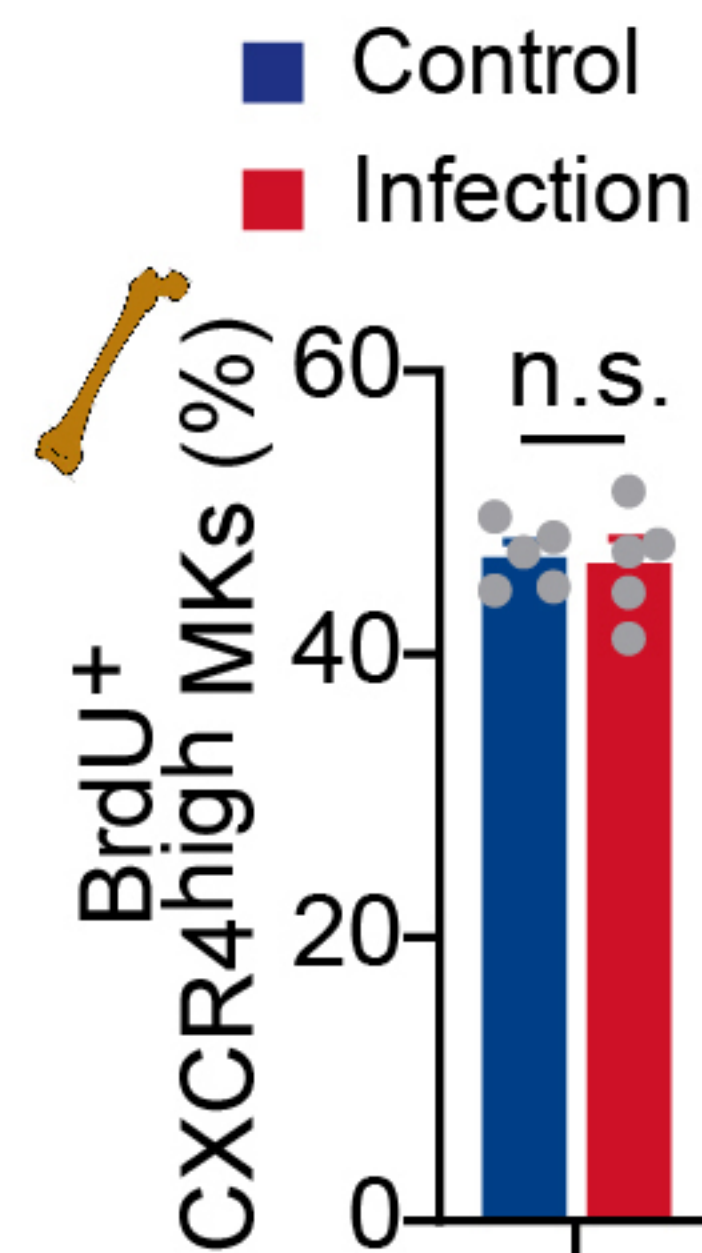
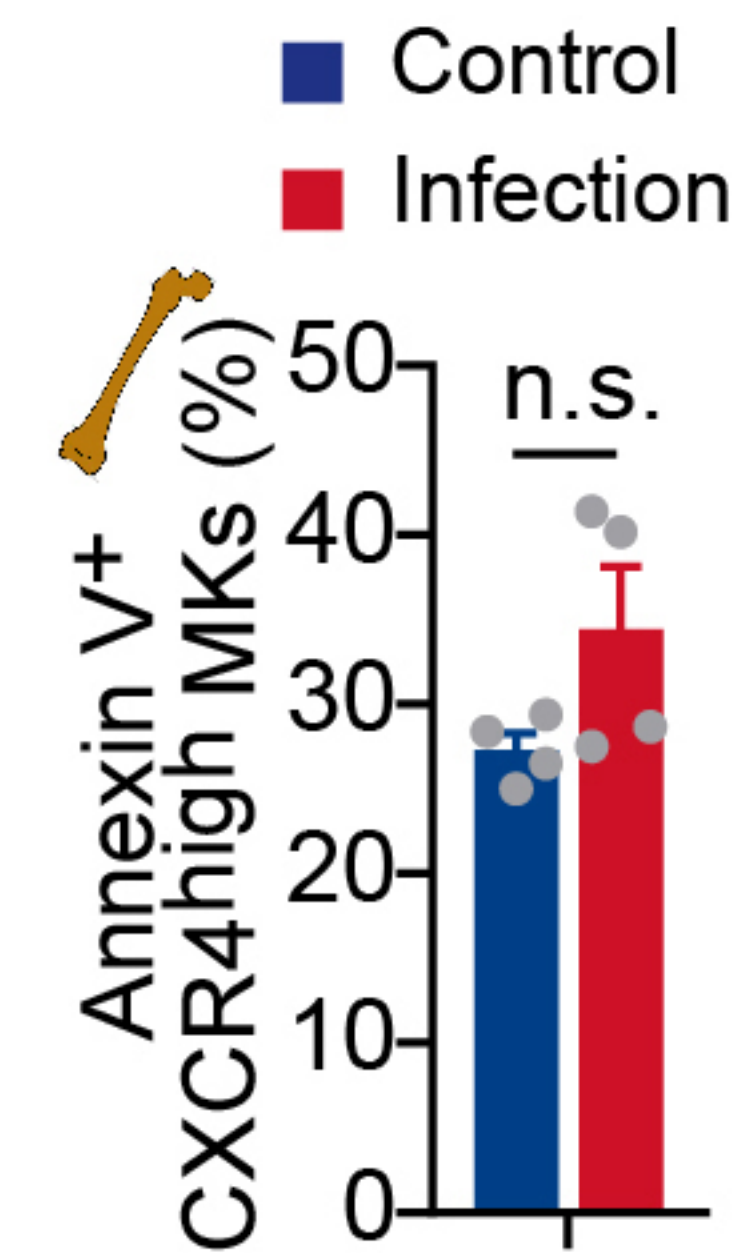
L. m.

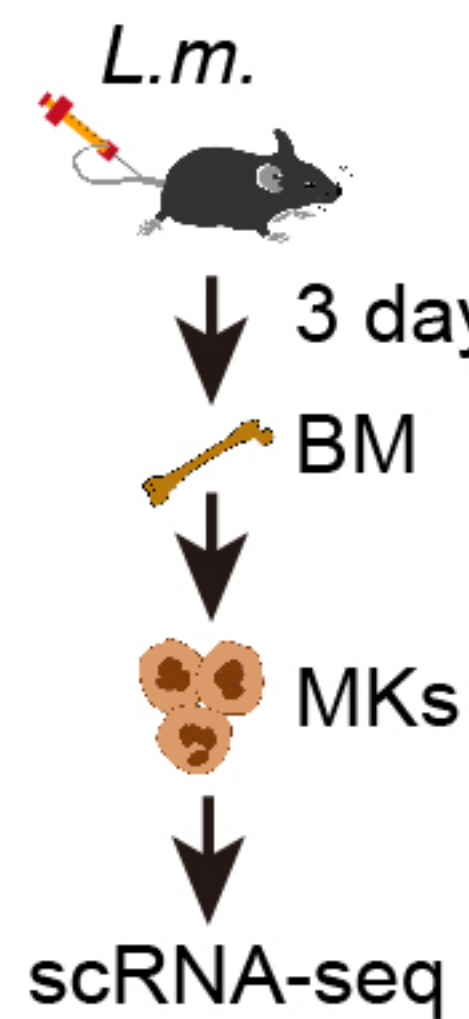
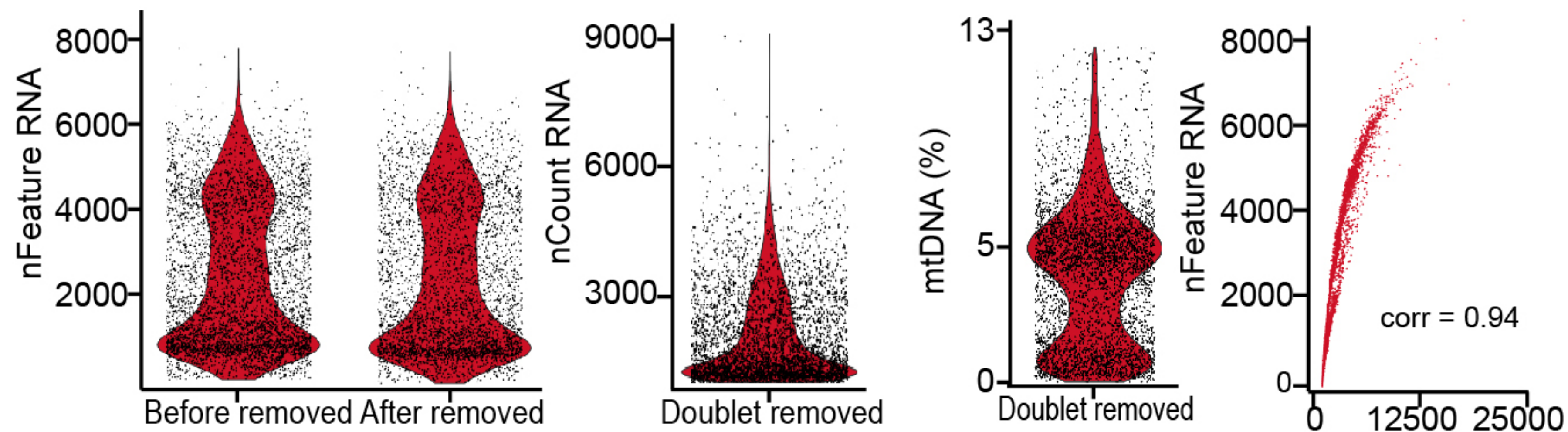
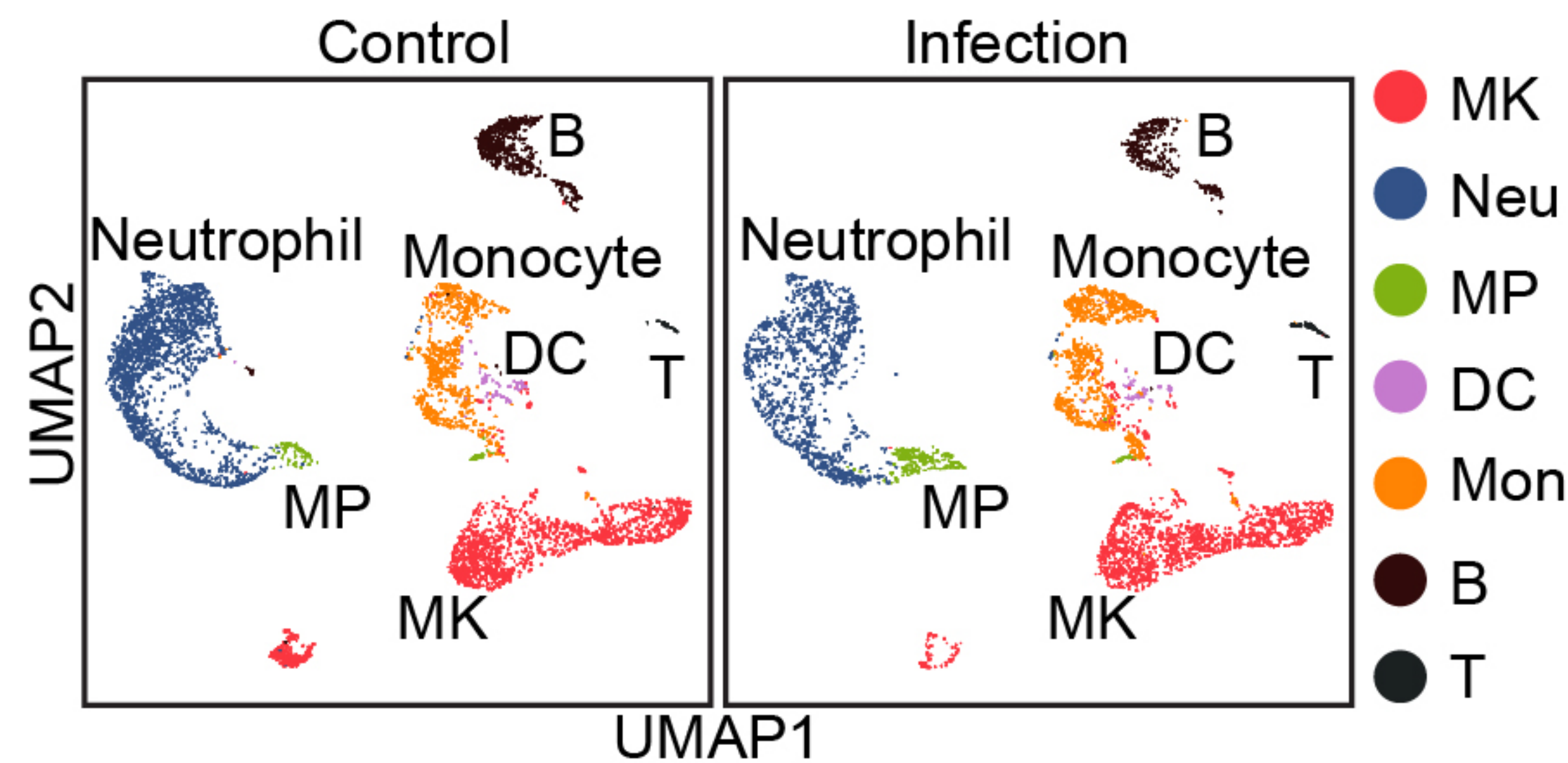
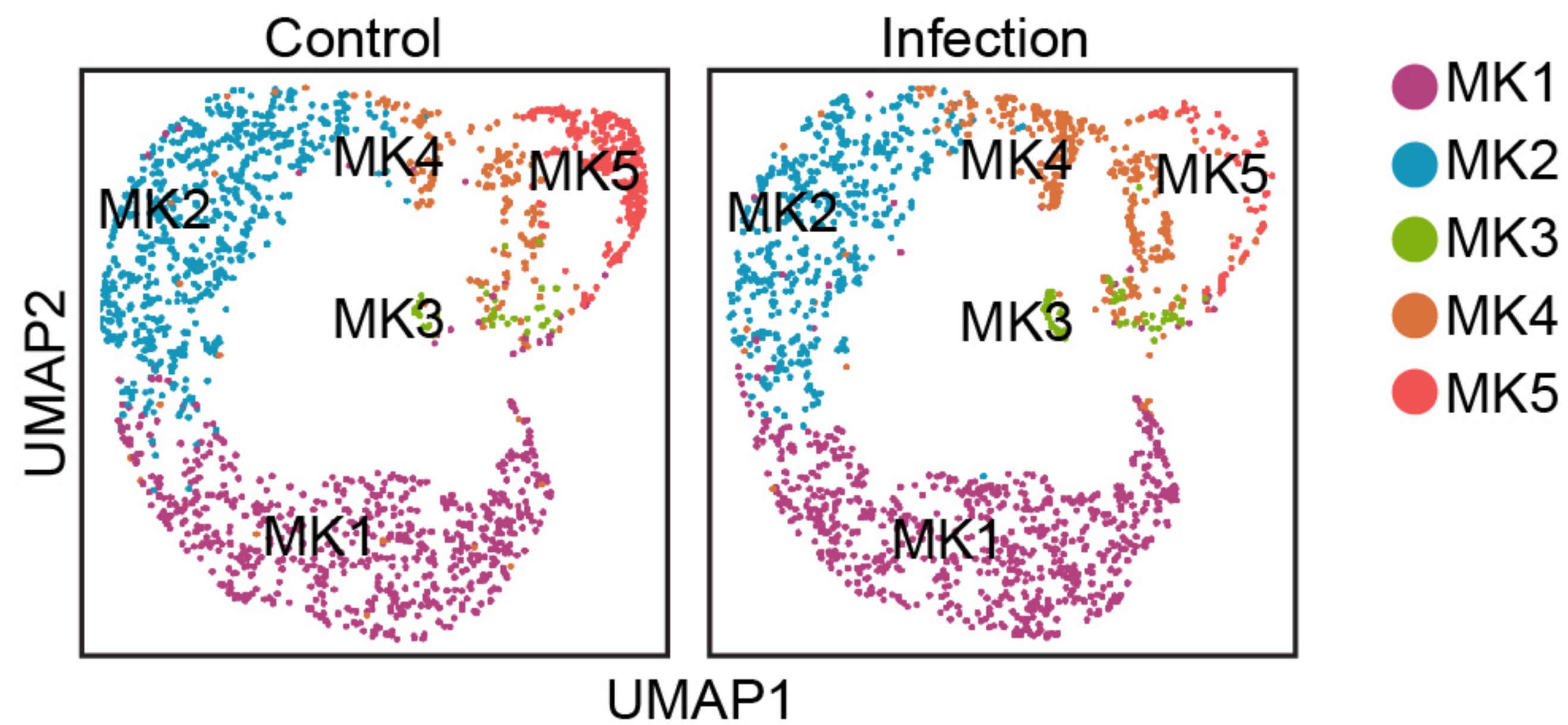
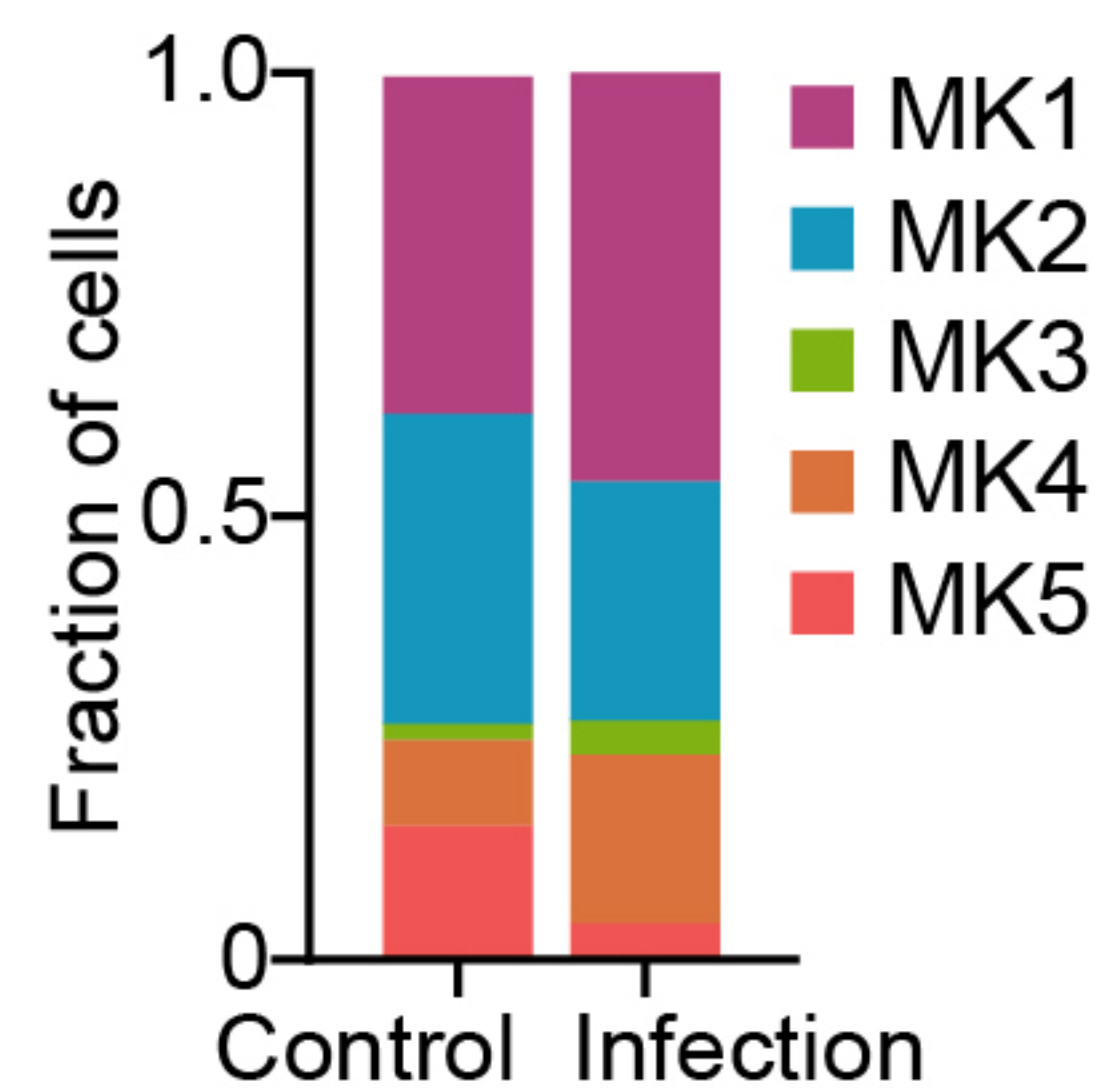
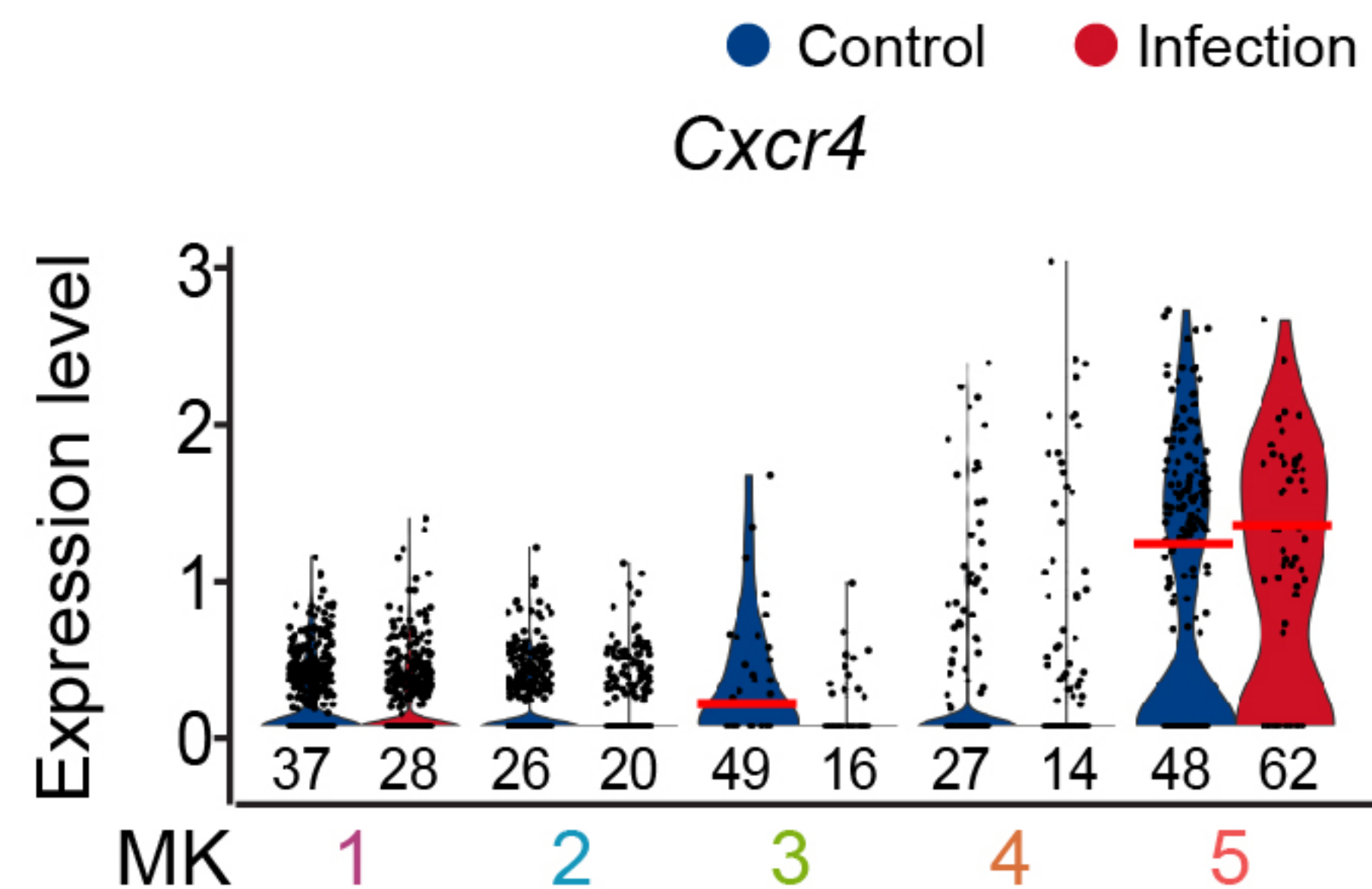
Harvest

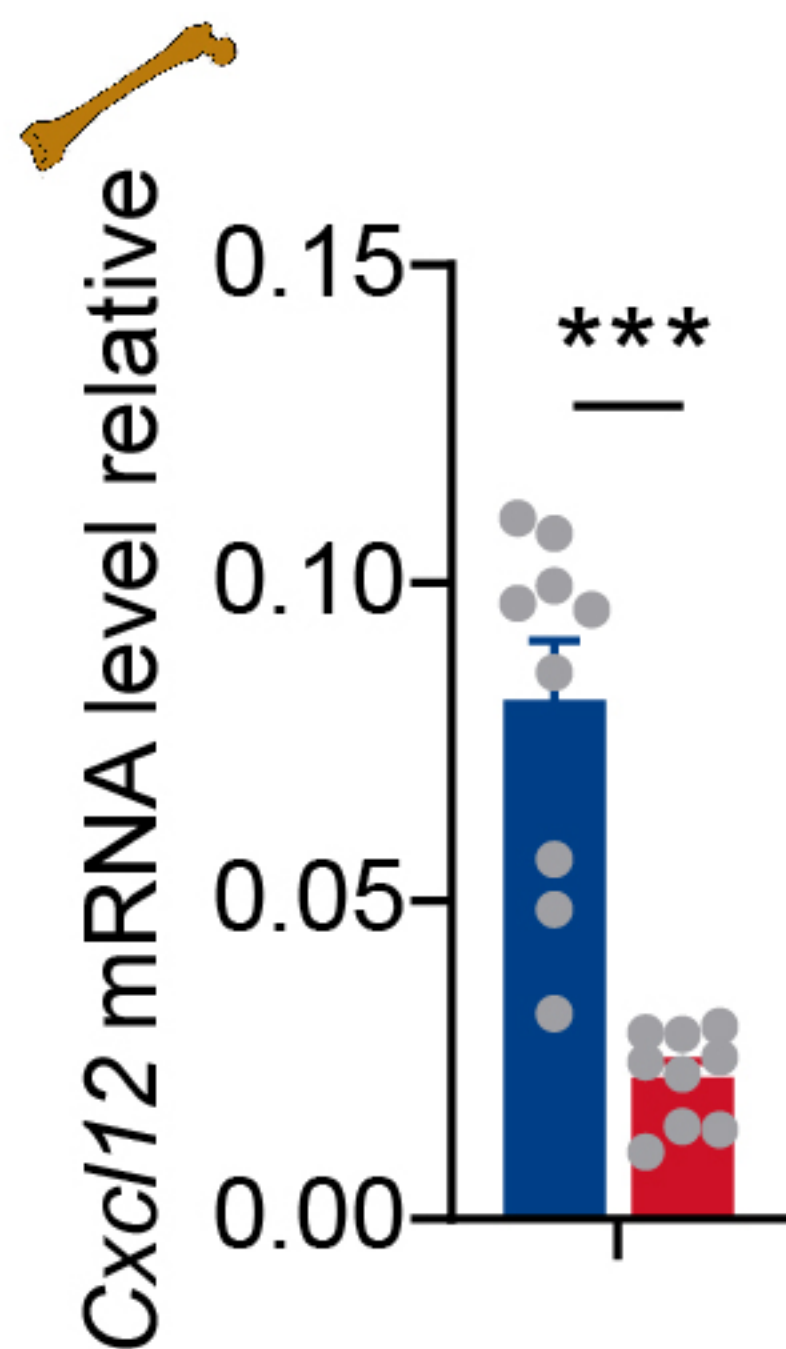
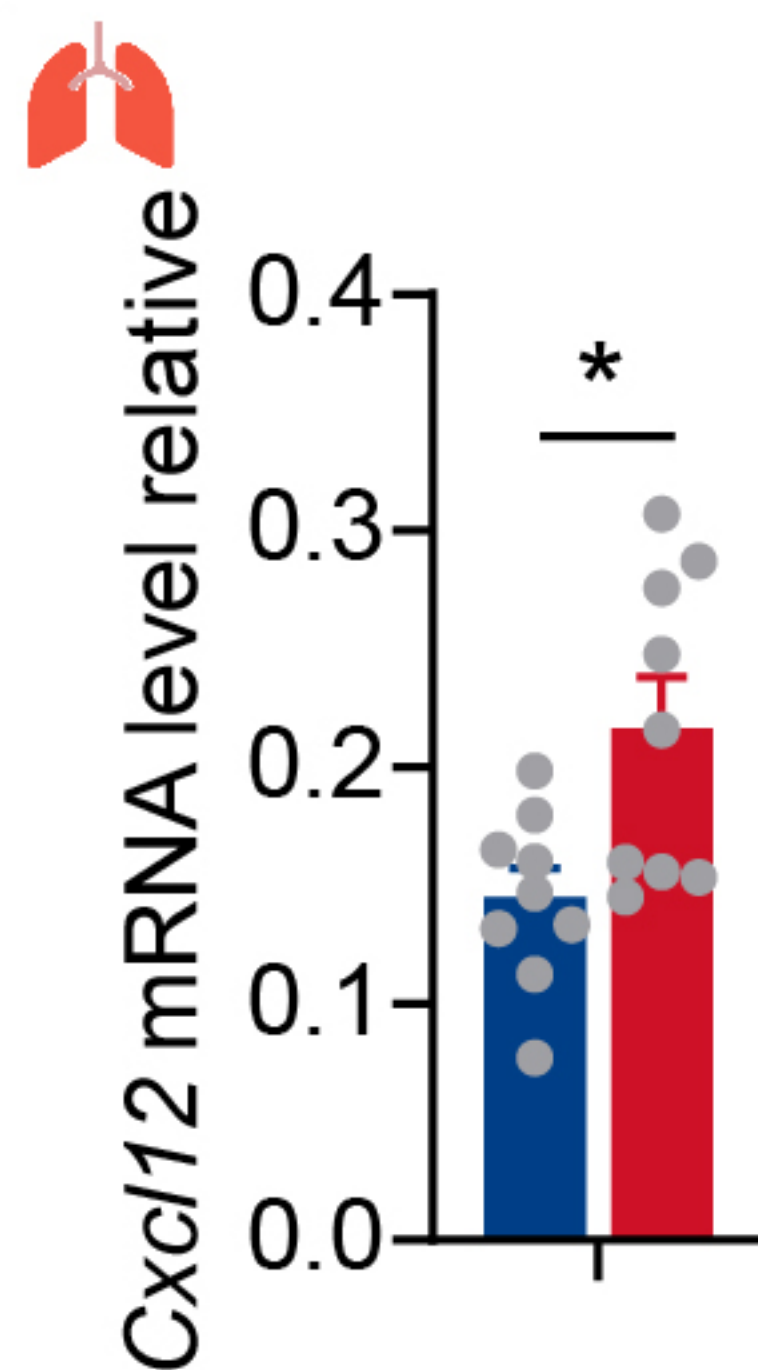
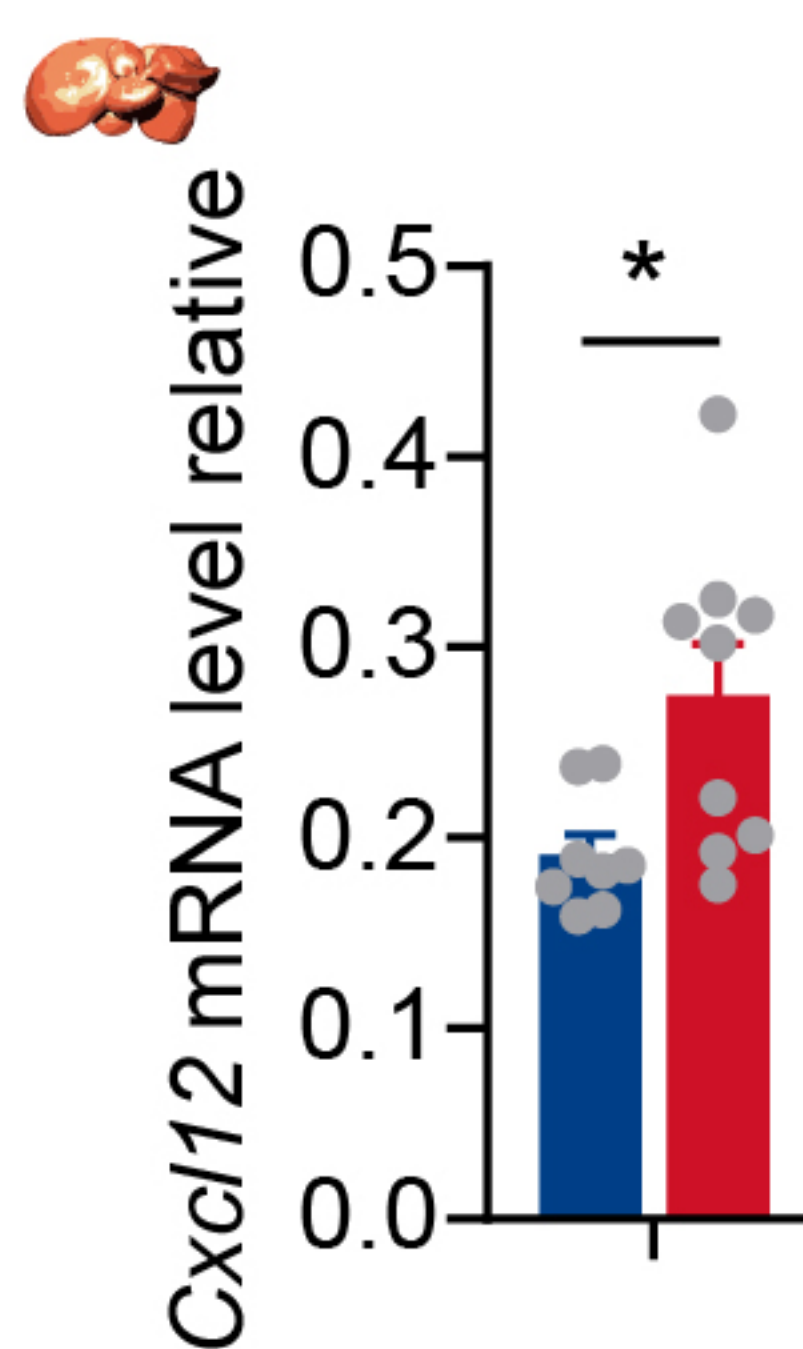
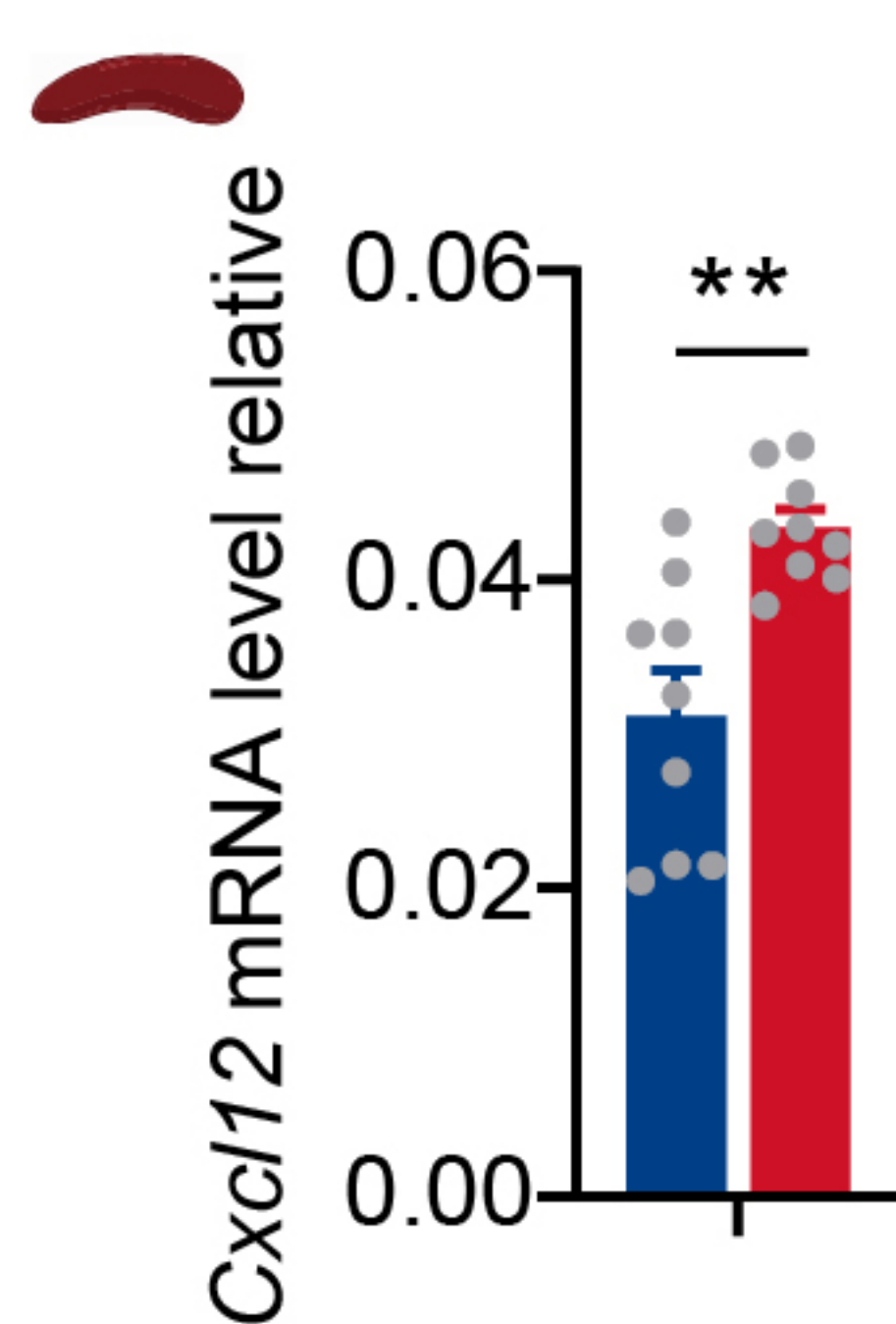
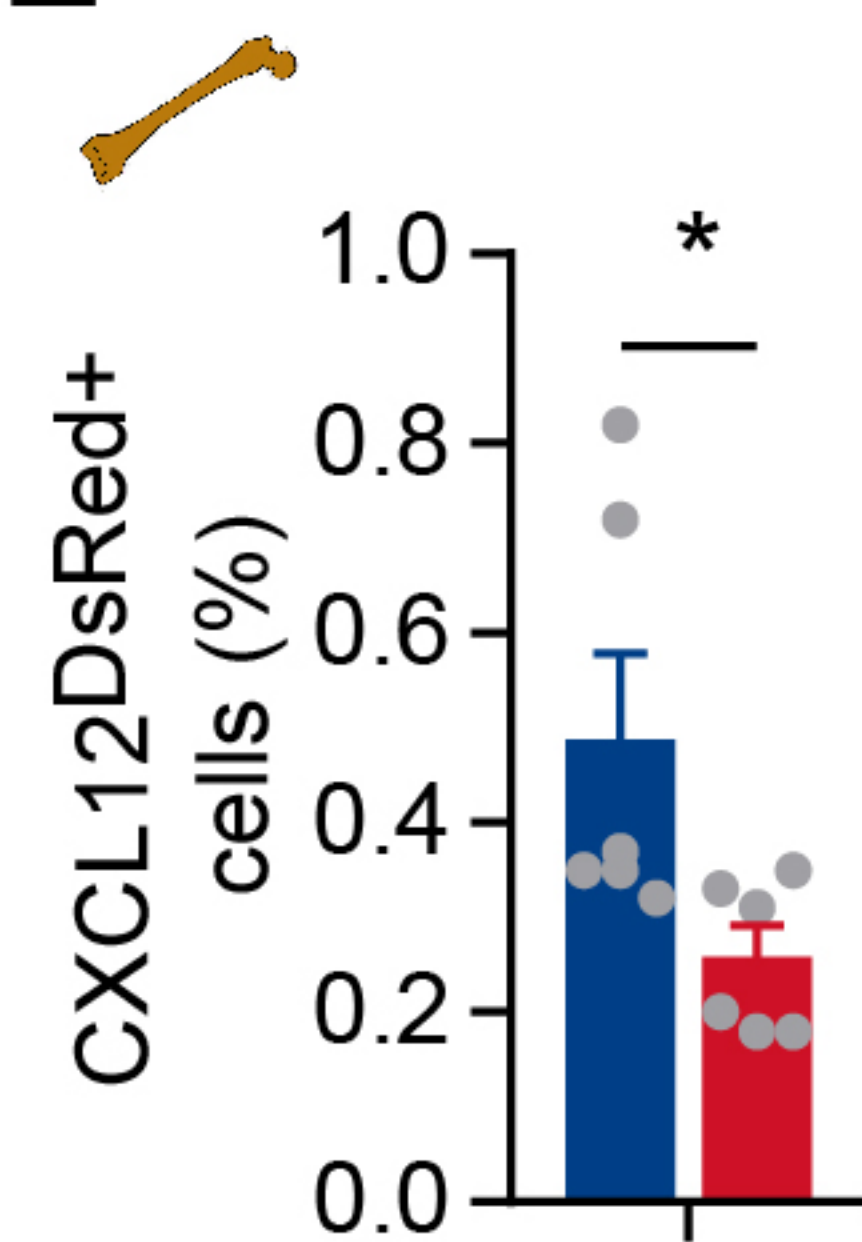
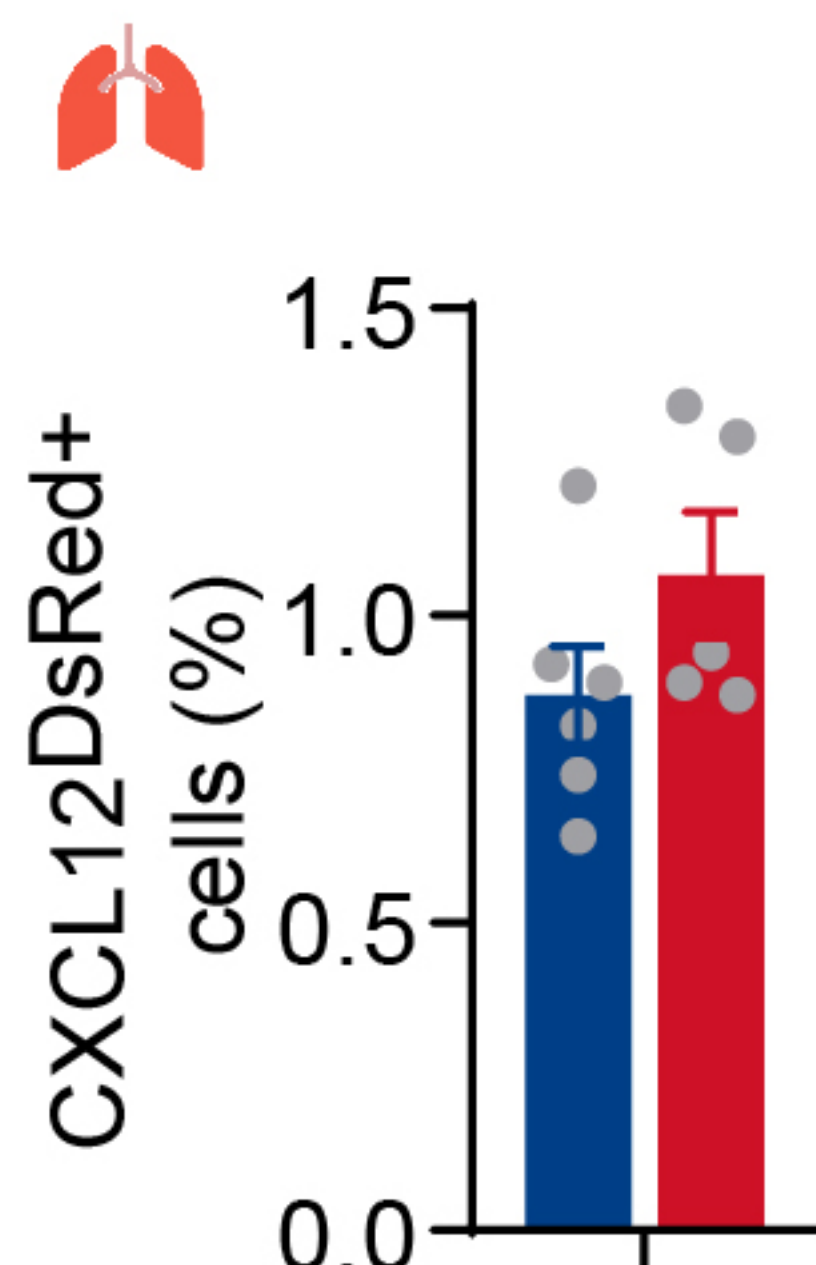
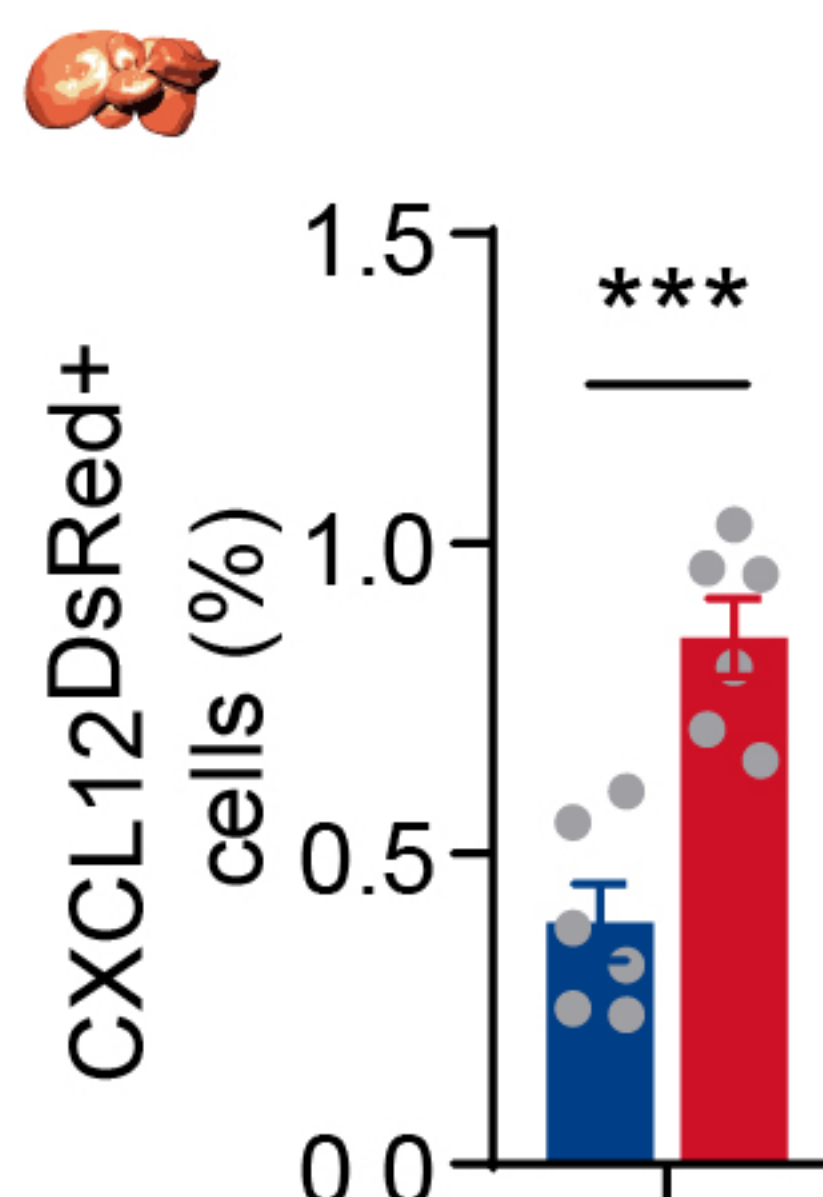
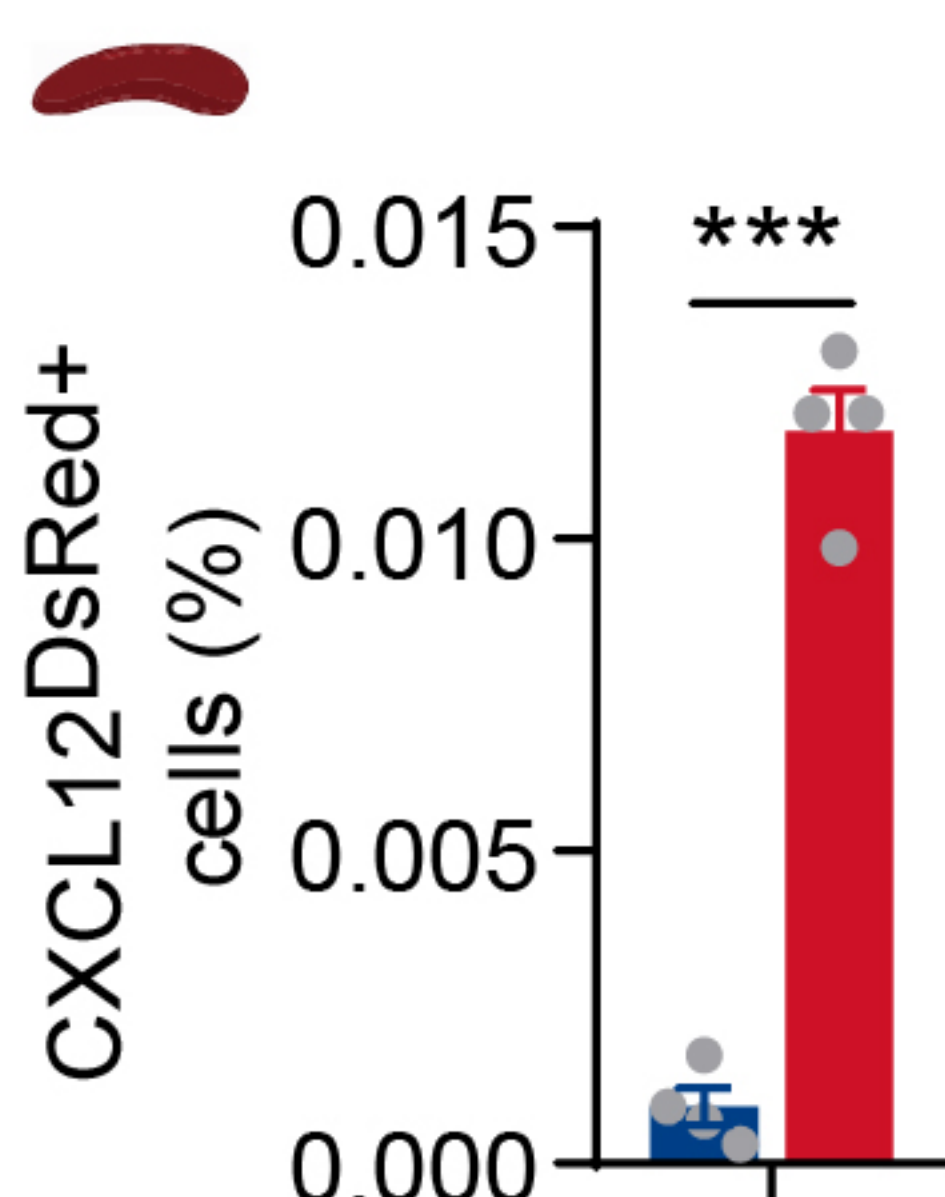
Pf4Cre^{+/+}
Rosa26^{fls-iDTR}+/-

B**C****D****E****F**



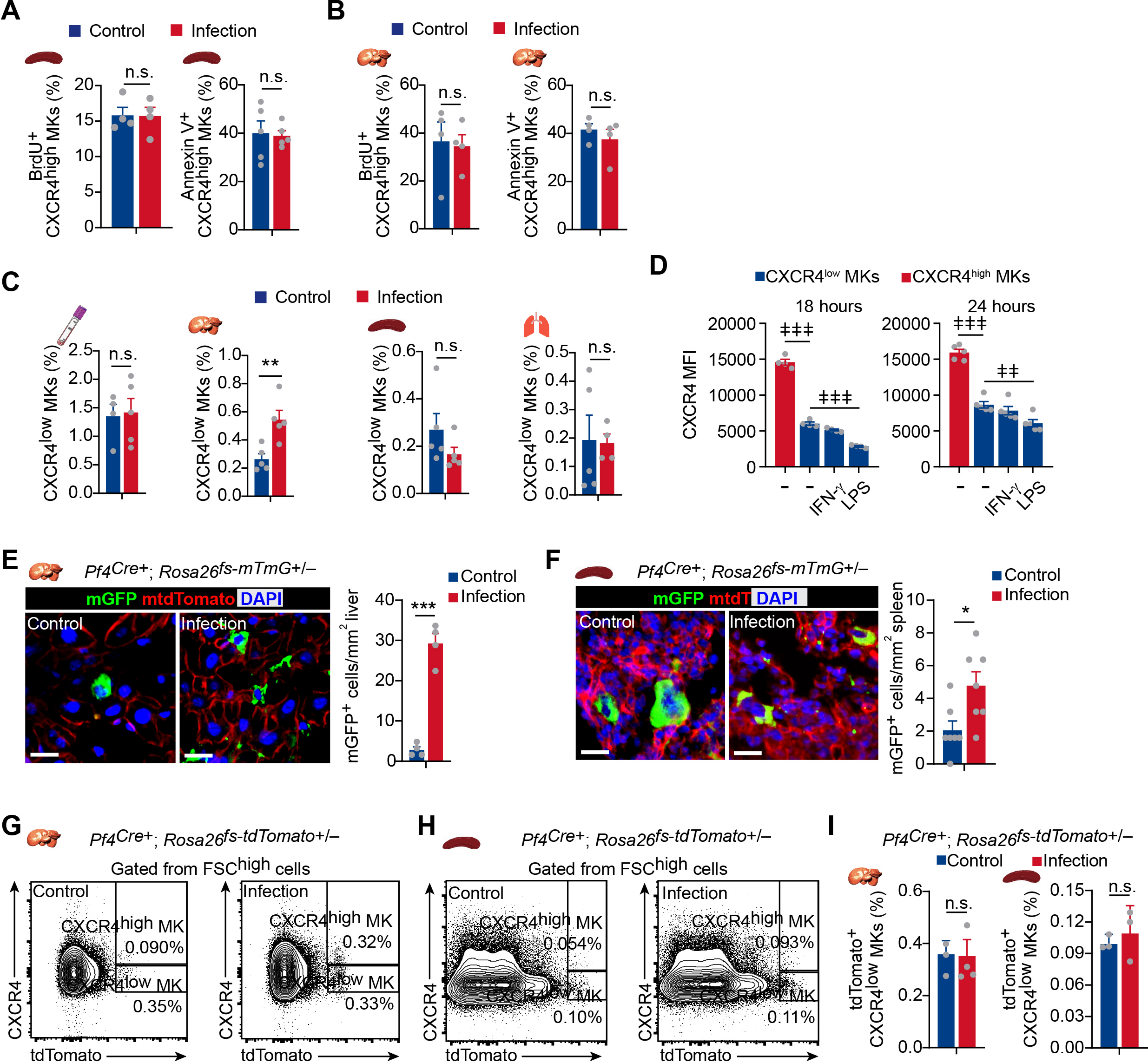
A**B****C****D****E****F**

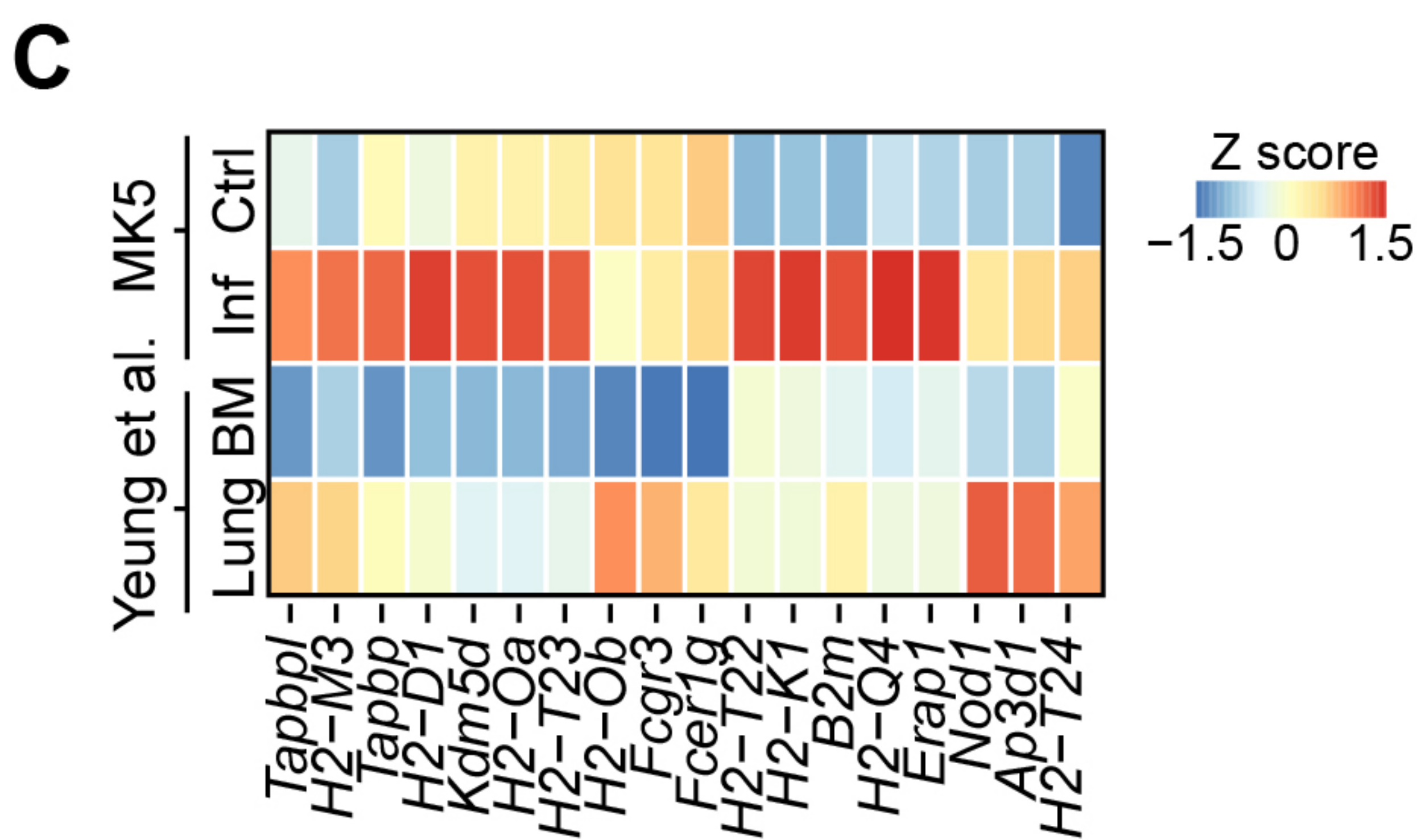
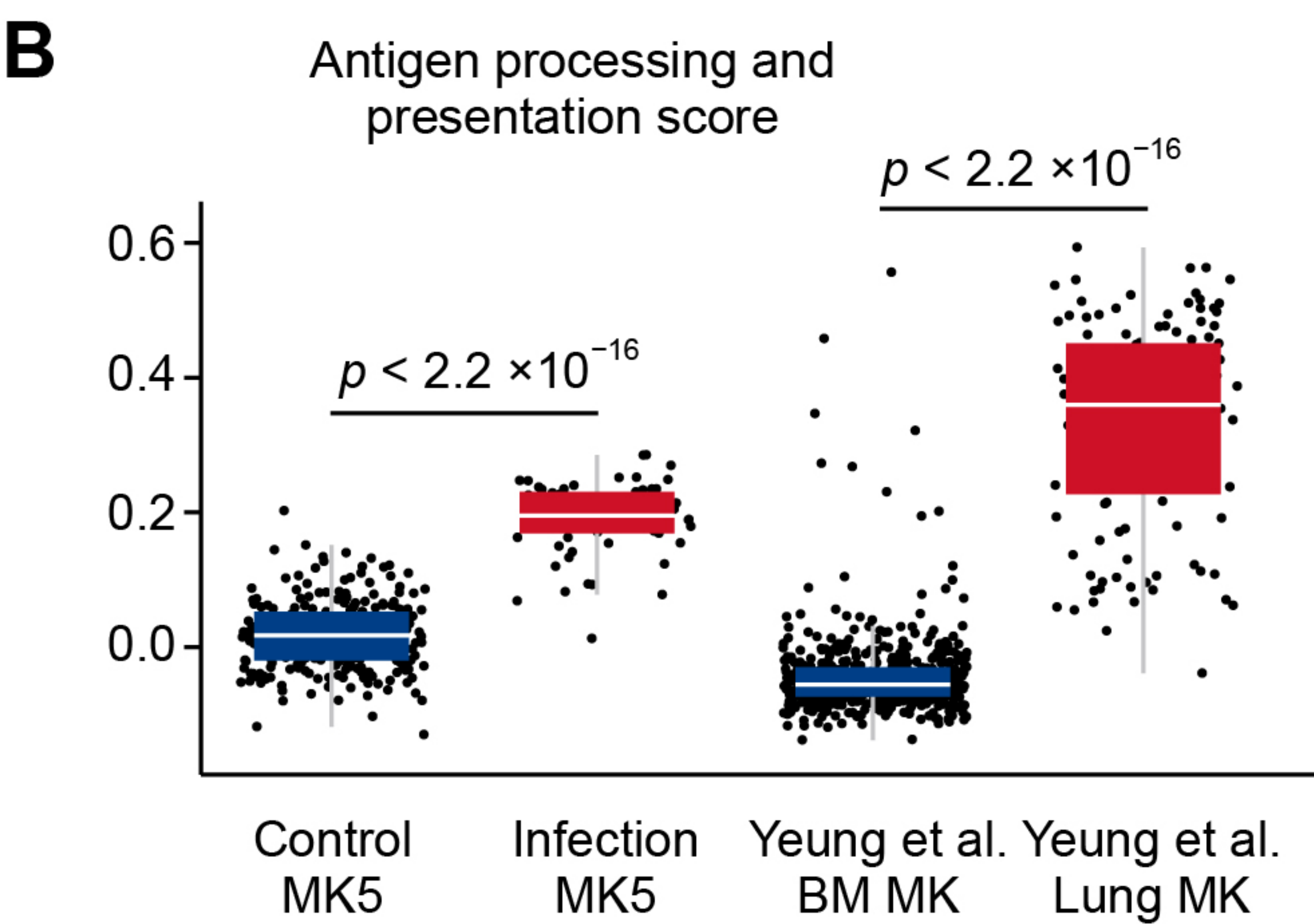
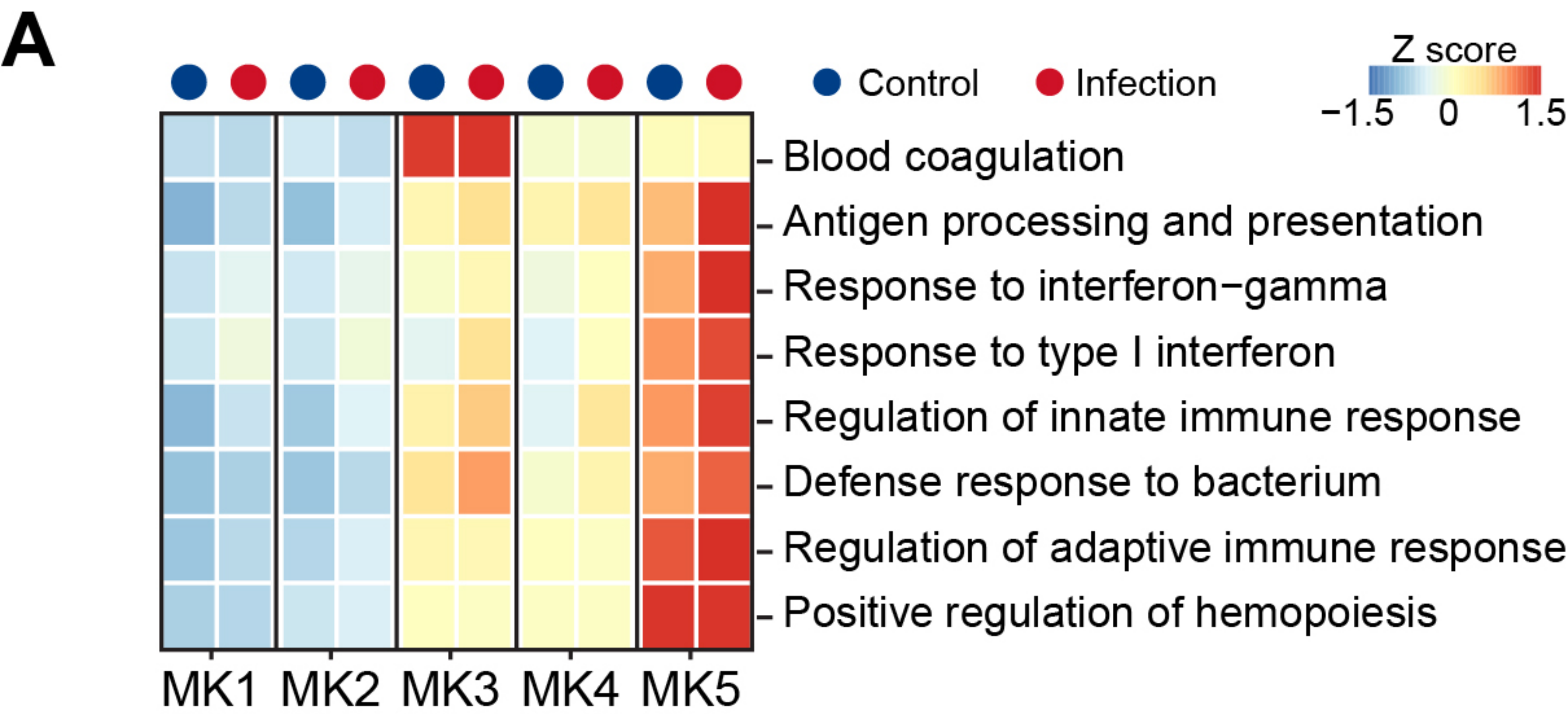
A**B****C****D****E****F**

A**B****C****D****E****F****G****H**

■ Control

■ Infection

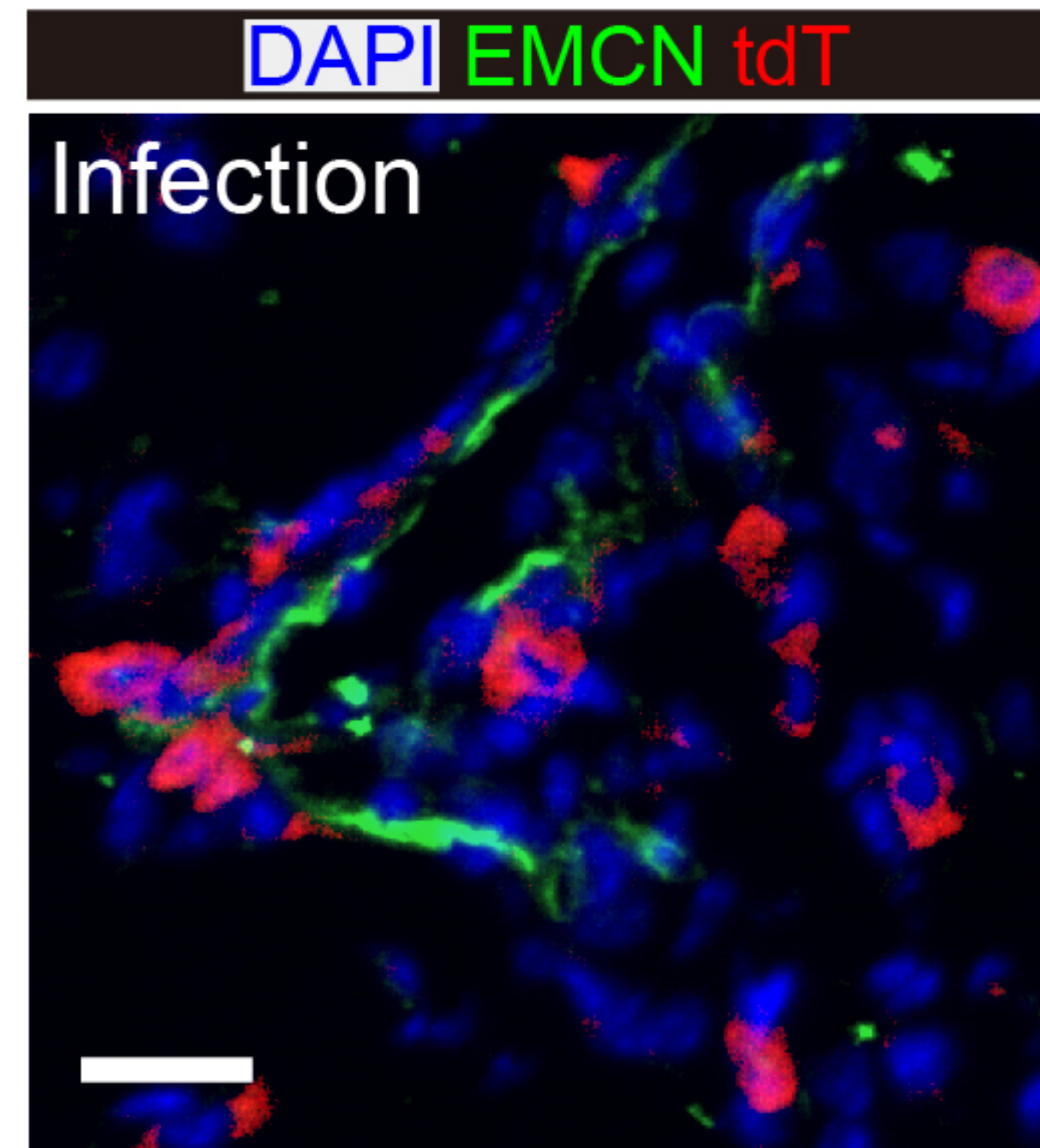




A



B



C

